Ruthenium Complexes of New Heterocyclic Ligands

A thesis submitted in partial fulfilment
of the requirements for the Degree
of
Master of Science in Chemistry
at the
University of Canterbury
by
Thomas William Davison

Department of Chemistry, University of Canterbury, Christchurch,
New Zealand
2014

“This book was written using 100% recycled words.”
― Terry Pratchett, Wyrd Sisters

Table of Contents

Acknowledgements

I wish to thank my supervisors, Professor Peter J. Steel and Dr Chris M. Fitchett, for their help and guidance during the course of this work. Thanks to Dr Chris Richardson and Professor Richard Keene for their discussions and advice.

I also wish to thank the students of Room 658, with particular mention to Siji Rajan and Robert Currie, for their support and advice over the course of my study. My thanks also to the technical and postdoctoral staff who helped me during my work, with special thanks to Marie Squire for her help with NMR and mass spectroscopy, Paula Brooksby and Lita Lee for their help with electrochemistry, Matthew Polson for his help with crystallography and his health and safety work, and to Alistair Duff, Robert Stainthorpe and Laurie Anderson for (among other things) their enjoyable afternoon tea discussions.

And finally, I wish to thank my family and friends, whose love and support have helped me get where I am today.

Abbreviations

bpy	2,2'-bipyridine
CIS	Coordination induced shift
COSY	Correlation spectroscopy
DCM	Dichloromethane
DPV	Differential pulse voltammetry
ESI	Electrospray ionisation
ESI/MS	Electrospray ionisation mass spectrometry
EtOAc	Ethyl acetate
EtOH	Ethanol
HMBC	Heteronuclear multiple bond correlation
HOMO	Highest occupied molecular orbital
HSQC	Heteronuclear single quantum correlation
I.R.	Infra-red
LUMO	Lowest unoccupied molecular orbital
MC	Metal centred
MeCN	Acetonitrile
MeOH	Methanol
MLCT	Metal-to-ligand charge transfer
NMR	Nuclear magnetic resonance
PF_6^-	Hexafluorophosphate anion
$[Ru(bpy)_3]^{2+}$	Tris(2,2'-bipyridine)ruthenium(II)
TLC	Thin-layer chromatography
TOCSY	Total correlation spectroscopy
TOF	Time-of-flight
UV-Vis	Ultraviolet–visible spectroscopy

Abstract

The coordination chemistry of eight chelating heterocyclic ligands is described. These ligands all contain heterocyclic ring systems with bridgehead nitrogens, and have received little attention in the literature. The ring systems examined are, specifically, imidazo[1,2-a]pyridine, imidazo[1,5-a]pyridine and triazolo[1,5-a]pyridine.

The coordination complexes synthesised are mononuclear ruthenium(II) complexes, of the type $[Ru(bpy)_2(L)]^{2+}$. Complexes have been examined by a combination of ^{1}H and ^{13}C NMR, UV-visible spectroscopy, cyclic voltammetry, and X-ray crystallography, in order to study their metal-ligand interactions. A total of six complexes were analysed by single crystal X-ray diffractometry, and the resulting structures are described herein.

In general, the inclusion of these ligands had the effect of raising the HOMO and lowering the LUMO, relative to the $[Ru(bpy)_3]^{2+}$ complex. As a result, the complexes were easier to oxidise, harder to reduce, and absorb visible light at longer wavelengths.

Chapter 1

Introduction

Coordination complexes have been of interest for hundreds of years (e.g. Alizarin 450 B.C., Prussian Blue 1704), however the theory behind these compounds was always a topic of debate. It wasn't until Alfred Werner first proposed the octahedral geometry of cobalt(III) in 1893[1,2] that our understanding of coordination chemistry really began. Many different ligands have been examined over the years,[3,4] and an important class of ligands in transition metal coordination chemistry has been the nitrogen containing aromatic heterocycles. Within this class, the two main groups of interest are the five-membered azoles (e.g. pyrrole) and the six membered azines (e.g. pyridine) (Fig 1.1).

Fig 1.1 Examples of aromatic nitrogen heterocycles.

Azines and azoles have rather different electronic features, which can be explained by examining their resonance structures.[5] Using pyridine as an example of a simple azine (Fig 1.2), we can observe that in three of the five resonance contributors, there is a partial negative charge located on the nitrogen, while there is a partial positive charge located on the α/γ carbons of the ring. This resonance, in addition to the electron withdrawing nature of nitrogen (nitrogen being more electronegative than carbon), creates a permanent dipole towards the nitrogen. As such, pyridine and other related heterocycles have been described as electron poor, or π-deficient. Their π* orbitals are relatively low lying, and as such form stable complexes with transition metals; the ligand acts as a good π-acceptor, so the coordination bonds are stabilised by back-bonding of the metal d-orbitals into the π-system of the ligand.

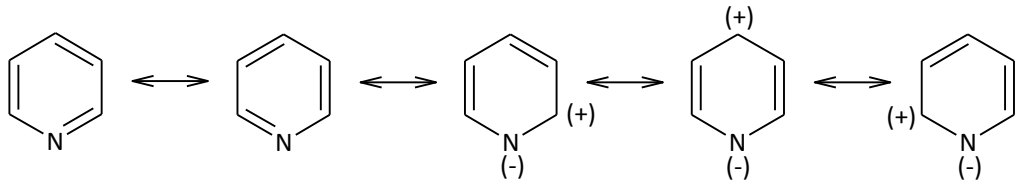

Fig 1.2 Resonance contributors of pyridine.

Conversely, examining the resonance structures of a simple azole (pyrrole, Fig 1.3) shows a partial positive charge centred on the nitrogen, with a partial negative charge on the carbons. This creates a permanent dipole away from the nitrogen. While the electron withdrawing nature of nitrogen will act in opposition to this dipole, the resonance effect is the more significant factor as the dipole is still observed to point away from nitrogen. Azoles are termed electron rich/π-excessive, and due to the nitrogen's lone pair being part of the six-electron aromatic system their binding potential can be increased by creating the anionic form (pK_a = 16.5).

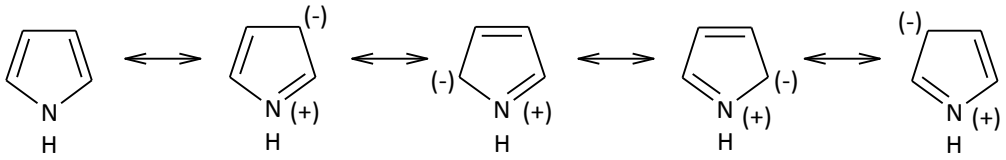

Fig 1.3 Resonance contributors of pyrrole.

Pyridine is one of the most well-known nitrogen heterocycles, and its extensive study has seen interest in its coordination chemistry. Octahedral binding of six pyridines is typically disfavoured, as steric effects caused by the hydrogens α to the nitrogen hamper coordination. As such, octahedral complexes with coordinating counteranions $M(py)_4(anion)_2$ are common,[6] with other geometries such as the square planar $M(py)_2(anion)_2$ having also been observed. It has been observed that the presence of large non-coordinating counterions, such as PF_6^-, can sometimes stabilise the octahedral $M(py)_6^{2+}$ form. To force an octahedral arrangement, pyridine rings could be bound together, in a way that disfavours square planar binding and increases the binding potential through the chelate effect. In this way, the synthesis of 2,2'-bipyridine (bpy) opened up many possibilities.

First reported in 1888,[7] bpy has been the subject of many studies over the last 125 years, owing to its ability to form stable complexes with most transition metals[8] and the interesting electrochemical, photochemical and photophysical properties[9,10] that result. Bipyridine's stability in complexes stems from a combination of effective back-bonding between the π-deficient azines and the metal d-orbitals, and the stabilising effects of bidentate chelation.

Of the possible transition metal complexes of bpy, tris(2,2'-bipyridine)ruthenium(II), $[Ru(bpy)_3]^{2+}$ (Fig 1.4), has been the most studied, due to its many favourable properties as a coordination complex. First synthesised by Burstall[11] in 1936, the first spectroscopic analysis carried out was a luminescence investigation by Paris and Brant in 1959.[12] Extensive studies have revealed a raft of interesting properties. It absorbs light in the visible region of the electromagnetic spectrum, with a strong absorption at 452 nm (ε = 13600) due to metal-to-ligand charge transfer, and has a comparatively long lived excited state (890 ns in acetonitrile at room temperature).[13] The long lifetime is due to the first excited state existing as a triplet, while the ground state is a singlet; transition between these spin states is forbidden, and so will occur over an extended period of time. $[Ru(bpy)_3]^{2+}$ has interesting and reversible redox properties and stability; in acetonitrile solution vs a saturated calomel electrode (SCE) one reversible metal based oxidation is observed at +1.26 V, in addition to three reversible bpy-based reductions (-1.33 V, -1.51 V and -1.79 V). Additionally, $[Ru(bpy)_3]^{2+}$ is both chemically photochemically stable. The combination of visible light absorption and a long lived excited state has made $[Ru(bpy)_3]^{2+}$ of interest in the production of photocatalysts, particularly for the splitting of water to hydrogen and oxygen.[14]

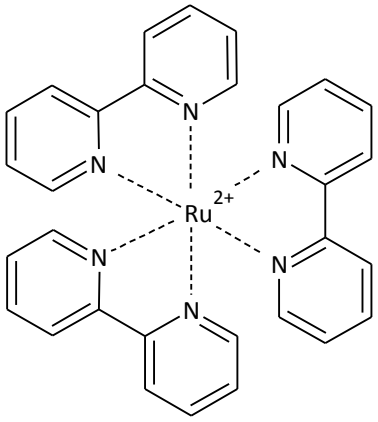

Fig 1.4 Tris(2,2'-bipyridine)ruthenium(II) cation.

The excited state of $[Ru(bpy)_3]^{2+}$ results from the transfer of an electron between the metal and ligands. Knowing this, we can tune the nature of the excited state by altering the ligands; by modifying or replacing one or more of the pyridine rings with either substituted derivatives or other heterocycles.[11] The most pronounced results come from replacing the entire pyridine ring with another heterocycle, and as such many have been investigated.[15] The simplest modifications involve substitution on the pyridine ring; 4,4′-dimethyl-2,2′-bipyridine is a popular modification made to ancillary bipyridine rings, as it helps to resolve the ^{1}H NMR when the ligand being investigated contains pyridine. Other simple modifications involve the replacement of pyridine with a diazine or a benzo-fused azine,[11,15] while more exotic modifications require replacement of bpy with a π-excessive azole.[15] Previous work by our group has focused on further modifying these azole moieties, either with more nitrogens (triazoles[16] and tetrazoles),[17] substituting oxygen or sulphur into the ring system (1,2,3-thiadiazoles[18] and 1,2,5-thiadiazoles,[19,20] 1,2,4-oxadiazoles[21] and 1,2,5-oxadiazoles),[20] or by fusing the five-membered system with benzene (benzotriazole,[22] benzothiazole and benzoxazole)[23] (Fig 1.5).

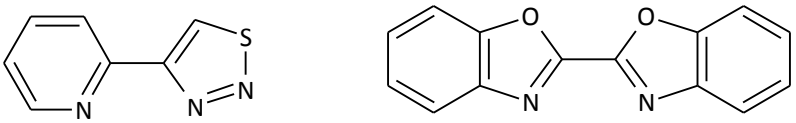

Fig 1.5 Examples of 1,2,3-thiadiazole and benzoxazole ligands.

The present work examines the properties of a series of systems containing a bridgehead nitrogen; that is, pyridine fused imidazoles and triazoles (Fig 1.6), and their nature as bidentate chelating ligands for ruthenium(II). There has been very little study carried out on these classes of ligands, and even less on their complexes, as will be described in subsequent chapters. This thesis examines a series of [1,2-a]- and [1,5-a]-imidazopyridines and [1,5-a] triazolopyridines, bound either to pyridine or to itself to form a bidentate ligand. Chapters 2 and 3 will examine the imidazoles, whilst Chapter 4 will examine the triazoles.

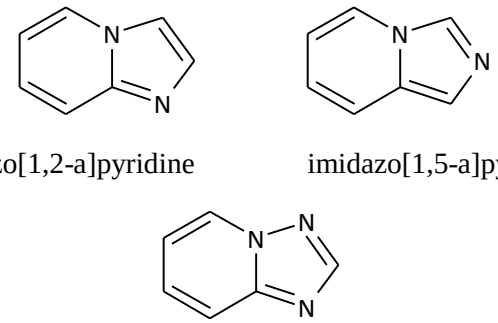

imidazo[1,2-a]pyridine imidazo[1,5-a]pyridine

triazolo[1,5-a]pyridine

Fig 1.6 Moieties examined in this work.

Limited data exist for ruthenium(II) complexes of related ligands (Fig 1.7); Pradhan and Das[24] examined a ruthenium(II) complex containing [3-(2-pyridyl)[1,2,4]triazolo[4,3-a]pyridine for use in organic bistable memory applications, while our own group has examined the [1,2,3]triazolo[1,5-a]pyridines, forming ruthenium(II) complexes with 3-(pyridin-2-yl)[1,2,3]triazolo[1,5-a]pyridine and 3,3'-bi[1,2,3]triazolo[1,5-a]pyridine.[25]

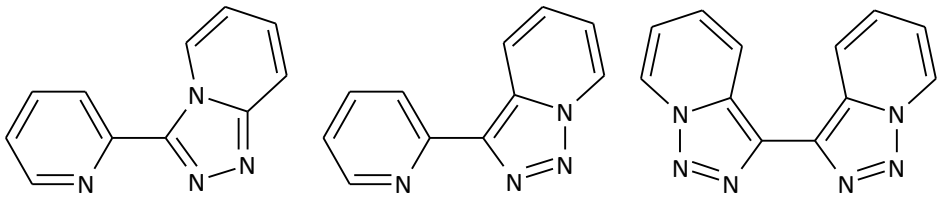

Fig 1.7 Related ligands with previously reported ruthenium complexes.

The numbering of these ring systems can be the source of confusion. The ring systems are named first (as in Fig 1.8), while a separate numbering system is used to label substituents on the ring. The [X,Y-z] label is determined by where the 5-membered ring is fused to pyridine. The letter z is dictated by which bond of pyridine the 5-membered ring is fused across (Fig 1.8a). The X and Y labels relate to which two atoms of the 5-membered ring are fused to the pyridine ring, and X is always the atom closest to the pyridyl nitrogen (or the nitrogen itself). As such, Fig 1.8b illustrates some imidazole and pyrazole based systems.

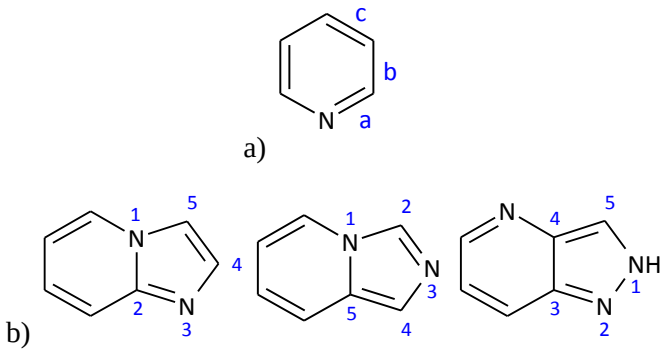

Fig 1.8 a) Labelling of the bonds of pyridine; b) example numbering of some fused systems ([1,2-a], [1,5-a] and [4,3-b]).

Numbering for substituents follows a separate system. For my fused systems, it is typical to label such that the pyridyl nitrogen is the fourth atom. Using the first two structures of Fig 1.8b as an example, atom 1 would be the atom labelled 3 and 4, respectively.

The ligands and complexes reported in this work were characterised by ^{1}H and ^{13}C NMR, with one- and two-dimensional correlation techniques carried out to assist in the assignment process. Assignment typically starts by recording the ^{1}H-^{1}H homonuclear correlation spectroscopy (COSY) spectrum. This two-dimensional technique identifies spins that are coupled to each other, and from this we can determine which peaks belong to discrete ring systems. However, when peaks are not well separated, assignment by COSY can become difficult. In these instances, one-dimensional total correlation spectroscopy (1-D TOCSY) can be used. By this method we irradiate a single, well separated proton resonance, and observe the transfer of magnetisation as it moves to the other protons in the same spin system. An example from complex **9** is shown in Fig 1.9, where the doublet at 8.16 ppm is initially irradiated. This can be seen to first transfer magnetisation to the triplet at 7.92 ppm, then to the triplet at 7.10 ppm, and finally to the doublet at 7.53 ppm. By Trace V, the magnetisation has started to transfer back to the triplet at 7.10 ppm, and with more readings would be seen to return to the initial proton. To assign the ^{13}C NMR spectrum, two-dimensional heteronuclear correlations are performed. Heteronuclear single-quantum correlation spectroscopy (HSQC) detects the correlation between a hydrogen and the atom one bond away (i.e. the carbon it is bound to). Heteronuclear multiple-bond correlation spectroscopy (HMBC) detects the correlation between a hydrogen and the atoms two-to-four bonds away. This method is useful for locating quaternary carbons, as without bonds to hydrogen these atoms are not detectable by HSQC analysis.

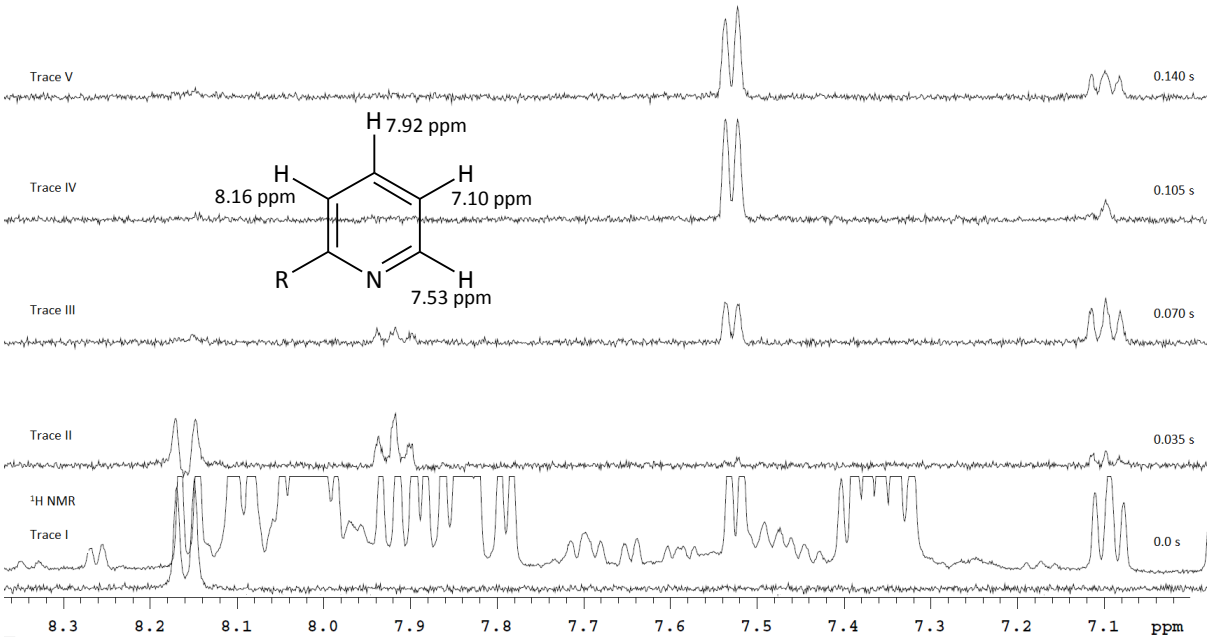

Fig 1.9 Example of a 1-D TOCSY, performed on complex **9** at 8.16 ppm.

Other analyses that will be used include mass spectroscopy, UV-Visible spectroscopy, cyclic voltammetry and X-ray diffraction.

The specific mass spectroscopy technique used here was electrospray ionisation (ESI), time-of-flight (TOF) mass spectroscopy (MS). ESI is known as a 'soft ionisation' technique, as it is able to produce ions with little in the way of fragmentation; this allows spectra to be more easily assigned. Ions are formed after the electrospray cone aerosolises the supporting liquid, when this volatile liquid evaporates. TOF is used to separate ions based on their mass-to charge ratio; as an ions relative velocity through an applied electric field is determined by this ratio, the time it takes for an ion to reach the detector can be used to calculate the relevant ratio.

UV-Vis spectroscopy examines a compounds ability to absorb light in the ultraviolet-visible region of the electromagnetic spectrum. Light can promote an electron from the highest occupied molecular orbital (HOMO) to the lowest unoccupied molecular orbital (LUMO), and for ruthenium(II) complexes, absorption in the visible region generally occurs between a π bonding orbital (or an *n* non-bonding orbital) and a π^* anti-bonding orbital. As the wavelength of light is inversely proportional to its energy, a compound that absorbs at a

longer wavelength requires less energy to promote this electron (i.e. it has a smaller HOMO-LUMO energy gap).

Cyclic voltammetry is used to examine the redox potentials and electrochemical reactions of a compound. By sweeping an applied potential, we can measure the resulting current and plot the results as a compound is oxidised or reduced. The current reaches a maximum as the potential approaches the redox potential of the analyte, and drops away as the concentration of the analyte remaining at the surface of the electrode decreases. Reversible redox couples can be observed when the potential is reversed; where the previously oxidised analyte is reduced, with the current of reverse polarity producing a peak with a similar shape to the forward scan.

X-Ray diffraction is a crystallography technique whereby a single crystal is subjected to an X-ray beam. The resulting diffraction pattern contains a number of regularly spaced spots (or reflections), and a number of these patterns are recorded as the crystal is rotated in the source. We can subsequently build these patterns into a 3-D model, and the appropriate mathematical solutions can transform this into a 3-D electron density map. Using the relative intensities and our chemical knowledge of the sample crystal, these electron densities can be rationalised to individual atoms, and further into complete crystal structures. In this work we obtained crystal structures for six of the reported complexes.

Chapter 2

Imidazo[1,2-a]pyridines

2.1 Introduction

In this chapter we examine a pair of imidazo[1,2-a]pyridine based heterocyclic ligands and their ruthenium complexes. The heterocyclic ring system and ring numbering are shown in Figure 2.1.

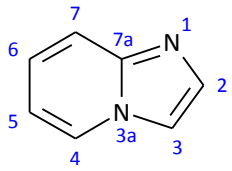

Fig 2.1

The compounds are, specifically, 2-(pyridin-2-yl)imidazo[1,2-a]pyridine (**1**) and 2,2'-biimidazo[1,2-a]pyridine (**2**) (Fig 2.2).

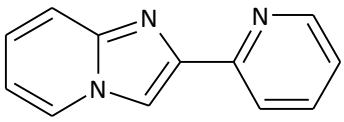

1

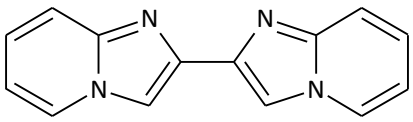

2

Fig 2.2

The parent imidazo[1,2-a]pyridine was first synthesised in 1925 by Tschitschibabin (Chichibabin),[26] who used high temperatures (150-200°C) and a sealed tube to react 2-aminopyridine with bromoacetaldehyde. A simpler method of synthesis was described by Mosby in 1961;[27] it had been determined that heat was not necessary, and that chloro- or bromoacetaldehyde would react with 2-aminopyridine simply in the presence of sodium bicarbonate and alcohol solution. Over the years numerous other methods of synthesising

imidazo[1,2-a]pyridine and substituted derivatives have been examined, in an effort to attain a wider range of useable substituents with increased efficiency. Roe[28] examined the reaction between imidazole and diketones, as well as a modified Tschitschibabin method using dioxane as the solvent. This modified method has been further adapted by other groups condensing 2-aminopyridines with α-halocarbonyls.[29] Due to the limited number of α-halocarbonyls available, a number of one-pot reactions have been developed in an effort to synthesise a wider array of derivatives. Investigated one-pot reactions include the reaction between aldehydes, isocyanides, and 2-aminopyridines,[30] and metal catalysed three component coupling reactions between aldehydes, alkynes and 2-aminopyridines; transition metal salts containing copper[31-33] are the most commonly used, however studies with other metals such as silver[33] and indium[34] have also been reported.

The importance of determining effective methods of synthesising substituted imidazo[1,2-a] pyridines is linked to their biological activity. This fused heterocycle can be found within a number of pharmacologically important structures, which exhibit a range of properties. These include antiviral,[35,36] antibacterial, anti-inflammatory,[37] and antiulcer actions, among others. This ring system is present in a number of commercial drugs, such as alpidem[32,38] (anxiolytic), zolpidem[39] (sedative), olprinone[40] (cardiotonic agent), minodronic acid (osteoporosis), zolimidine[41] (antiulcer), saripidem and necopidem (sedative/anxiolytic).

Despite the parent imidazo[1,2-a]pyridine unit having been first synthesised nearly a century ago, the ligands examined herein have been curiously ignored. Using SciFinder® to examine the literature, a search for compound **1** returns a total of three results; two papers, by Cyrański *et al*.[42] and Chandra Mohan *et al.*,[43] and a patent from Aries.[44] A literature search for compound **2** yielded even fewer results, with this compound yet to be reported in any form. Because the few publications of these compounds focus solely on their synthesis, the complexation of these ligands has yet to be examined with any transition metals.

Cyrański *et al*.[42] examined a new synthesis of 2-substituted imidazo[1,2-a]pyridines based on a two-step reaction; an Ortoleva-King reaction, followed by cyclisation of the resulting pyridinium salt by base (Scheme 2.1). Ortoleva[45] and King[46] found that pyridinium salts could be formed by heating active methyl compounds in the presence of iodine and pyridine.

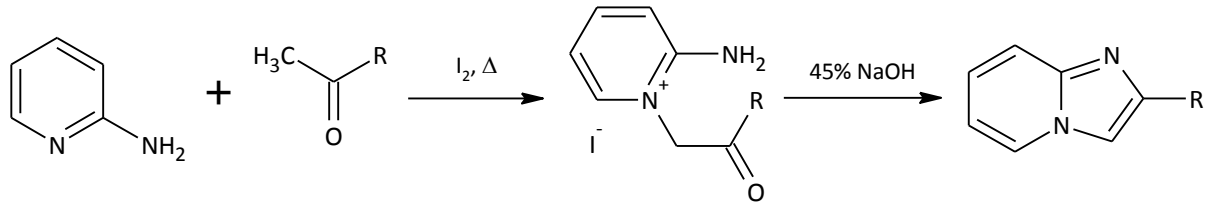

Scheme 2.1 An Ortoleva-King reaction, followed by cyclisation in base.

Cyclisation of the pyridinium salt would occur quickly under basic conditions, and the resulting 2-imidazo[1,2-a]pyridine could be obtained in reasonable yield (~50%) with a variety of different R groups, depending on the methyl ketone used.

Chandra Mohan *et al.*[43] examined another new synthetic method, again reacting methyl ketones with 2-aminopyridine. In this work, instead of pre-activating the ketone with iodine, CuI/$BF_3 \cdot Et_2O$ was used as a catalyst, with O_2 as an oxidant. This method allowed them to synthesise a range of substituted imidazo[1,2-a]pyridines, in good yields. As an interesting aside, they successfully synthesised zolimidine; achieving in a single step what typically requires multiple steps. The proposed mechanism of this reaction, shown in Scheme 2.2, sees the 2-aminopyridine form an imine/enamine with the methyl ketone, before oxidative addition of CuI with O_2 forms a Cu(III) complex. Reductive elimination regenerates the catalyst while closing the ring system.

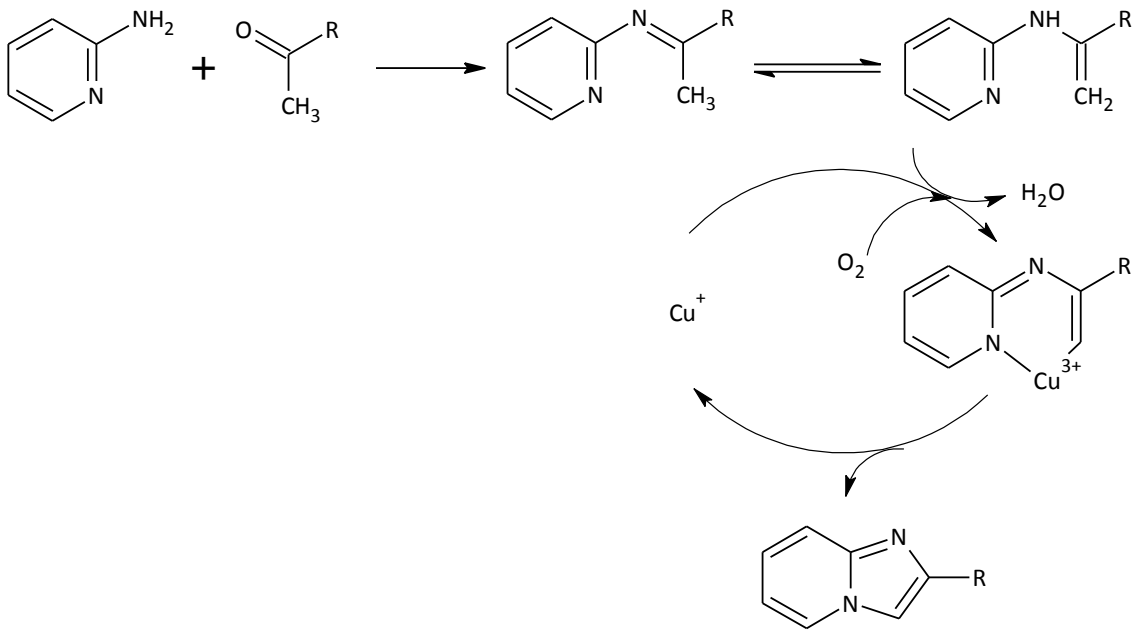

Scheme 2.2 Proposed mechanism for Cu(I) catalysed synthesis of imidazo[1,2-a]pyridines.[43]

The following sections will examine the synthesis of compounds **1** (synthesised via a literature procedure) and **2** (reaction of 1,4-dibromo-2,3-butanedione with 2-aminopyridine), and their subsequent complexation with bis(2,2'-bipyridine)ruthenium(II) dichloride to form complexes **3** and **4,** respectively. The ligands were analysed by ^{1}H and ^{13}C NMR, while the complexes were additionally examined by UV-visible spectroscopy, cyclic voltammetry and, where possible, crystal structures were obtained by X-ray diffraction.

2.2 Synthesis of Ligands

Following the method detailed by Cyrański *et al.*[42] 2-(pyridin-2-yl)imidazo[1,2-a]pyridine (**1**) was synthesised (Scheme 2.3), and its presence was confirmed by ^{1}H NMR. However, this spectrum also showed the presence of excess 2-aminopyridine. Separation of the product from the 2-aminopyridine proved problematic, with both eluting at a similar rate when subjected to column chromatography. A stock of **1** synthesised by a previous member of our group, Dr Chris Richardson, was used for the subsequent complex synthesis and analysis.

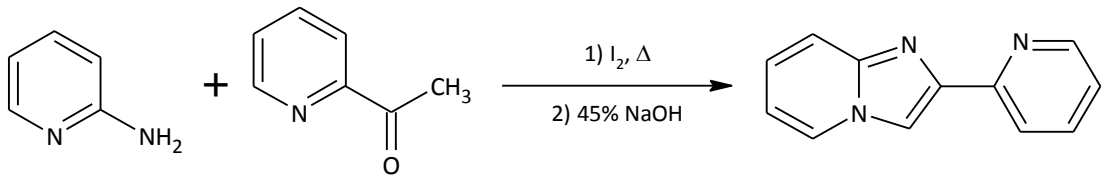

Scheme 2.3 Synthesis of 2-(pyridin-2-yl)imidazo[1,2-a]pyridine (**1**).

2,2'-Biimidazo[1,2-a]pyridine (**2**) was synthesised via the cyclocondensation of 2-aminopyridine with 1,4-dibromo-2,3-butanedione, as shown in Scheme 2.4. However, as with **1**, separating the product from the excess 2-aminopyridine proved difficult, and as such very low yields were obtained.

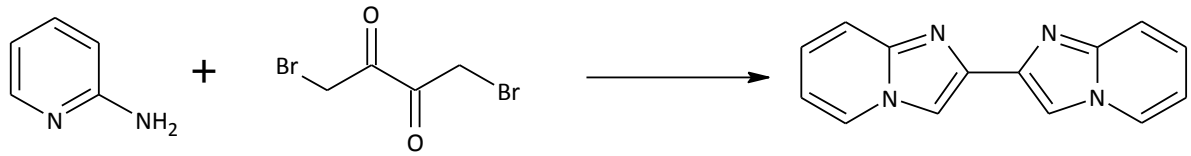

Scheme 2.4 Synthesis of 2,2'-biimidazo[1,2-a]pyridine (**2**).

Other attempts at synthesising this compound involved adding sodium bicarbonate and heat to the reaction, however this did not produce any noticeable improvements; problematic purification still led to low yields.

The ^{1}H- and ^{13}C NMR spectra of ligands **1** and **2** were recorded in deuterated chloroform, with additional ^{1}H NMR measurements recorded in deuterated acetonitrile to allow Coordination Induced Shift (CIS) analysis. Full proton and carbon assignments, made by a combination of 2-D experiments (COSY, HSQC, HMBC), can be found in the Experimental section (Chapter 6).

2.3 Synthesis and Characterisation of Complexes

2.3.1 Synthesis of Bis(2,2'-bipyridine)[2-(pyridin-2-yl)imidazo[1,2-a]pyridine]ruthenium(II) bis(hexafluorophosphate) (3)

Ligand **1** was reacted with bis(2,2'-bipyridine)ruthenium(II) dichloride, $[Ru(bpy)_2Cl_2]$, in a 1:1 ratio. The reactants were added to a 3:1 mixture of ethanol:water, and heated with stirring at reflux overnight. After workup, the product $[Ru(bpy)_2(\mathbf{1})](PF_6)_2$, (**3**), was obtained in excellent yield (95%) (Fig 2.3).

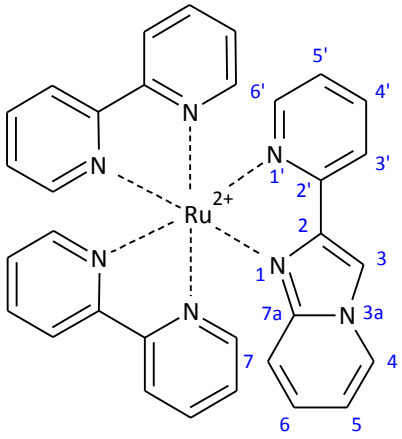

Fig 2.3 Structure of the cation of complex **3.**

Complex **3** contains 25 aromatic protons; 16 from the ancillary bpy ligands, and 9 from ligand **1**. The ^{1}H NMR spectrum of the product displayed the expected 25 proton signals. The chemical shifts and Coordination Induced Shifts (CIS) for **1** and **3** are shown in Table 2.1. The ^{1}H NMR spectrum of **3** is shown in Figure 2.4.

Table 2.1 ^{1}H NMR Chemical Shifts[a] and Coordination Induced Shifts[b] of the coordinated imidazo[1,2-a]pyridine rings of **3** and the chemical shifts of **1**.

	H3	H4	H5	H6	H7	H3'	H4'	H5'	H6'
3	8.65	8.43	7.00	7.11	5.59	8.23	7.95	7.25	7.55
1	8.30	8.34	6.85	7.24	7.54	8.15	7.82	7.27	8.58
CIS	+0.15	+0.09	+0.15	-0.13	-1.95	+0.08	+0.13	-0.02	-1.03

[a] Solvent: deuterated acetonitrile (MeCN-*d3*). [b] CIS = ($\delta_{complex}$ - δ_{ligand}).

The proton with the chemical shift of 5.59 ppm is assigned to H7 of the ligand. The large upfield shift (CIS -1.95 ppm) is due to heavy shielding, caused by the ring-current anisotropy of the nearby pyridine ring. A combination of 2-D COSY and HMBC experiments was used to assign the rest of the ligand and the bpy protons. While it was possible to distinguish each of the ring systems with a COSY, this type of analysis does not allow us to determine which pyridine ring of bpy is *cis*, and which is *trans* to the ligand. The pyridine ring of the ligand is easy to determine, as its protons experience significant shifts relative to those of the bpy pyridines. The proton signals for 2-substituted pyridine rings could be expected to occur at similar positions. In **3**, as each pyridine ring does not exist in an identical environment, the related protons will experience a small shift relative to each other. The resulting multiplet clusters occur at characteristic shifts, and are consistent across the range of ruthenium complexes examined in this work. There is a slight exception when examining H6 protons. Like the H7 proton of the ligand, these protons experience anisotropic shielding of varying magnitudes, depending on the other ligands present. One pyridine H6 appears to shift much further than the others; this can be assigned to the H6' proton of the ligand, as being part of **1** will position it closer to neighbouring pyridine rings than if it were part of a bipyridine. This closer proximity was confirmed by X-ray diffraction analysis.

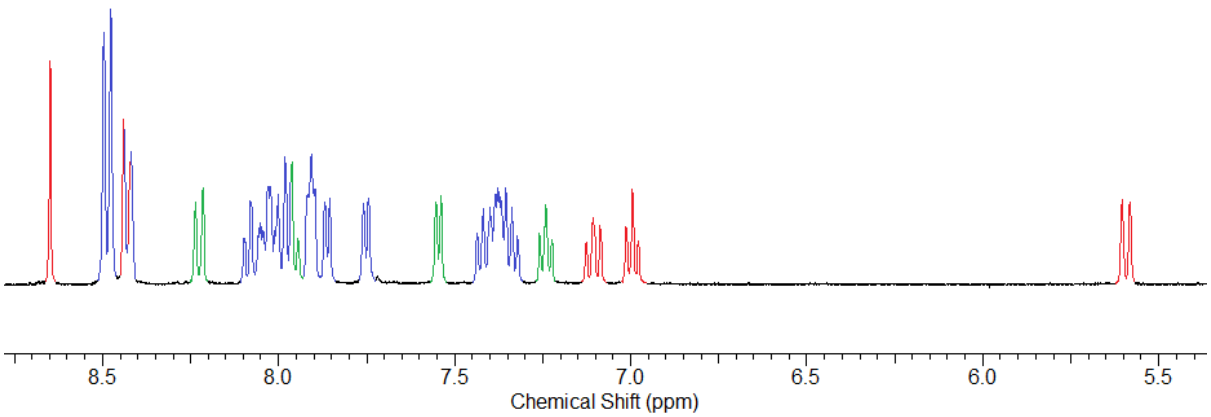

Fig 2.4 ^{1}H NMR spectrum of $[Ru(bpy)_2(\mathbf{1})]^{2+}$, (**3**), in MeCN-*d3*. Red = **1** (H4-H7), Green = **1** (H3'-H6'), Blue = 2,2'-bipyridine.

The UV-visible spectrum for complex **3** shows a λ_{max} at 463 nm (Fig 2.5, Table 2.2). This metal-to-ligand charge-transfer (MLCT) band is at a longer wavelength (and thus a lower energy) than $[Ru(bpy)_3]^{2+}$ (452 nm), and it corresponds to the (M)d-(L)π* transition. The shoulder at 427 nm can likely be assigned to the (M)d-(bpy)π* transition, while the transitions at <326 nm are ligand centred. As the energy of MLCT bands have been shown to

indicate the relative size of the HOMO-LUMO energy gap,[11] we can conclude that this gap is smaller in **3** than in $[Ru(bpy)_3]^{2+}$; **3** will be easier to excite than $[Ru(bpy)_3]^{2+}$ as a result. However, while easier to excite, a smaller molar absorption coefficient indicates that this complex does not absorb light as strongly as $[Ru(bpy)_3]^{2+}$. We can predict that the $\Delta E_{ox\text{-}red1}$ value for **3**, obtained through electrochemical techniques, will be smaller than that of $[Ru(bpy)_3]^{2+}$, as the same molecular orbitals are involved ((M)d-(L)π*).

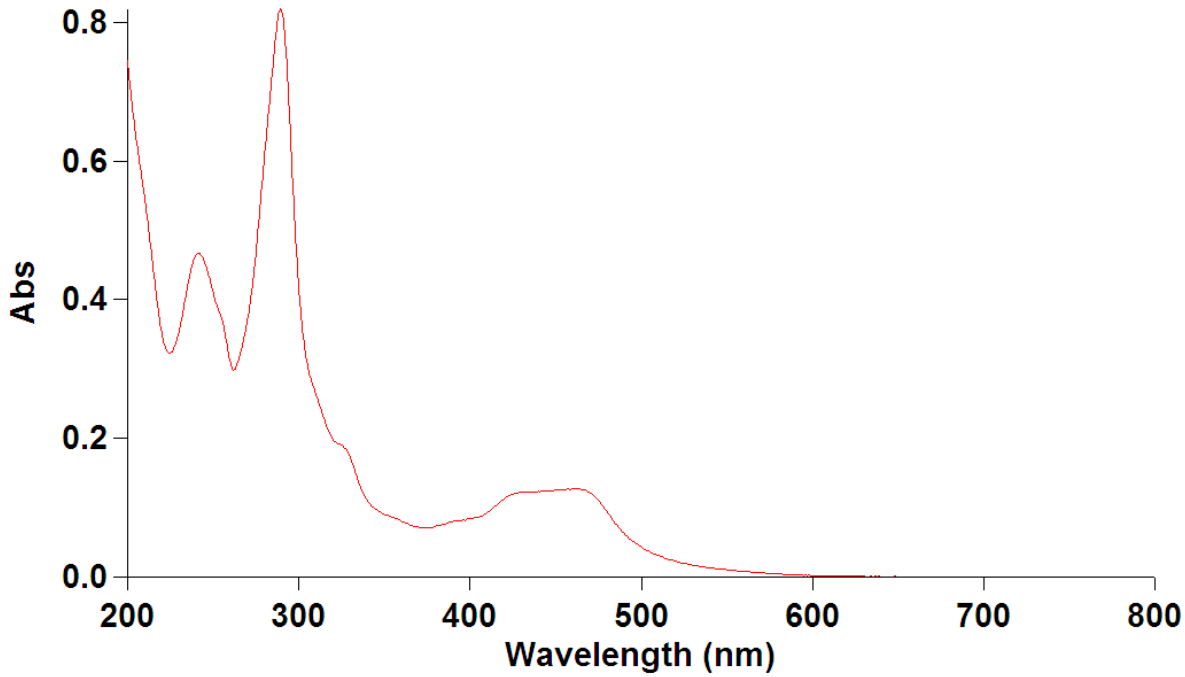

Fig 2.5 UV-Vis spectrum of $[Ru(bpy)_2(\mathbf{1})]^{2+}$, (**3**).

Table 2.2 Absorption Maxima[a] with Molar Absorption Coefficients[b] and Redox Potentials[c] of complex **3**.

Complex	λ_{max} (ε)	E_{ox}	E_{red1}	E_{red2}	E_{red3}	$\Delta E_{ox\text{-}red1}$
$[Ru(bpy)_3]^{2+}$	452 (13600)	+1.26	-1.33	-1.51	-1.79	2.59
3	463 (8000)	+0.99(78)	-1.47(81)	-1.69(83)	-	2.46

[a] In nanometres. [b] $M^{-1}cm^{-1}$. [c] In volts vs SCE.

The cyclic voltammogram (CV) of complex **3** (Fig 2.6) shows a reversible oxidation at +0.99 V, and two reversible reductions (Table 2.2). Complex **3** is easier to oxidise than $[Ru(bpy)_3]^{2+}$ (+1.26 V), while it is noticeably harder to reduce; only two of three potential ligand based reduction peaks occurred within the solvent limit. Additionally, as these reductions are in agreement with the second and third reductions found in $[Ru(bpy)_3]^{2+}$, this indicates that if reduction of the coordinated **1** occurs, it must be past the solvent limit. With oxidation

occurring at the metal centre, the decrease in oxidation potential between $[Ru(bpy)_3]^{2+}$ and **3** indicates that the ruthenium atom in **3** is more electron rich than $[Ru(bpy)_3]^{2+}$. Likewise, the fact that **3** is harder to reduce than $[Ru(bpy)_3]^{2+}$ indicates that **1** is a more electron rich ligand than bipyridine. Both of these features likely result from the π-excessive nature of the fused azole in **1** (compared with the π-deficient nature of bipyridine).[5] As predicted, the $\Delta E_{ox\text{-}red1}$ value of **3** is smaller than that of $[Ru(bpy)_3]^{2+}$, which further points towards a lower energy gap.

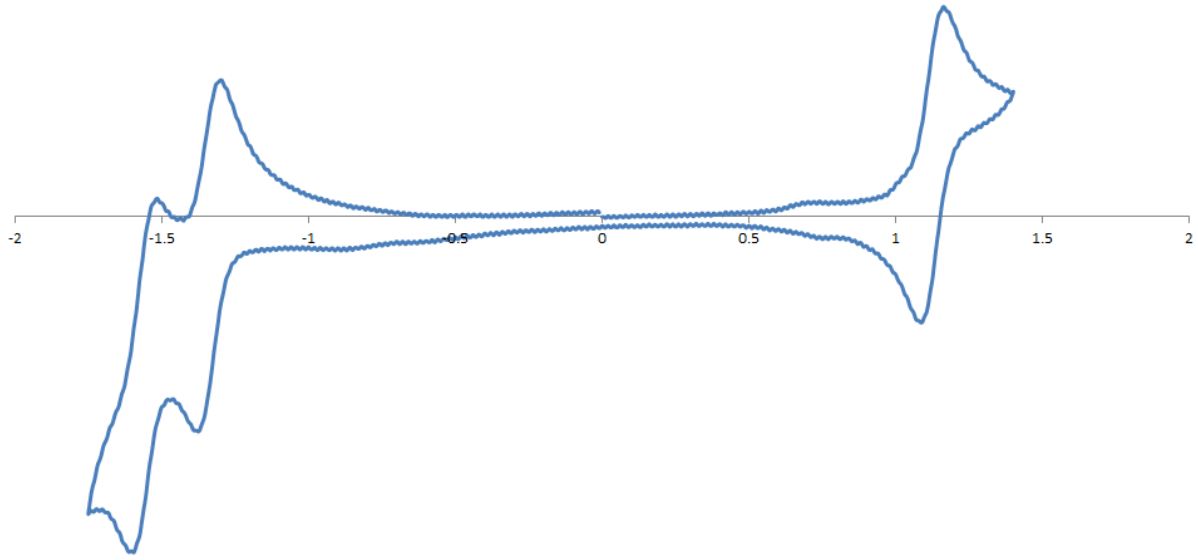

Fig 2.6 Cyclic Voltammogram of $[Ru(bpy)_2(\mathbf{1})]^{2+}$, (**3**), in volts vs silver wire.

Crystals of complex **3** were grown by slow diffusion of petroleum ether into a solution of acetone containing the complex. X-Ray diffraction analysis was carried out on one of these crystals, and the resulting structure solved in the monoclinic space group C2/c. The asymmetric unit contains one full cation, two hexafluorophosphate counteranions and one and a half acetone solvate molecules. Twinning has led to disorder within this structure, with the ruthenium atom located in two locations in a 2:1 ratio, and an acetone solvent molecule being rotationally disordered. Although the ruthenium atom of the twinned structure is a major peak, those of its coordinated ligands are much weaker, to a degree that makes modelling this twin unfeasible. Figure 2.7 presents a perspective view of the complex cation, with solvent molecules, counteranions, and the minor ruthenium atom Ru1A omitted for clarity.

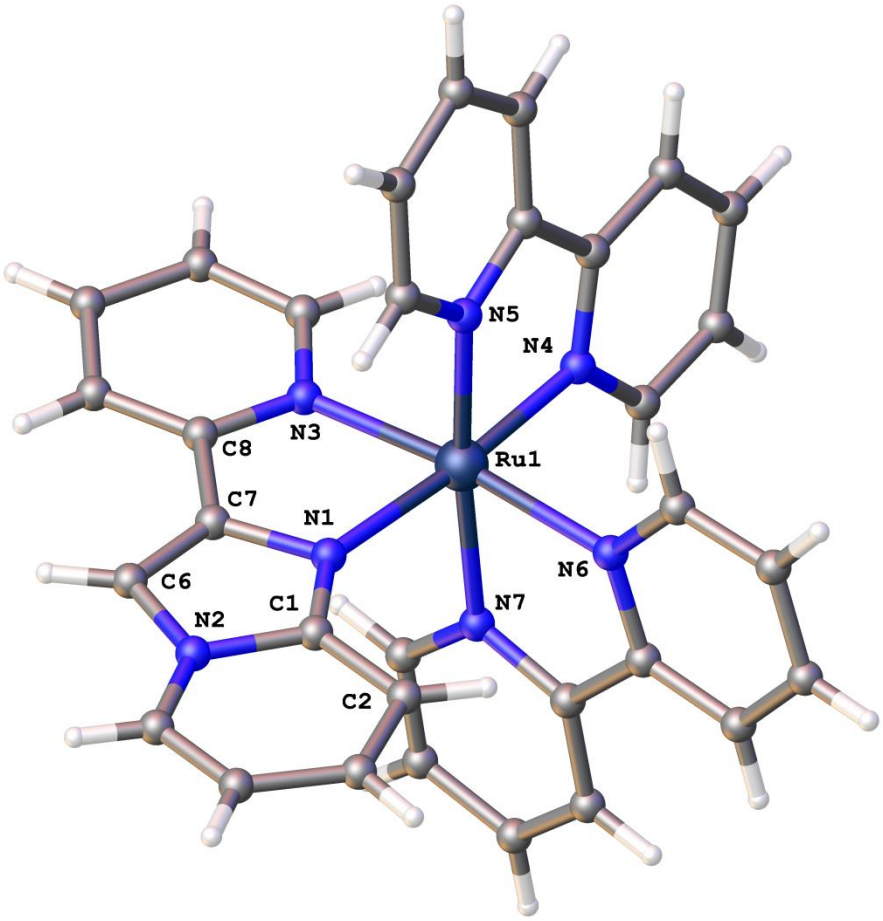

Fig 2.7 Perspective view of complex **3** cation, with partial labelling. Selected bond lengths (Å) and angles (°): Ru1-N1 2.123(7), Ru1-N3 2.083(6), Ru1-N4 1.970(6), Ru1-N5 2.043(5), Ru1-N6 2.118(6), Ru1-N7 2.086(5), N1-Ru1-N3 78.9(3), N4-Ru1-N5 80.8(2), N6-Ru1-N7 76.5(2), N1-C1 1.289(9), N1-C7 1.402(8), N2-C1 1.406(8), N2-C6 1.388(12), C6-C7 1.373(11), N1-C1-N2 111.8(8), N1-C7-C6 108.6(8), N2-C6-C7 107.3(7), C1-N1-C7 107.1(6), C1-N2-C6 105.3(6).

While including the second ruthenium centre in the solved structure greatly improves the R-factor (7.35% vs 12.44%), it has the effect of pushing the main atom slightly off centre. This leads to a slight skewing of bond lengths and angles between the ligands and the ruthenium centre. While this skewing is not obvious in the data between **1** and ruthenium (being a newly complexed ligand), the data for bpy is slightly more telling; these angles and bond lengths are fairly consistent across a range of complexes, as can be seen in the literature[47] and later on in this work, and the range of values reported here indicate a clear discrepancy.

The data relating the minor ruthenium atom Ru1A to the ligands often varies wildly each side of the expected values, and as such will not be examined here. This data, along with the

remaining distances and angles, is available from the Department of Chemistry, University of Canterbury.

The bond length from ruthenium (Ru1) to the imidazo[1,2-a]pyridine nitrogen of **1** (N1) is 2.123(7) Å, and to the pyridine nitrogen (N3) is 2.083(6) Å. Ruthenium-to-bipyridine bond lengths are typically fairly consistent; for example, Rillema *et al.*[47] reported an average Ru-N bond length of 2.056(6) Å for $[Ru(bpy)_3]^{2+}$, while Steel *et al.* reported ranges of 2.051(3)-2.061(3) Å and 2.048(3)-2.058(3) for the $[Ru(bpy)_2(L)]^{2+}$ complexes of 2-(2-pyridyl)benzoxazole[23] and 3-(2-pyridyl)[1,2,3]triazolo[1,5-a]pyridine,[25] respectively.

The bond lengths reported for **1** are thus longer than those expected of bipyridine, and this agrees with previously examined data. From the UV-vis and cyclic voltammetry data, we know that **1** is overall more electron rich than bipyridine, and as such does not experience the same level of stabilisation through back bonding as bpy. This, along with a greater steric bulk, would naturally lead to longer Ru-N bond lengths compared to bpy. Within **1**, the imidazopyridine system is π-excessive, while the pyridine system is π-deficient; back bonding from the metal d-orbitals to the pyridines π-system results in the shorter length for Ru1-N3. The bite angle for N1-Ru1-N3, [78.9(3)°], is in agreement with related complexes. Both these bond lengths and angles are in reasonable agreement with those of the related complex **4**, discussed later in this chapter.

While the data regarding Ru1-**1** conforms to predicted values, the data for Ru1-bpy is a little more variable. As previously discussed, the average Ru-bpy bond length tends to be around 2.05 Å. The bipyridine ligand containing nitrogens N4 and N5 is located the closest to Ru1, with bond lengths of 1.970(6) Å and 2.043(5) Å, respectively; compare this to the N6/N7 bipyridine, with bond lengths of 2.118(6) Å and 2.086(5) Å, respectively. This mixture of bipyridine ligands being closer and further away from the central ruthenium adds credence to the assumption that the major ruthenium atom in this solution is located slightly off centre. Interestingly, the average of these bond lengths is 2.054 Å. Bond lengths are not the only values that lie either side of the predicted values, with the bipyridine bite angles shifting in accordance with the bonds (N4/N5 80.8(2)° and N6/N7 76.5(2)°), either side of the bite angle in $[Ru(bpy)_3]^{2+}$ of 78.7°.

When examining the ^{1}H NMR of complex **3**, the large upfield shift of the H7 proton was proposed to be due to ring-current anisotropic shielding of this proton by the pyridine ring that it points into. This can be seen in the crystal structure in Figure 2.7, with the proton of C2 pointing towards the N6 containing ring. It is possible to approximate the distance from this proton to the centre of the pyridine ring (the position of hydrogens cannot be obtained from X-ray diffractometry, and are typically set to a fixed position in structural refinement), and from this we can get an indication of the relative distances involved. To emphasise the inherent inaccuracy of these calculations, values have been rounded to one decimal place. The distance between H7 and the N6 pyridine ring is calculated at *ca.* 2.9 Å. The H6'-N4 ring distance is *ca.* 3.1 Å, while the bpy H6 distances are as follows: to N3 *ca.* 3.3 Å, to N5 *ca.* 3.4 Å, and to N7 *ca.* 3.2 Å. The distance from a bpy H6 to the fused pyridine of the ligand is the longest calculated, at a distance of *ca.* 4.0 Å. As this illustrates, H7 is predicted to be closest to the neighbouring pyridine ring, explaining the large upfield shift of H7. H6' is predicted to be closer than the bpy H6 protons, explaining its larger upfield shift compared to these similar protons.

2.3.2 Synthesis of Bis(2,2'-bipyridine)[2,2'-biimidazo[1,2-a]pyridine]ruthenium(II) bis(hexafluorophosphate) (4)

Ligand **2** was reacted with bis(2,2'-bipyridine)ruthenium(II) dichloride, $[Ru(bpy)_2Cl_2]$, in a 1:1 ratio. The reactants were added to a small volume of ethylene glycol and irradiated in a microwave at 450 W; the reaction was monitored by thin-layer-chromatography (TLC) at 2 minute intervals, for a total reaction time of 6 minutes. After precipitating the PF_6^- salt (addition of aqueous KPF_6), the product $[Ru(bpy)_2(\mathbf{2})](PF_6)_2$, (**4**), was recrystallised by the addition of excess diethyl ether to the precipitate dissolved in the minimum amount of acetonitrile, in moderate yield (66%) (Fig 2.8).

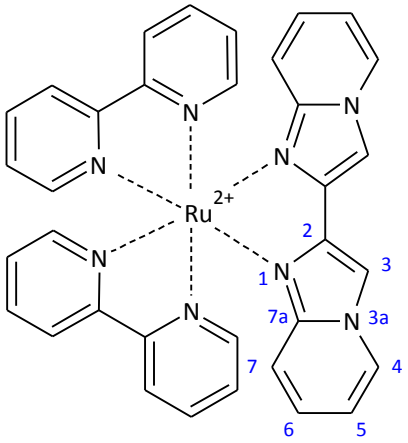

Fig 2.8 Structure of the cation of complex **4** .

Complex **4** contains a total of 26 aromatic protons. A total of 13 signals were seen in the ^{1}H NMR spectrum, arising from the fact that **4** contains a two-fold rotational axis of symmetry. The chemical shifts and CIS values for **2** and **4** are shown in Table 2.3, and the ^{1}H NMR spectrum of **4** is shown in Figure 2.9.

Table 2.3 ^{1}H NMR Chemical Shifts[a] and Coordination Induced Shifts[b] of the coordinated imidazo[1,2-a]pyridine rings of **4** and the chemical shifts of **2**.

	H3	H4	H5	H6	H7
4	8.43	8.42	6.95	7.06	5.48
2	8.15	8.33	6.83	7.22	7.51
CIS	+0.28	+0.09	+0.12	-0.16	-2.03

[a] Solvent: deuterated acetonitrile (MeCN-*d3*). [b] CIS = ($\delta_{complex}$ - δ_{ligand}).

As could be expected, the ^{1}H NMR spectrum of **4** shares similarities to that of **3**. The H7 proton experienced a larger shift than in **3**, which indicates this proton is located closer to the neighbouring pyridine ring (closer proximity leads to greater anisotropic shielding). A 2-D COSY helped to assign the rest of the ligand and bpy protons.

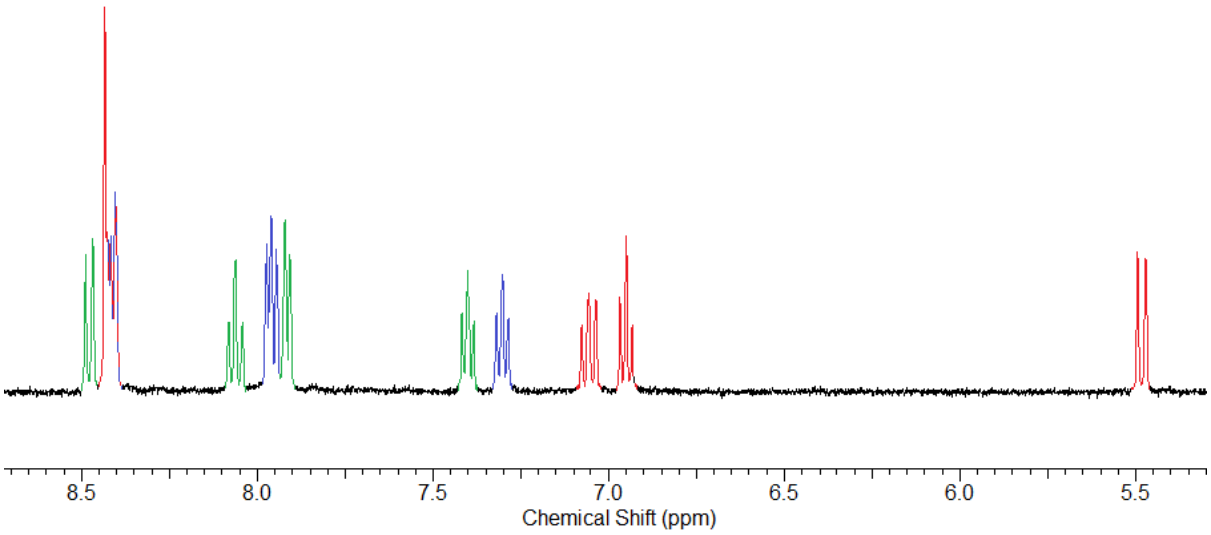

Fig 2.9 ^{1}H NMR spectrum of $[Ru(bpy)_2(\mathbf{2})]^{2+}$, (**4**), in MeCN-*d3*. Red = **2**, Blue/Green = bpy.

The (M)d-(L)π* absorption band of complex **4** has shown a significant increase in wavelength, with a λ_{max} of 480 nm (Fig 2.10, Table 2.4). This is almost 30 nm longer than that of $[Ru(bpy)_3]^{2+}$, and 20 nm longer than complex **3**. As will be seen in later chapters, this is the longest wavelength for the (M)d-(L)π* absorption band reported in this work, and indicates that **4** has the lowest HOMO-LUMO energy gap of all the complexes examined. By substituting the pyridine ring containing ligand **1** with the double imidazo[1,2-a]pyridine ligand **2**, we have significantly reduced the energy required to promote the complex from its ground state to its excited state. We have also reduced the molar absorption coefficient compared to $[Ru(bpy)_3]^{2+}$, meaning that while easier to excite, complex **4** does not absorb light as strongly.

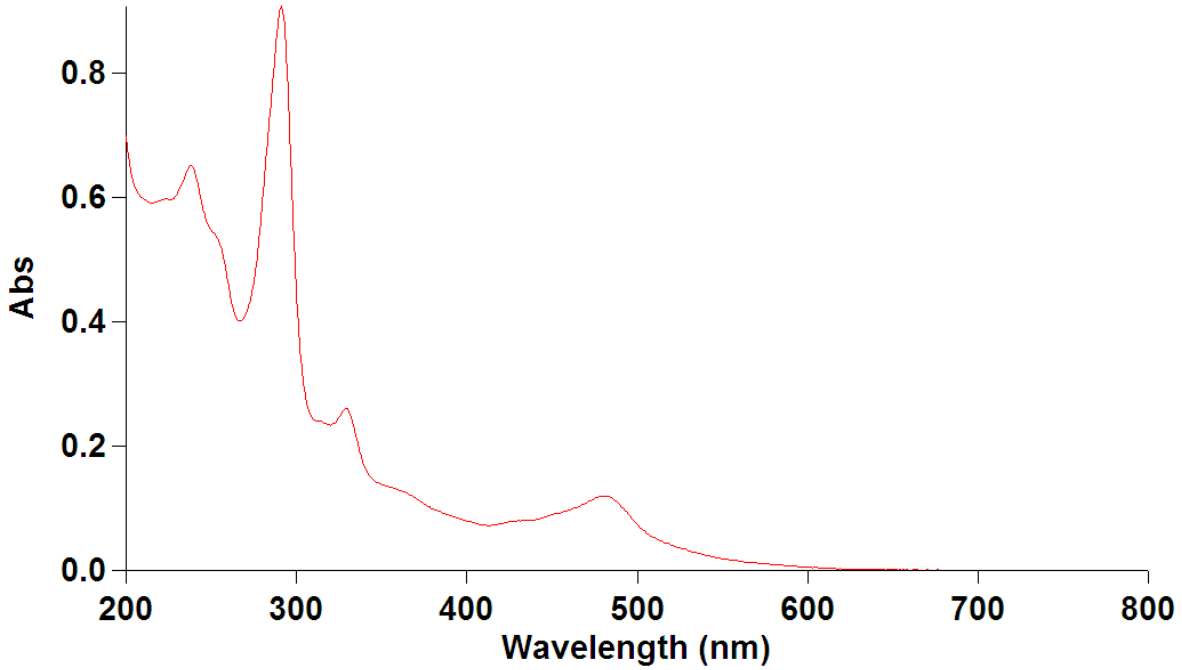

Fig 2.10 UV-Vis spectrum of $[Ru(bpy)_2(\mathbf{2})]^{2+}$, (**4**).

Table 2.4 Absorption Maxima[a] with Molar Absorption Coefficients[b] and Redox Potentials[c] of complex **4.**

Complex	λ_{max} (ε)	E_{ox}	E_{red1}	E_{red2}	E_{red3}	$\Delta E_{ox\text{-}red1}$
$[Ru(bpy)_3]^{2+}$	452 (13600)	+1.26	-1.33	-1.51	-1.79	2.59
4	480 (8100)	+0.89(80)	-1.50(70)	-1.74(85)	-	2.39

[a] In nanometres. [b] $M^{-1}cm^{-1}$. [c] In volts vs SCE.

The cyclic voltammogram of complex **4** (Fig 2.11) shows a reversible oxidation at +0.89 V, and two reversible reductions (Table 2.4). Complex **4** is slightly easier to oxidise than **3** (+0.99 V), and is likewise harder to reduce. As was seen in the voltammogram of **3**, the reduction peaks observed are in agreement with those of $[Ru(bpy)_3]^{2+}$, leading to the conclusion that the reduction of coordinated **2** occurs beyond the solvent limit. By replacing the π-deficient pyridine found in **1** with an additional π-excessive imidazo[1,2-a]pyridine, coordination with **2** has further increased the electron density found on the ruthenium atom and on the ligand.

When comparing $[Ru(bpy)_3]^{2+}$ and **3**, we have replaced one π-deficient pyridine ring with a π-excessive imidazo[1,2-a]pyridine system. This has the effect of increasing the electron density found on the ligand π-system, reducing the back bonding ability of the ligand, and thus increasing the electron density on the metal. Complex **4** contains two π-excessive

imidazo[1,2-a]pyridine systems, which further reduces back bonding and increases electron density.

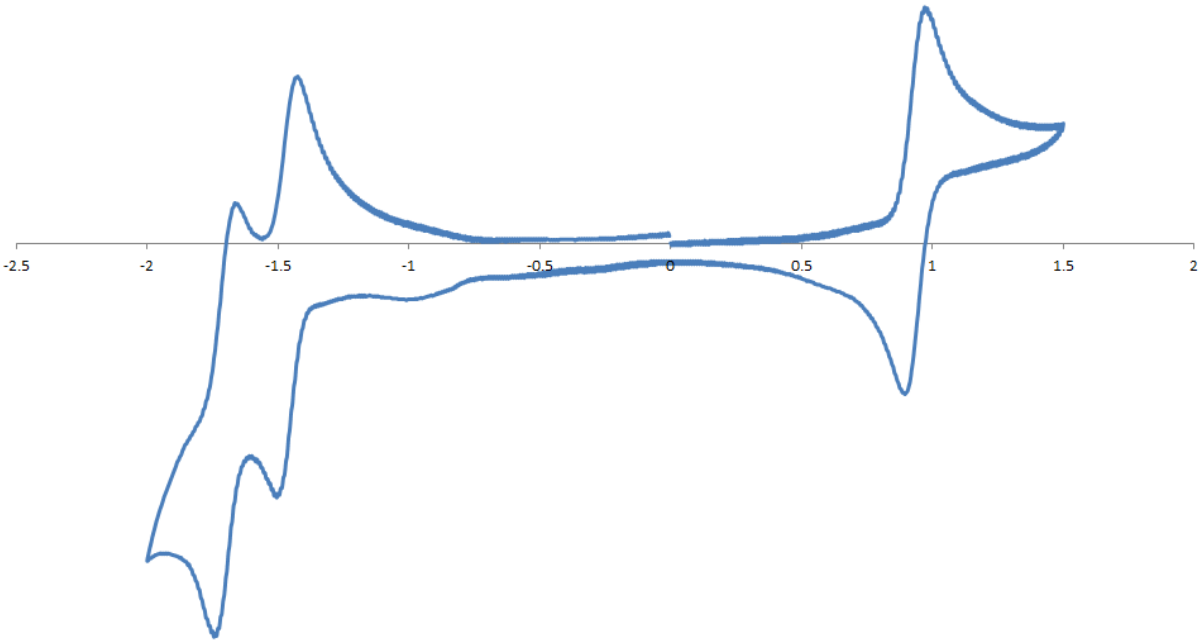

Fig 2.11 Cyclic Voltammogram of $[Ru(bpy)_2(\mathbf{2})]^{2+}$, (**4**), in volts vs silver wire.

Crystals of complex **4** were grown by the slow diffusion of petroleum ether into a solution of the complex in acetone. One of the needle-like crystals formed was used for X-ray diffraction analysis. Solving in the monoclinic space group C2/c, the asymmetric unit of **4** contains a full cation, two hexafluorophosphate counteranions and one and a half acetone solvate molecules. Figure 2.12 shows a perspective view of the cation, with the counteranions and solvent molecules omitted for clarity.

Unlike **3**, the only disorder present here is solvent based, with the complete acetone molecule showing signs of disorder. The Ru-N bond lengths of the coordinating nitrogens of **2** [N1 2.100(3) Å and N3 2.115(3) Å] are slightly longer than those of the bpy ligands [2.038(3) Å to 2.062(3) Å], and indicate that that **2** is a poorer electron donor than bipyridine.[48] The bite angle of **2** is 77.834(11)°, compared with those of bpy [78.512(13)° and 78.963(11)°]. For both bond lengths and bite angles, the results are comparable to those of the structurally similar 2,2'-bibenzoxazole complex [Ru-L 2.104(5), 2.116(5) Å, 77.6(2)°; Ru-bpy 2.032(5)-2.091(5) Å, 78.5(2)-78.6(2)°],[23] and the results for bpy are in agreement with those previously reported for $[Ru(bpy)_3]^{2+}$ in the literature [2.056(6) Å, 78.7(2)°, 79.4(2)°].[47]

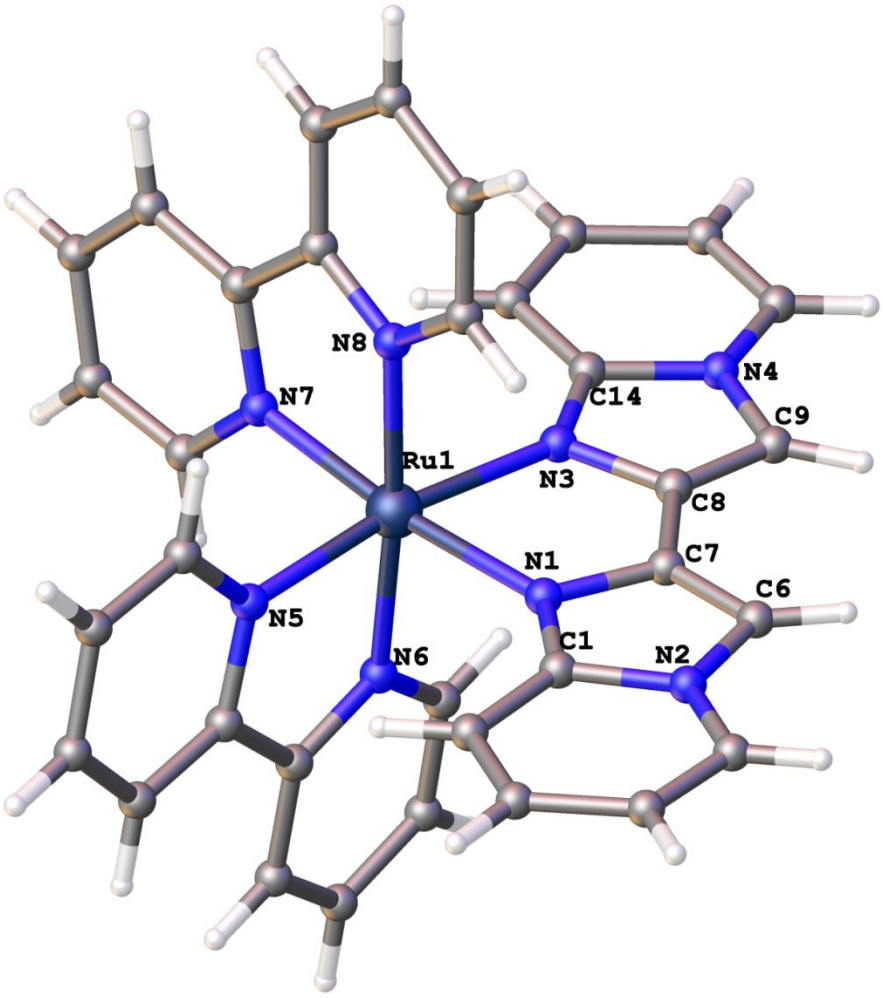

Fig 2.12 Perspective view of **4**, with partial labelling. Selected bond lengths (Å) and angles (°): Ru1-N1 2.115(3), Ru1-N3 2.100(3), Ru1-N5 2.038(3), Ru1-N6 2.051(3), Ru1-N7 2.044(3), Ru1-N8 2.062(3), N1-Ru1-N3 77.8(11), N5-Ru1-N6 78.9(11), N7-Ru1-N8 78.5(13), N1-C1 1.339(5), C1-N2 1.386(5), N2-C6 1.375(5), C6-C7 1.359(5), C7-N1 1.381(5), C7-C8 1.446(5), N1-C1-N2 109.1(3), C1-N2-C6 108.3(3), N2-C6-C7 105.5(3), C6-C7-N1 110.9(3), N1-C7-C8 115.8(3).

As was previously touched on, the structure of **4** shows obvious similarities with that of complex **3**. The ruthenium-to-imidazopyridine bond lengths are consistent between the two complexes [2.100(3) Å and 2.115(3) Å *vs* 2.123(7) Å].

As illustrated with **3**, we can view the cause of the large negative CIS value for H7 by examining the distances between protons and the centre of the ring into which they point. The distance of the H7 protons to their adjacent pyridine rings were calculated as *ca.* 2.7 Å and *ca.* 2.9 Å. These are comparable to, or just slightly shorter than, **3**, which explains the slightly larger CIS value in **4** than in **3**; as the H7 proton is closer to the centre of the pyridine ring, this proton experiences greater shielding and is thus shifted further upfield. The average bpy

H6 to ligand pyridine was *ca.* 3.9Å, and the average bpy H6 to bpy pyridine was *ca.* 3.2Å, both of which are in agreement with the corresponding values for **3**.

Chapter 3

Imidazo[1,5-a]pyridines

3.1 Introduction

In this chapter we examine a set of imidazo[1,5-a]pyridine based heterocyclic chelating ligands and their ruthenium complexes. The heterocyclic ring system and ring numbering are shown in Figure 3.1.

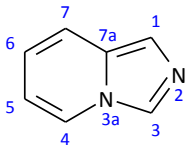

Fig 3.1

The compounds examined are, specifically, 1-(pyridin-2-yl)imidazo[1,5-a]pyridine (**5**), 1,1'-biimidazo[1,5-a]pyridine (**6**) (attempted synthesis), 3-(pyridin-2-yl)imidazo[1,5-a]pyridine (**7**) and 3,3'-biimidazo[1,5-a]pyridine (**8**) (Fig 3.2).

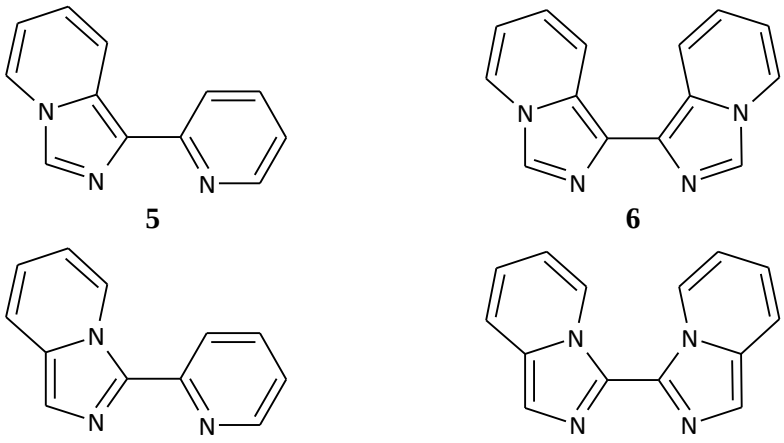

5 **6**

7 **8**

Fig 3.2

One of the first syntheses of imidazo[1,5-a]pyridine was reported by Bower and Ramage[49] in 1955. *N*-(2-Pyridinylmethyl)-formamide was refluxed in benzene with phosphoryl chloride, undergoing a Vilsmeier-type cyclisation to the imidazopyridine product. Further study was focused on various 1- and 3-substituted derivatives.

While the above method still proves popular, various other synthetic pathways to imidazo[1,5-a]pyridine and its derivatives have been examined. Shibahara *et al.*[50,51] examined a similar reaction using *N*-2-pyridylmethyl thioamides. In contrast to the method of Bower and Ramage, this synthesis could be carried out under reasonably mild conditions, with reactions starting at 0°C and being raised to room temperature over the course of the reaction. Iodine was used to mediate oxidative desulphurisation, which in turn led to cyclisation and an imidazopyridine product. Shibahara *et al.* have developed a number of other methods of synthesising imidazo[1,5-a]pyridines and their 1-/3-substituted derivatives. They examined a method of cyclising aryl aldehydes with aryl-2-methylpyridine using elemental sulphur as an oxidant,[52] as well as a number of cross-coupling reactions to produce 3- and 1,3-substituted derivatives.[53,54] Other methods based on an oxidative pathway include those of Bluhm *et al.*,[55,56] Moulin *et al.*[57] (thioacylation by Lawesson's reagent, followed by ring closure by mercury(II) acetate), Ostermeie *et al.*[58] (oxidation of 1,4-bis(2-pyridylmethyl)piperazine by iron(III) chloride), and Niyomura *et al.*[59] (cyclisation of 2-(aminomethyl)pyridine with selenium dioxide). Methods involving an acid-mediated condensation include those of Wang *et al.*,[60,61] Siddiqui *et al.*[62] (condensation using ionic liquids), and Crawforth and Paoletti[63] (one-pot synthesis using propane phosphonic acid anhydride (T3P®)).

Imidazo[1,5-a]pyridines are attractive molecules for use in a number of fields. They have been examined for potential application in organic light-emitting diodes (OLEDs)[64] and organic thin-layer field effect transistors (FETs),[65] and as possible precursors for *N*-heterocyclic carbenes (NHCs).[66-68] Like imidazo[1,2-a]pyridines, these compounds are bioactive, and have been used in a range of pharmaceuticals, such as HIV-protease inhibitors,[69] cardiotonic agents,[70] and thromboxane A2 synthase inhibitors.[71]

Similar to **1**, **5** has seen little study, with a literature search only finding two references; a 1992 paper from Grigg *et al.*,[72] and a 2002 paper from Hajos and Riedl.[73] In comparison, the synthesis of **7** has been thoroughly examined, with 20 papers and patents detailing a variety of synthetic methods and modifications. Compounds **6** and **8** have never been reported. The

only reported transition metal complex of any of these ligands is a manganese(II) complex of **7**; Álvarez *et al.*[74] used manganese(II) and ammonium cations to promote the dimerization of pyridine-2-carboxaldehyde on the metal.

Grigg *et al.*[72] examined an interesting reaction between 2,2'-dipyridyl ketone and α-amino acids, which led to a range of 1,3-disubstituted imidazo[1,5-a]pyridines (Scheme 3.1). Heated in methanol, the dipyridyl ketone reacts with an α-amino acid, and the resulting imine undergoes decarboxylation to form an azomethine ylide. This ylide subsequently undergoes 1,5-electrocyclisation and aromatisation to give a 3-substituted-1-(2'-pyridyl)-imidazo[1,5-a]pyridine. The moiety of the 3-substituent is dictated by the α-amino acid used, and can range from simple (R = H, glycine, leading to **5**), to more complex (R = indole, tryptophan). Addition of a small amount of acetic acid was important to the reaction, as it had a notable catalytic effect; care must be taken though, as some amino acid moieties were found to undergo side-reactions when catalytic acid was present (e.g. histidine and tryptophan were found to undergo Pictet-Spengler cyclisations.).

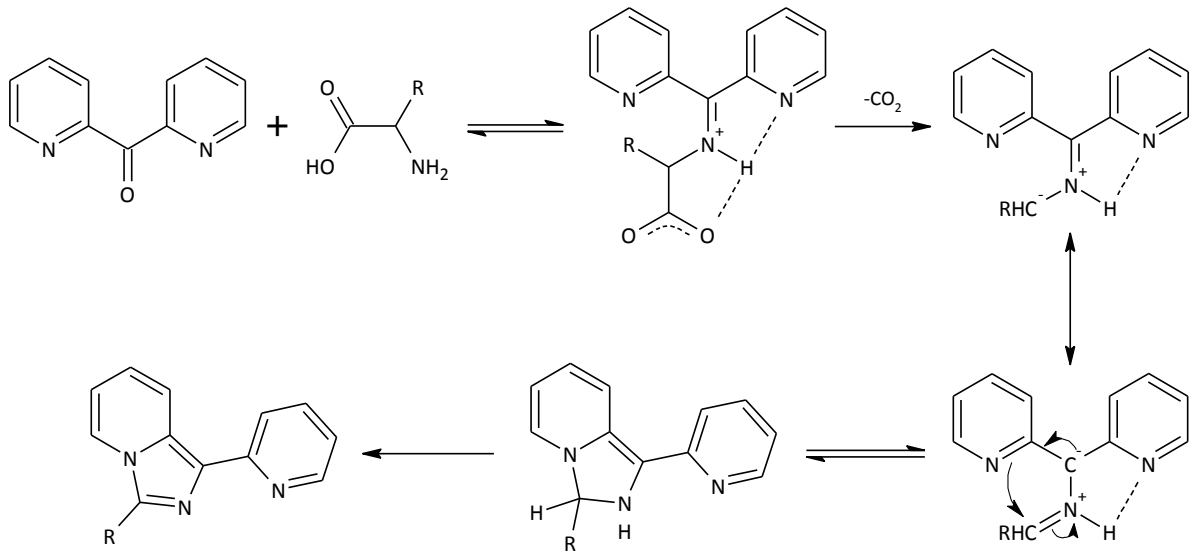

Scheme 3.1 Proposed mechanism of formation of derivatives of **5**.[72]

The earliest reported synthesis of compound **7** appears to be in 1971, published by Abushanab.[75] While attempting to synthesise 2-(diethoxymethyl)-pyrazine (using pyrazine carboxaldehyde and methyl orthoformate, with ammonium chloride as a catalyst), an unusual by-product was obtained (10% yield). A combination of ^{1}H NMR, mass spectrometry, and UV-visible spectroscopy strongly indicated that this by-product was 3-(2-

pyrazinyl)imidazo[1,5-a]pyrazine. This reaction was further examined by reacting 2-pyridine carboxaldehyde with ammonium chloride and, despite a low yield (7%), the presence of 3-(2-pyridinyl)imidazo[1,5-a]pyridine was confirmed by ^{1}H NMR and mass spectrometry.

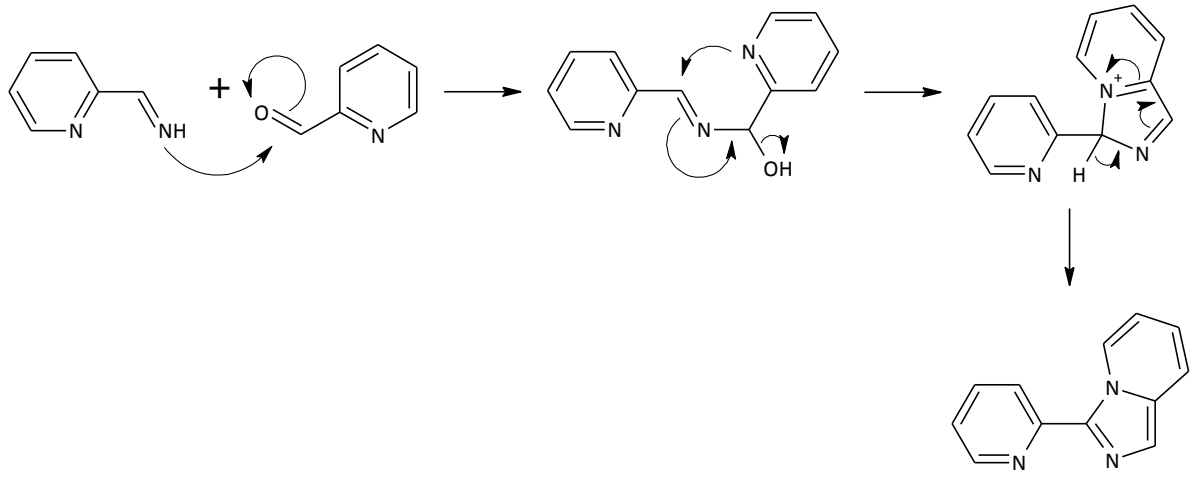

Scheme 3.2 Proposed mechanism of formation of **7**.[75]

In 2011, Huang *et al.*[76] and Yamaguchi *et al.*[54] examined a series of cross-coupling reactions, catalysed by palladium(II) acetate and $[Pd(phen)_2](PF_6)_2$, respectively. In each example, imidazo[1,5-a]pyridine was reacted with a range of aryl halides (aryl bromides and aryl iodides, respectively), with C-3 arylation of the imidazopyridine occurring selectively in moderate to excellent yield (46-99%). While Huang *et al.* reported no arylation at the C-1 carbon, Yamaguchi *et al.* found that under certain conditions this could occur, but only subsequent to the C-3 arylation (producing a diarylated product). Compound **7** was synthesised by both these methods, and was consistently one of the lowest reported yields (48-49%), due to the electron deficient nature of the pyridine ring.

During this work, attempts were made at growing crystals of each complex that would be suitable for analysis by X-ray diffraction. Unfortunately, only one of the three complexes produced suitable crystals; **9** was crystallised by slow diffusion of diisopropyl ether into a solution of acetone containing the complex. A number of solvent systems were tested, including acetone or acetonitrile (with a drop of toluene) as the mother liquor, and diethyl ether, petroleum ether, diisopropyl ether, nitromethane, benzene or toluene as the diffusing solvent. Complex **10** grew some tiny crystals in acetone/diisopropyl ether, however these repeatedly failed to diffract when mounted on the diffractometer; the rest of the samples, failed to furnish single crystals.

3.2 Synthesis of Ligands

Ligand **5** was synthesised as per the procedure detailed by Grigg *et al.*[72] (Scheme 3.1, R = H). Di(2-pyridyl)ketone and glycine were added to methanol in a 1:1 ratio, along with a drop of glacial acetic acid. The reaction mixture was stirred at reflux for 24 hours, and monitored by TLC (silica, EtOAc) and ^{1}H NMR. After column chromatography (silica, EtOAc), a final yield of 39% was obtained.

Based on the synthesis of **5**, an attempt at synthesising **6** was made by reacting 2,2'-pyridil with excess glycine (Scheme 3.3). After the reaction mixture was subjected to column chromatography, analysis of the fractions by ^{1}H NMR and mass spectrometry indicated that the desired product had not been formed.

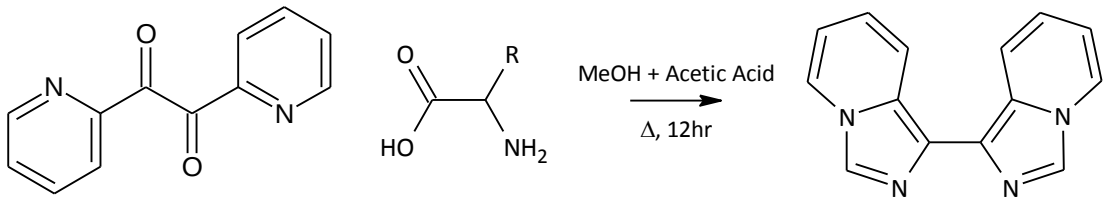

Scheme 3.3 Proposed synthesis of **6**.

A subsequent attempt at synthesising **6** followed a synthesis from Garino *et al.*,[77] who had previously synthesised the 3-methyl derivative of **5**. 2,2'-Pyridil and formaldehyde were added to a glacial acetic acid solution containing ammonium acetate. The reaction mixture was refluxed under nitrogen for 5 hours, and after cooling was neutralised by addition of sodium chloride and sodium bicarbonate. After extraction, ^{1}H NMR and mass spectroscopy indicated that the desired product had not been produced.

Ligands **7** and **8** were received with gratitude from Dr Chris Richardson.

3.3 Synthesis and Characterisation of Complexes

3.3.1 Synthesis of Bis(2,2'-bipyridine)[1-(pyridin-2-yl)imidazo[1,5-a]pyridine]ruthenium(II) bis(hexafluorophosphate) (9)

Ligand **5** was reacted with bis(2,2'-bipyridine)ruthenium(II) dichloride, $[Ru(bpy)_2Cl_2]$, in a 1:1 ratio. Added to a 3:1 mixture of ethanol:water, the reaction mixture was stirred at reflux overnight. After workup, the product $[Ru(bpy)_2(\mathbf{5})]$, (**9**), was obtained in excellent yield (90%) (Fig 3.3).

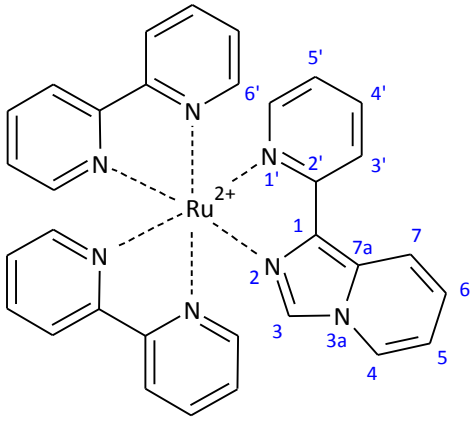

Fig 3.3 Structure of the cation of complex **9**.

Complex **9** contains a total of 25 aromatic protons; 16 from the two bpy ligands and 9 from ligand **5**. Integration of the ^{1}H NMR spectrum revealed a total of 25 signals. The chemical shifts and CIS values for **5** and **9** are shown in Table 3.1, and the ^{1}H NMR spectrum of **9** is shown in Figure 3.4.

Table 3.1 ^{1}H NMR Chemical Shifts[a] and Coordination Induced Shifts[b] of the coordinated imidazo[1,2-a]pyridine rings of **9** and the chemical shifts of **5**.

	H3	H4	H5	H6	H7	H3'	H4'	H5'	H6'
9	7.87	8.10	6.97	7.36	8.10	8.16	7.92	7.10	7.53
5	8.22	8.16	6.71	6.97	8.54	8.11	7.75	7.12	8.57
CIS	-0.35	-0.06	+0.26	+0.39	-0.44	+0.05	+0.17	-0.02	-1.04

[a] Solvent: deuterated acetonitrile (MeCN-*d3*). [b] CIS = ($\delta_{complex}$ - δ_{ligand}).

Altering the shape of the ligand has significantly altered the ^{1}H NMR spectrum. Unlike the imidazo[1,2-a]pyridine ligands (Chapter 2), the H7 proton of **9** is not in a position where it can experience serious anisotropic shielding; H6' is now the proton that experiences the most shielding, with H3 is only slightly shielded by anisotropy. The upfield shift of H4 is likely due to a reduced through-space effect from the neighbouring bpy system. Because we no longer see H7 far upfield, we must look to other information to assign the different rings. The H6' proton of **5** is the easiest to determine, as its shift to 7.53 ppm is characteristic of this proton. The other protons in this ring were determined by COSY analysis (Fig 3.5), and follow a similar shift pattern to those seen in related complexes. Determination of the imidazopyridine protons required a 1-D TOCSY analysis of the multiplet at 8.10 ppm (Fig 3.6); this proved that both the H4 and H7 signals were found in this multiplet, as irradiation of this peak showed only the triplets of H5 and H6.

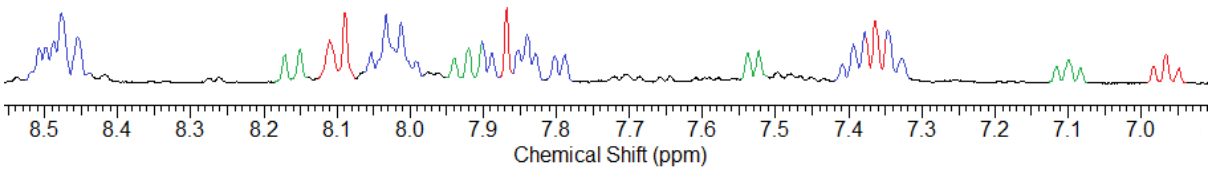

Fig 3.4 ^{1}H NMR spectrum of $[Ru(bpy)_2(\mathbf{5})]^{2+}$, (**9**), in MeCN-*d3*. Red = **5** (H4-H7), Green = **5** (H3'-H6'), Blue = bpy.

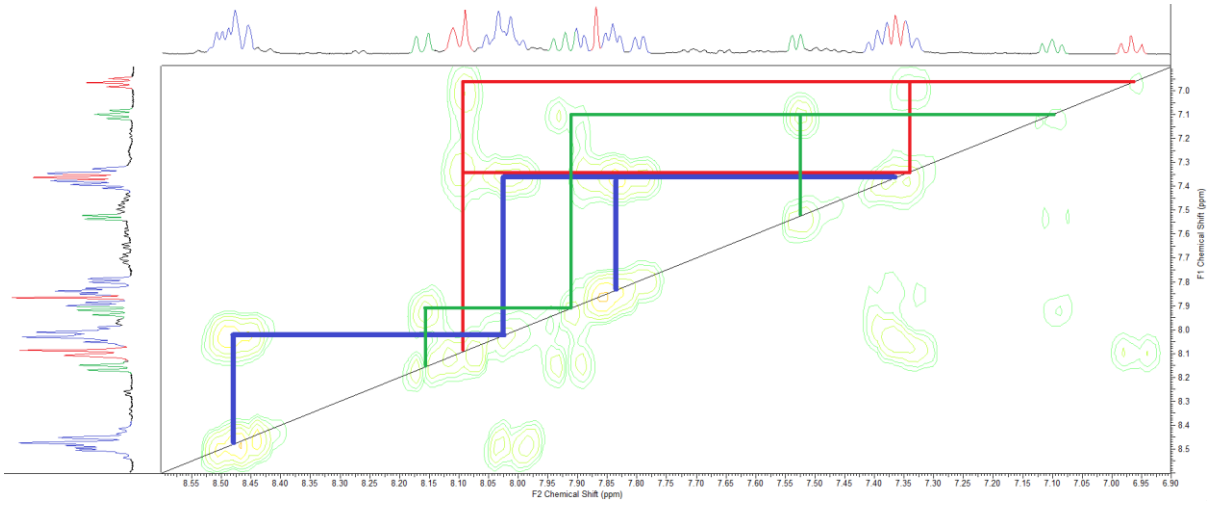

Fig 3.5 2-D COSY of **9** in MeCN-*d3*. Red = **5** (H4-H7), Green = **5** (H3'-H6'), Blue = bpy.

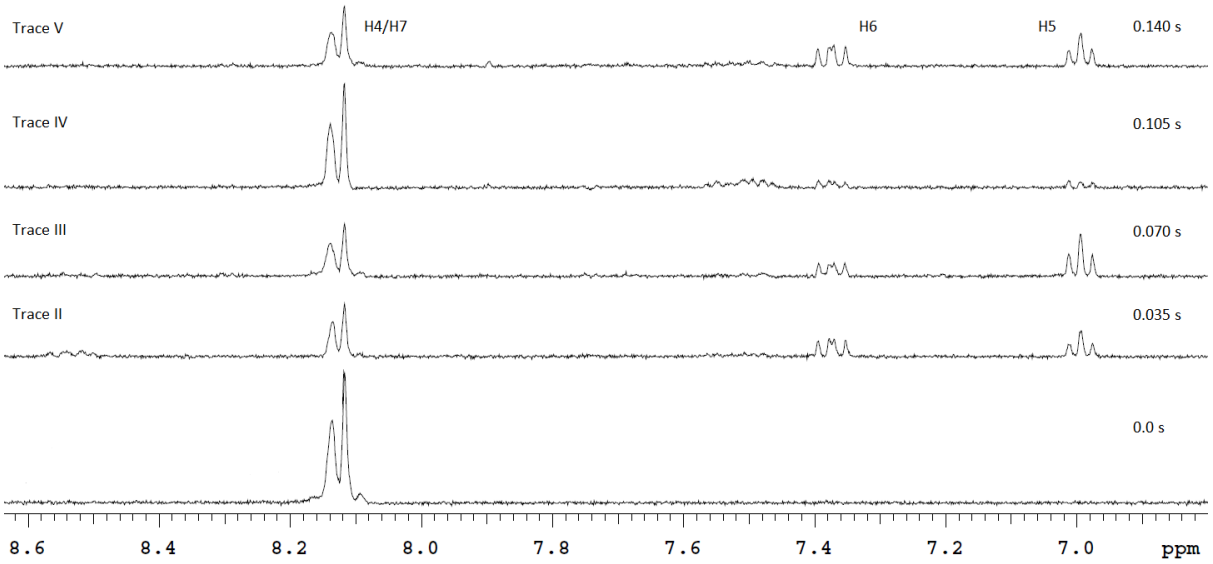

Fig 3.6 1-D TOCSY of **9** in MeCN-*d3*.

By examining the conformation of the free ligand and when it is chelated, we can propose two ways to potentially explain the larger negative CIS value for H7. The first is that this proton is being shielded. When chelating to ruthenium, the conformation that ligand **5** will have to adopt may place the H7 and H3' protons in a close environment. To relieve the steric stress that would result, the two rings may be tilted relative to one another. This situation would lead to H4 and H3' lying above the opposite ring's pyridine system, resulting in each proton experiencing an anisotropic shielding effect. This situation seems unlikely however, as H3' shows no upfield shift due to shielding. On the contrary, H3' has been shifted downfield in this complex. The theory is further disproven upon examination of the crystal structure of **9** (see below), in which the chelating **5** shows little in the way of distortion from planarity.

The second explanation is that, rather than experiencing *more* shielding, the proton is experiencing less *de*shielding upon chelation.[78] The H7 proton of the free ligand is at 8.54 ppm (compare with the other imidazopyridine H7 signals of 7.51-7.65 ppm). This indicates that H7 is in fact deshielded, and the most likely cause for this is the nitrogen of the pyridine ring. In solution, to limit the steric interactions of H7 and H3' discussed above, the conformation of the uncomplexed ligand will be such that the nitrogens are *trans* to each other with respect to the inter-ring bond (Fig 3.7).[79]

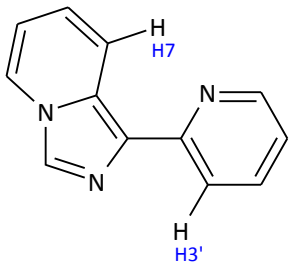

Fig 3.7

We might expect the H3' proton to experience a similar deshielding effect to H7, however examining the shifts and CIS values indicate this is not the case. It is possible that the proximity of H7 to the pyridyl nitrogen *versus* that of H3' to the imidazo nitrogen could explain the difference; a simple simulated 3-D model (created with ACD/Labs ChemSketch and 3D Viewer programs)[80,81] of **5** in a planar conformation calculated the distances as *ca.* 2.24 Å and *ca.* 2.67 Å respectively.

In complex **9**, the λ_{max} corresponding to the (M)d-(L)π^* transition occurs at 462 nm (Fig 3.8), almost identical to that found in the imidazo[1,2-a]pyridine complex **3**, although with a greater extinction coefficient (ε = 10000 *vs* 8000 $M^{-1}cm^{-1}$) (Table 3.2). Similarly, the (M)d-(bpy)π^* transition occurs as a shoulder at 423 nm, while the ligand centred transitions occur <330 nm. The HOMO-LUMO energy gap is again smaller than that found in $[Ru(bpy)_3]^{2+}$.

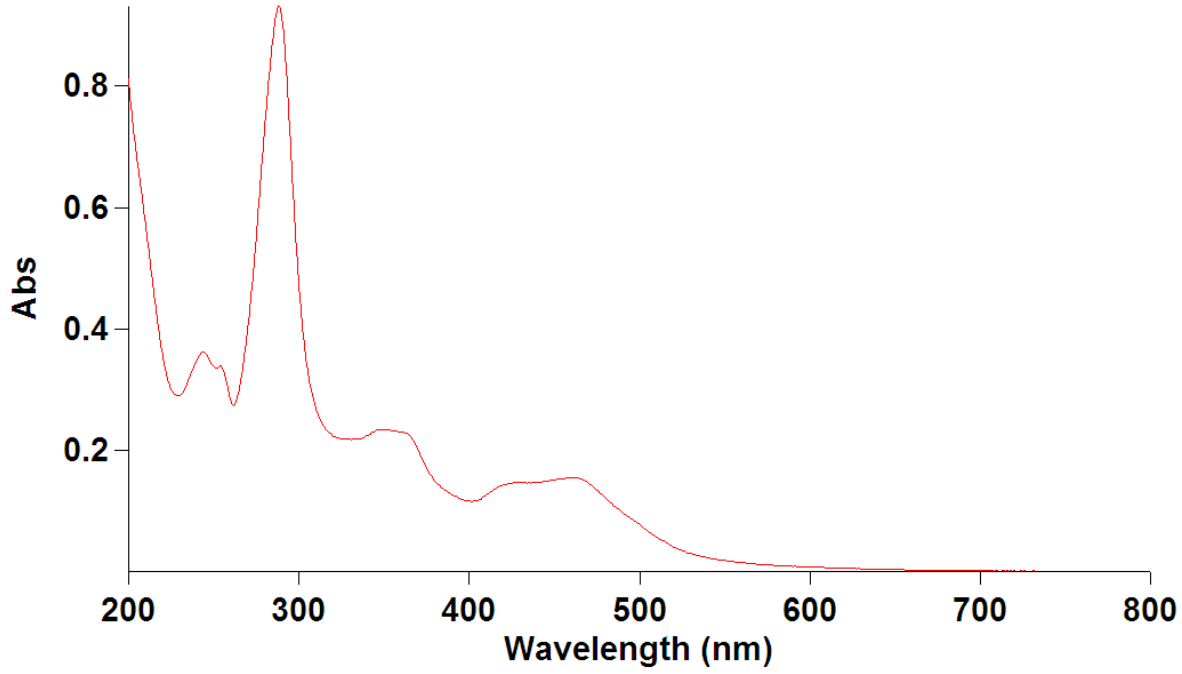

Fig 3.8 UV-Vis spectrum of $[Ru(bpy)_2(\mathbf{5})]^{2+}$, (**9**).

Table 3.2 Absorption Maxima[a] with Molar Absorption Coefficients[b] and Redox Potentials[c] of complex **9**.

Complex	λ_{max} (ε)	E_{ox}	E_{red1}	E_{red2}	E_{red3}	$\Delta E_{ox\text{-}red1}$
$[Ru(bpy)_3]^{2+}$	452 (13600)	+1.26	-1.33	-1.51	-1.79	2.59
9	462 (10000)	+1.09(90)	-1.49(103)	-1.69(100)	-	2.58

[a] In nanometres. [b] $M^{-1}cm^{-1}$. [c] In volts vs SCE.

Minor impurities in the sample led to a less well defined cyclic voltammogram for **9**, although this does not prevent us from examining the reversible nature of the peaks (Fig 3.9). As previously seen with the imidazo[1,2-a]pyridines (Chapter 2), the cyclic voltammogram contains three reversible peaks; one oxidation at a lower potential than $[Ru(bpy)_3]^{2+}$, and two bpy-based reductions, placing the reduction potential of **5** past the solvent limit. As such, **9** is easier to oxidise, and harder to reduce than $[Ru(bpy)_3]^{2+}$.

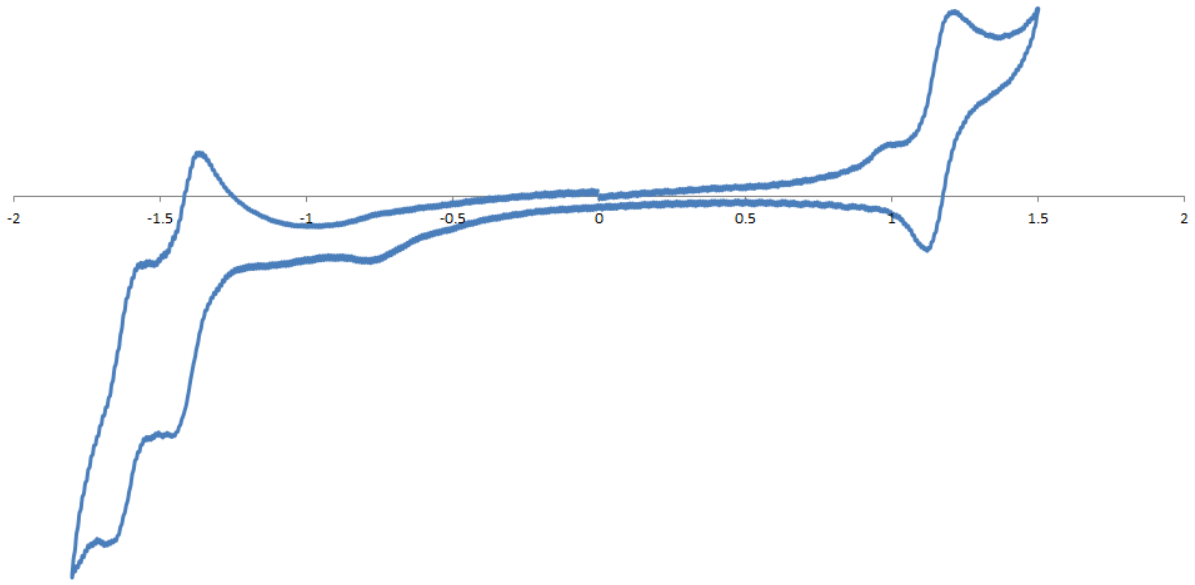

Fig 3.9 Cyclic Voltammogram of $[Ru(bpy)_2(\mathbf{5})]^{2+}$, (**9**), in volts vs silver wire.

Crystals suitable for X-ray analysis of **9** were grown by the slow diffusion of diisopropyl ether into a solution of **9** dissolved in acetone. Crystallising in the monoclinic space group $P2_1/n$, the asymmetric unit contains a full cation and two hexafluorophosphate counterions. Interestingly, this is the only structure reported in this work that solved without acetone solvate molecules being present. The cation is shown in Fig 3.10, with counterions omitted for clarity. Examining the coordination bonds between the central ruthenium atom and the ligands, the longest is that of Ru1-N1, from the metal to the pyridine ring of **5** [2.083(2) Å].

Conversely, the bond between ruthenium and the imidazo[1,5-a]pyridine ring is one of the shorter bonds [2.052(3) Å], and is very similar to those found in the ancillary bpy ligands [2.050(2) Å - 2.065(2) Å]. These results are contrary to what was observed in the previous chapter, where the ruthenium to imidazo bond was the longer, and the ruthenium to pyridine bond was shorter. This indicates that the imidazopyridine system is a good donor and may coordinate more strongly with ruthenium, and that the longer bond lengths in the previous chapter may have been the result of steric hindrance, caused by the position of the fused pyridine. A similar set of values can be observed in the ruthenium complex of the analogous [1,2,3]triazolopyridine;[25] the triazolopyridine unit is located even closer to the central ruthenium [Ru-L(tri) 2.33(3) Å], as this system is more electron rich than the imidazopyridine. The rest of the bond lengths in this complex [Ru-L(py) 2.083(3) Å; Ru-bpy 2.051(3)-2.061(3) Å] are consistent with those reported for **9**.

The bite angles (**5** [78.40(10)°], bpy [78.47(10)°, 79.03(10)°]) are fairly regular, and those of bpy (along with the corresponding bond lengths) are in agreement with those previously reported in the literature.[25,47]

As before, the chemical shifts present in the ^{1}H NMR spectrum can be rationalised by calculating the distance between modelled hydrogens and the centre of the adjacent bpy pyridine systems. The distance between H3 and the N5 ring system is calculated at *ca.* 3.3 Å, while the distance from H4 to the N5 ring system is *ca.* 5.8 Å. The distance between H6’ and the N7 ring system is *ca.* 3.3 Å.

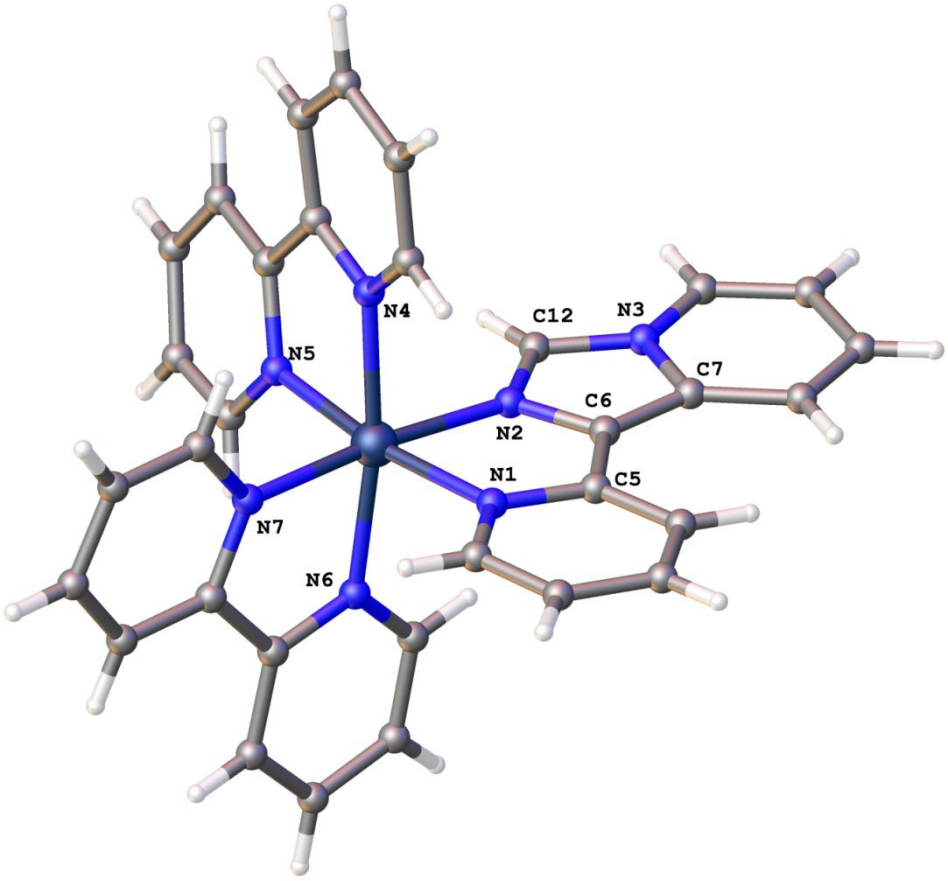

Fig 3.10 Perspective view of **9**, with partial labelling. Selected bond lengths (Å) and angles (°): Ru1-N1 2.083(2), Ru1-N2 2.052(3), Ru1-N4 2.065(2), Ru1-N5 2.050(2), Ru1-N6 2.056(2), Ru1-N7 2.051(3), N1-Ru1-N2 78.40(10), N4-Ru1-N5 79.03(10), N6-Ru1-N7 78.47(10), N2-C6 1.378(4), C6-C7 1.390(4), N3-C7 1.382(4), N3-C12 1.374(4), N2-C12 1.316(4), C5-C6 1.458(4), N2-C6-C7 110.0(3), C6-C7-N3 104.5(3), C7-N3-C12 108.4(3), N2-C12-N3 110.2(3), C12-N2-C6 106.9(3), N2-C6-C5 116.0(3).

3.3.2 Synthesis of Bis(2,2'-bipyridine)[3-(pyridin-2-yl)imidazo[1,5-a]pyridine]ruthenium(II) bis(hexafluorophosphate) (10)

Ligand **7** was reacted with bis(2,2'-bipyridine)ruthenium(II) dichloride, $[Ru(bpy)_2Cl_2]$, in a 1:1 ratio. A small volume of ethylene glycol was added to the reactants and irradiated in a microwave at 450 W, in 2 minute intervals for a total of 6 minutes. After precipitating the PF_6^- salt (addition of aqueous KPF_6), the product $[Ru(bpy)_2(\mathbf{7})](PF_6)_2$, (**10**), was recrystallised by the addition of excess diethyl ether to the precipitate dissolved in the minimum amount of acetonitrile, in moderate yield (58%) (Fig 3.11).

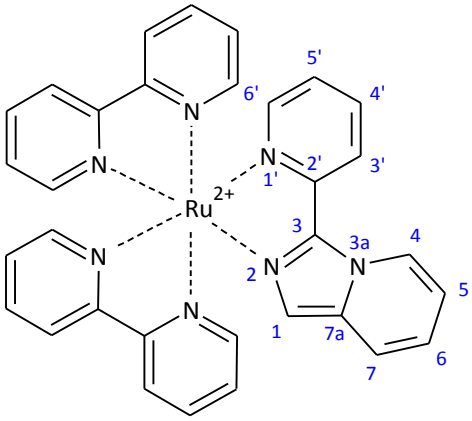

Fig 3.11 Structure of the cation of complex **10**.

Complex **10** contains a total of 25 aromatic protons. The correct number of signals was confirmed by integration of the multiplets present in the ^{1}H NMR spectrum. The chemical shifts and CIS values for **7** and **10** are shown in Table 3.3, and the ^{1}H NMR spectrum of **10** is shown in Figure 3.12.

Table 3.3 ^{1}H NMR Chemical Shifts[a] and Coordination Induced Shifts[b] of the coordinated imidazo[1,2-a]pyridine rings of **10** and the chemical shifts of **7**.

	H1	H4	H5	H6	H7	H3’	H4’	H5’	H6’
10	7.03	8.83	7.18	7.24	7.63	8.31	8.02	7.21	7.70
7	7.57	9.95	6.82	6.93	7.63	8.31	7.85	7.28	8.66
CIS	-0.54	-1.12	+0.36	+0.31	0	0	+0.17	-0.07	-0.96

[a] Solvent: deuterated acetonitrile (MeCN-*d3*). [b] CIS = ($\delta_{complex}$ - δ_{ligand}).

In complex **10**, both the H4 proton and the H6' proton have experienced sizable upfield shifts, while H7 and H3' have apparently seen no shift at all. As has been seen previously, the large negative CIS of H6' is the result of anisotropic shielding, as is the negative shift of H1 to a lesser degree.

With the characteristic cluster of bpy H3 protons at ~8.5 ppm, and the upfield shifted H3' signal at 8.31 ppm, the signal at 8.83 ppm was assigned to H4. COSY analysis was used to determine the rest of the signals in the ligand's two spin systems.

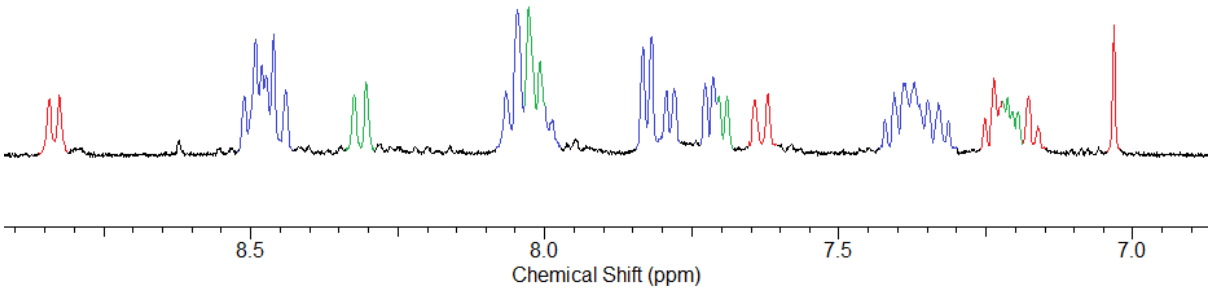

Fig 3.12 ^{1}H NMR spectrum of $[Ru(bpy)_2(\mathbf{7})]^{2+}$, (**10**), in MeCN-*d3*. Red = **7**, Green = **7** (H3'-H6'), Blue = bpy.

Changing the pyridine binding site of the imidazo[1,5-a]pyridine from C1 to C3 had some interesting effects on the proton NMR signals of the complex. The H7 signal of the free ligand **7** has been lowered in comparison to **5**, while the H4 signal has been pushed well downfield. Both of these shifts are the result of deshielding effects in the free ligand, as discussed for **9**. The H7 proton is no longer deshielded by the pyridyl nitrogen, with H4 now being the one deshielded. H4 is also moved downfield relative to H7 due to the electronegative nature of the neighbouring bridgehead nitrogen. Likewise, the H1 singlet is located further upfield than the H3 singlet of **9**, as there is no longer a nitrogen adjacent to this proton.

Both H7 and H3' experience CIS values of 0. Examining the values of related sites in previous complexes (those of H3' and H4 in **9** (the doublets not experiencing major shielding or deshielding effects)), correspondingly small CIS values are seen (-0.06 ppm to +0.09 ppm). For H7, it is proposed that the 0 CIS value results from the cancellation of two effects; a downfield shift due to coordination, coupled with an upfield shift caused by a minor through space effect.

The (M)d-(L)π* transition of complex **10** absorbs at very similar λ_{max} wavelength than that of $[Ru(bpy)_3]^{2+}$; *viz.* 454 nm (Fig 3.13). This indicates that the HOMO-LUMO energy gap in **10** is slightly smaller than that of $[Ru(bpy)_3]^{2+}$, while the extinction coefficient (11500) indicates that it is slightly harder to excite. The (M)d-(bpy)π* transition occurs at 424 nm, and the ligand based transitions occur at <300 nm (Table 3.4).

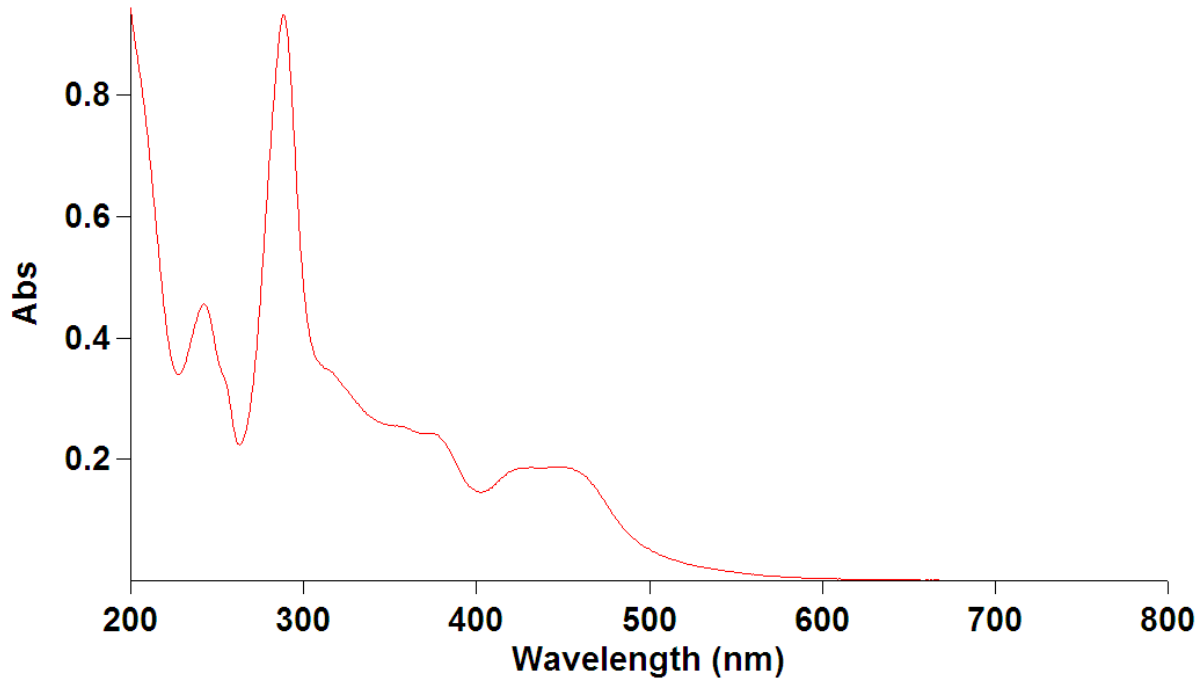

Fig 3.13 UV-Vis spectrum of $[Ru(bpy)_2(\mathbf{7})]^{2+}$, (**10**).

Table 3.4 Absorption Maxima[a] with Molar Absorption Coefficients[b] and Redox Potentials[c] of complex **10**.

Complex	λ_{max} (ε)	E_{ox}	E_{red1}	E_{red2}	E_{red3}	$\Delta E_{ox\text{-}red1}$
$[Ru(bpy)_3]^{2+}$	452 (13600)	+1.26	-1.33	-1.51	-1.79	2.59
10	454 (11500)	+1.10(84)	-1.47(83)	-1.67(88)	-	2.57

[a] In nanometres. [b] $M^{-1}cm^{-1}$. [c] In volts vs SCE.

Following the trend, compared to $[Ru(bpy)_3]^{2+}$ complex **10** is both easier to oxidise and harder to reduce, based on the reversible oxidation and reduction potentials shown in Figure 3.14. Complex **10** appears to be slightly harder to oxidise than **9**, however the inherent error associated with this measurement and equipment (±0.02 V) means their oxidation potentials could overlap.

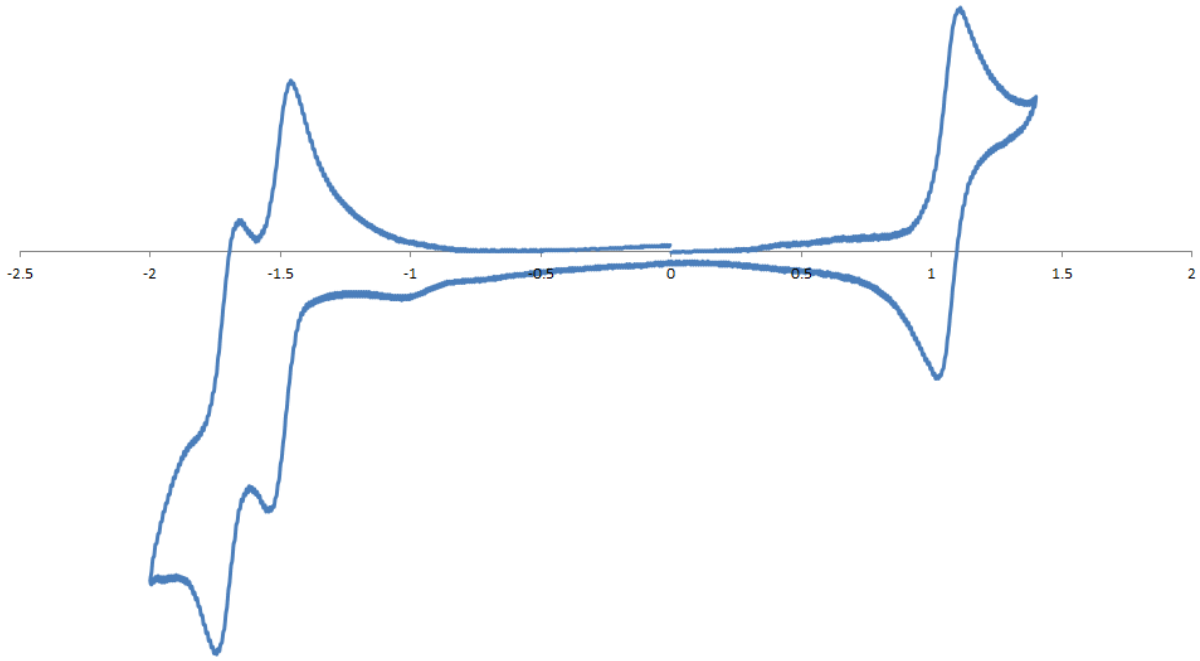

Fig 3.14 Cyclic Voltammogram of $[Ru(bpy)_2(\mathbf{7})]^{2+}$, (**10**), in volts vs silver wire.

3.3.3 Synthesis of Bis(2,2'-bipyridine)[3,3'-biimidazo[1,5-a]pyridine]ruthenium(II) bis(hexafluorophosphate) (11)

Ligand **8** was reacted with bis(2,2'-bipyridine)ruthenium(II) dichloride, $[Ru(bpy)_2Cl_2]$, in a 1:1 ratio. The reactants were added to a small volume of ethylene glycol and irradiated in a microwave at 450 W, in 2 minute intervals for a total of 8 minutes. After precipitating the PF_6^- salt (addition of aqueous KPF_6), the product $[Ru(bpy)_2(\mathbf{8})](PF_6)_2$, (**11**), was recrystallised by the addition of excess diethyl ether to the precipitate dissolved in the minimum amount of acetonitrile, and further subjected to column chromatography. Unfortunately, only a low yield of pure sample was obtained (~16%) (Fig 3.15).

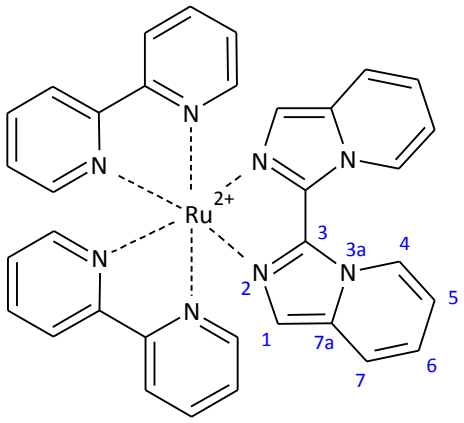

Fig 3.15 Structure of the cation of complex **11**.

Complex **11** contains 26 aromatic protons, and a two-fold rotational axis of symmetry; as such, from the 13 signals present in the spectrum, 8 signals result from the two bpy ligands, and 5 result from ligand **8**. The chemical shifts and CIS values for **8** and **11** are shown in Table 3.5. The ^{1}H NMR spectrum of **11** is shown in Figure 3.16.

Table 3.5 ^{1}H NMR Chemical Shifts[a] and Coordination Induced Shifts[b] of the coordinated imidazo[1,2-a]pyridine rings of **11** and the chemical shifts of **8**.

	H1	H4	H5	H6	H7
11	6.96	8.60	7.02	7.06	7.51
8	7.62	9.78	6.84	6.93	7.65
CIS	-0.66	-1.18	+0.18	+0.13	-0.14

[a] Solvent: deuterated acetonitrile (MeCN-*d3*). [b] CIS = ($\delta_{complex}$ - δ_{ligand}).

Like the comparison of **3** with **4**, there are a lot of similarities between the spectra of **10** and **11**. The ligand signals occur at similar shifts, and were definitively assigned through the use of a COSY experiment. Many of the rationalisations made about **9** and **10** also apply here. The H1 and H7 signals have a more negative shift than **10**, which indicate they are located closer to the neighbouring bipyridine ring; however, the lack of a crystal structure means this is unable to be definitively proven.

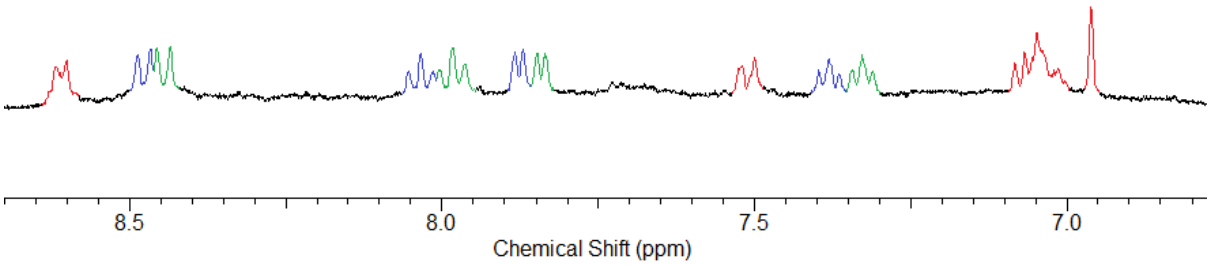

Fig 3.16 ^{1}H NMR spectrum of $[Ru(bpy)_2(\mathbf{8})]^{2+}$, (**11**), in MeCN-*d3*. Red = **8**, Blue/Green = bpy.

In a similar manner to the red shift seen when moving from complex **3** to complex **4**, we have likewise seen a red shift when moving from **10** to **11**. Despite the absorption spectrum displaying a broad absorption band (Fig 3.17), we can observe the (M)d-(L)π* transition occurring at the longer wavelength of 469 nm. The (M)d-(bpy)π* transition occurs at 428 nm, similar to that seen in other complexes, and the ligand centred transitions occur at <315 nm.

Table 3.6 Absorption Maxima[a] with Molar Absorption Coefficients[b] and Redox Potentials[c] of complex **11**.

Complex	λ_{max} (ε)	E_{ox}	E_{red1}	E_{red2}	E_{red3}	$\Delta E_{ox\text{-}red1}$
$[Ru(bpy)_3]^{2+}$	452 (13600)	+1.26	-1.33	-1.51	-1.79	2.59
11	469 (9200)	+0.88	-1.47	-1.70	-	2.35

[a] In nanometres. [b] $M^{-1}cm^{-1}$. [c] In volts vs SCE.

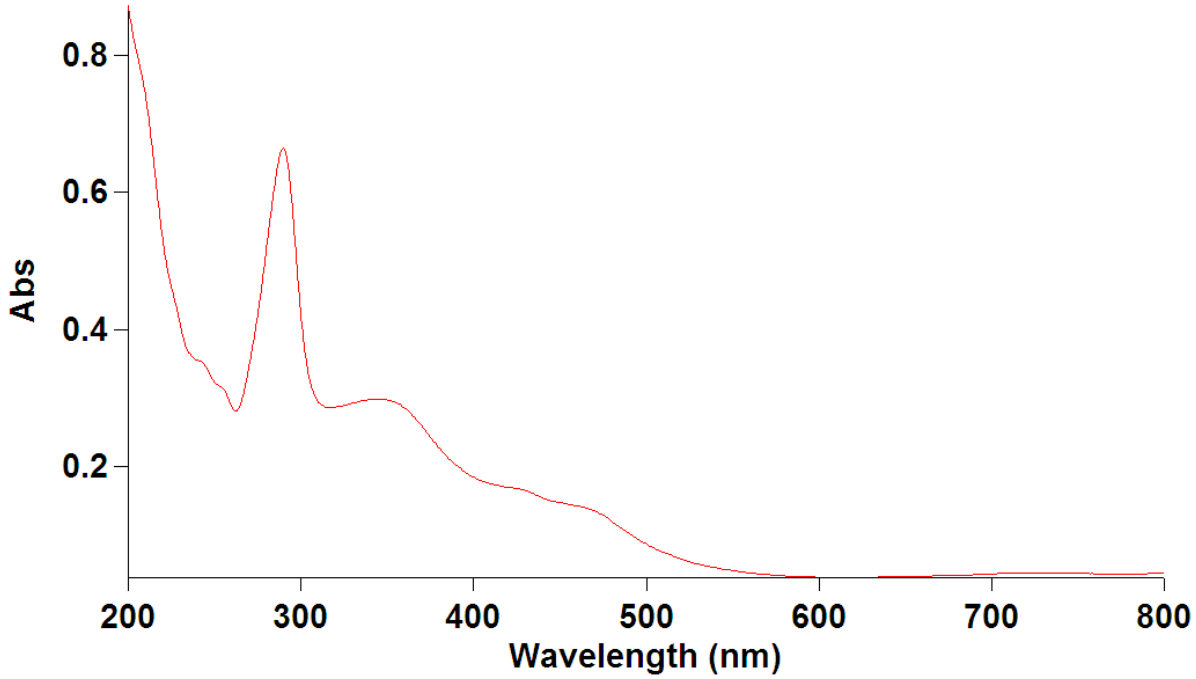

Fig 3.17 UV-Vis spectrum of $[Ru(bpy)_2(\mathbf{8})]^{2+}$, (**11**).

Due to a shortage of sample, we could not use cyclic voltammetry to examine the electrochemistry of complex **11**; instead, differential pulse voltammetry (DPV) was used. DPV is similar to linear sweep voltammetry, as each forward and reverse potential sweep is measured as a separate experiment. This technique is more sensitive that cyclic voltammetry, and while this means we can examine smaller sample sizes, it also means that minor impurities are more easily detected.

The DPV of **11** displayed three oxidation peaks; two reversible (+879 mV and +1.27 V) and one quasi-reversible (+1.07 V). Similar to previous complexes, two reversible bpy-based one-electron reduction peaks were observed (-1.47 V and -1.70 V). To determine which oxidation peak belongs to our complex of interest, we can examine the potentials alongside the absorption data. We know the oxidation of this type of complex is fully reversible, and as such the quasi-reversible E_{ox2} peak is an unlikely candidate. From previous examples we know that the values of $\Delta E_{ox\text{-}red1}$ and λ_{max} are linked; a longer wavelength gives a smaller ΔE value. With a λ_{max} of 469 nm, **11** has a longer absorption wavelength than $[Ru(bpy)_3]^{2+}$, and so $\Delta E_{ox\text{-}red1}$ must in turn be smaller than 2.59 V. The ΔE values for E_{ox1} and E_{ox3} are 2.35 V and 2.74 V, respectively, and as such the oxidation peak at +879 mV is attributed to **11**. This means **11** is quite easy to oxidise, and indicates that ligand **8** is quite electron rich.

E_{ox3} has a very similar potential to that of $[Ru(bpy)_3]^{2+}$, however the lack of matching reduction peaks means that $[Ru(bpy)_3]^{2+}$ is unlikely to be the cause. Another theory as to the contributor to E_{ox3} is that, due to its steric nature, the ligand **8** may photodissociate and lead to the formation of other complexes. $[Ru(bpy)_2(CH_3CN)_2]^{2+}$ was proposed, however a search of the literature suggests that the oxidation potential of this complex is +1.45 V.[82]

Chapter 4

[1,2,4]Triazolo[1,5-a]pyridines

4.1 Introduction

In this chapter we examine a pair of [1,2,4]triazolo[1,5-a]pyridine based heterocyclic ligands and their ruthenium complexes. The heterocyclic ring system and ring numbering is shown in Figure 4.1.

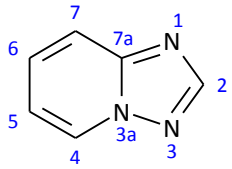

Fig 4.1

The compounds examined are, specifically, 2-(pyridin-2-yl)[1,2,4]triazolo[1,5-a]pyridine (**12**) and 2,2'-bi[1,2,4]triazolo[1,5-a]pyridine (**13**) (Fig 4.2).

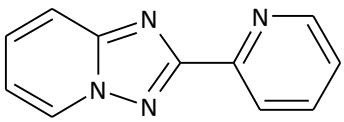

12

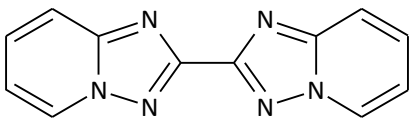

13

Fig 4.2

Subsequent to their synthesis of imidazo[1,5-a]pyridine in 1955,[49] Bower and Ramage published a follow-up paper in 1957,[83] wherein they detailed the synthesis of [1,2,4]triazolo[1,5-a]pyridines, [1,2,3]triazolo[1,5-a]pyridines, and pyrazolo[1,5-a]pyridines. To synthesise the [1,2,4]triazolo[1,5-a]pyridines, *N*-2-pyridylamidines were boiled in acetic acid, with lead tetraacetate used to promote oxidative ring closure to the triazolopyridine product (Scheme 4.1). They were able to successfully synthesise a number of 2-substituted

derivatives (R = Me, Ph, *p*-tolyl), however they were unable to successfully synthesise the parent triazolopyridine (R = H), as the necessary amidine had yet to be synthesised. A further synthesis of the phenyl derivative followed in 1964, when Grenda *et al.*[84] stumbled upon it while experimenting with azabenzimidazole synthesis. In a similar manner to Bower and Ramage, a *N*-2-pyridylamidine was cyclised to the final product, although on this occasion hydrochloric acid and sodium hypochlorite were used in place of lead tetraacetate.

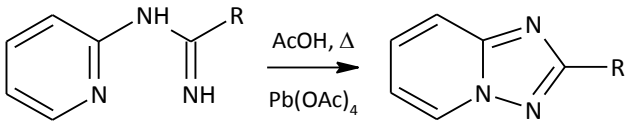

Scheme 4.1 Oxidative ring closure of amidines.[49]

The next attempt at synthesising this triazolopyridine was reported by Potts *et al.*[85] in 1966, where they examined a number of different synthetic methods. After further experimenting with the method of Bower and Ramage, they turned their attention to the cyclisation of 1,2-diaminopyridinium salts with organic acids (Scheme 4.2), and were successful in synthesising the parent [1,2,4]triazolo[1,5-a]pyridine using formic acid. Additionally, during their studies of the [1,2,4]triazolo[4,3-a]pyridine system,[86] it was found that heating these 3-substituted [4,3-a] systems in sodium hydroxide promoted a Dimroth rearrangement to the 2-substituted [1,5-a] system.[87] In this way, [1,2,4]triazolo[1,5-a]pyridine was synthesised by first rearranging 3-amino[1,2,4]triazolo[4,3-a]pyridine, and then deaminating the resulting 2-amino[1,2,4]triazolo[1,5-a]pyridine.

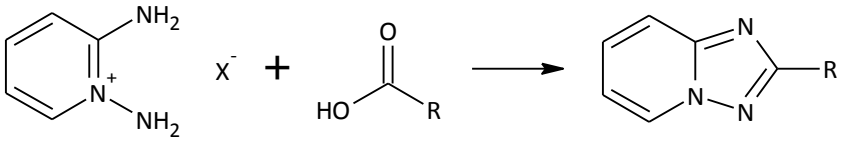

Scheme 4.2 Condensation of 1,2-diaminopyridium salts with carboxylic acid derivatives.[85]

Other synthetic methods include a 1,3-dipolar cycloaddition, where 1-aminopyridines react with nitriles to give 2-substituted triazolopyridines.[88,89] Ueda and Nagasawa[90] have reported a copper(I) catalysed reaction, occurring between 2-aminopyridines and aromatic nitriles, while Mammoliti *et al.*[91] have examined a reaction between a series of thiadiazoles and 2-chloro-3-nitropyridine (the expected [1,2,4]triazolo[4,3-a]pyridine was not seen, and has been predicted to have undergone a Dimroth rearrangement to the [1,5-a] product).[87]

Like the previous imidazopyridine systems, [1,2,4]triazolo[1,5-a]pyridines are of biological interest; while they themselves do not occur in nature, they share structural similarities with the important [1,2,4]triazole system. They have been examined as part of inhibitors of growth factor-β kinase receptors[92] and adenosine receptors,[93,94] antifungal agents,[95] and in the treatment of cancer[96] and diabetes.[97]

There are currently no journal articles listed for either compound **12** or **13**; the only literature available are four Japanese patents for **12**, submitted over 30 years ago by Kiyogo[98] and Tsukamoto *et al.*[99-101] As such, no transition metal complexes have been reported. The English abstracts of these patents provide a rough outline as to the reactions that were carried out. Both Kiyogo and Tsukamoto utilised the 1,2-diaminopyridine method of Potts *et al.*,[85] and while Kiyogo used nitrile derivatives in a 1,3-dipolar cycloaddition, as per Okamoto *et al.*,[88] Tsukamoto *et al.* used nitriles in a similar method to that used by Ueda and Nagasawa[90] (without the copper(I) catalyst). In addition, Tsukamoto *et al.* reacted 2-cyanopyridine with an alkoxide to give (2-pyridyl)formiminoether; after reaction with 2-aminopyridine, the resulting *N*-(2-pyridyl)-2-pyridinecarboxamidine was cyclised to form compound **12** (Scheme 4.3).

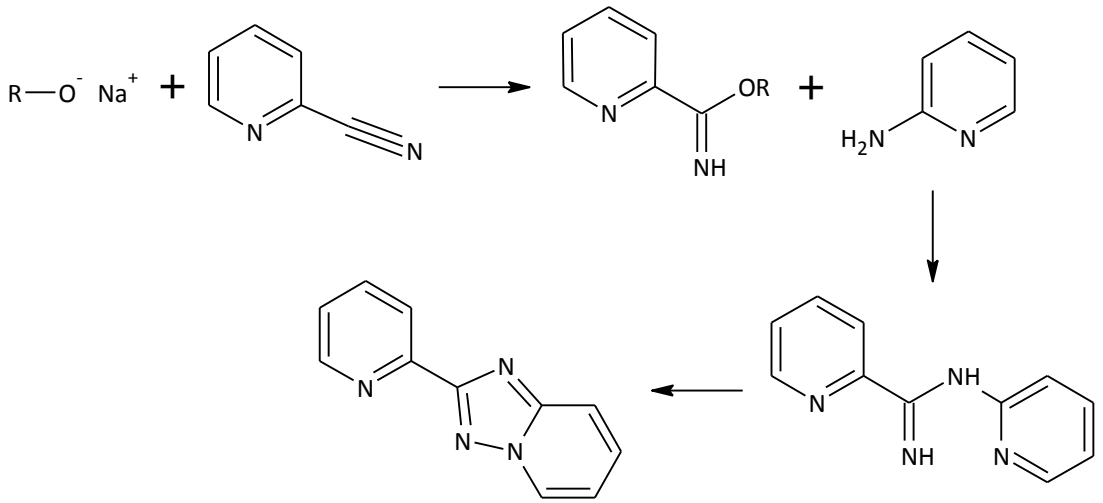

Scheme 4.3 Synthesis of *N*-(2-pyridyl)-2-pyridinecarboxamidine and cyclisation to form ligand **12**.[100]

4.2 Synthesis of Ligands

Mixing of 2-aminopyridine with O-p-tolylsulphonyl hydroxylamine[102] (TSH) formed the tosyl salt of 1,2-diaminopyridinium, which was subsequently cyclised with 2-pyridinecarboxaldehyde at room temperature. After purification, the product, 2-(pyridin-2-yl)[1,2,4]triazolo[1,5-a]pyridine (**12**), was recovered in excellent yield (91%) (Scheme 4.4).

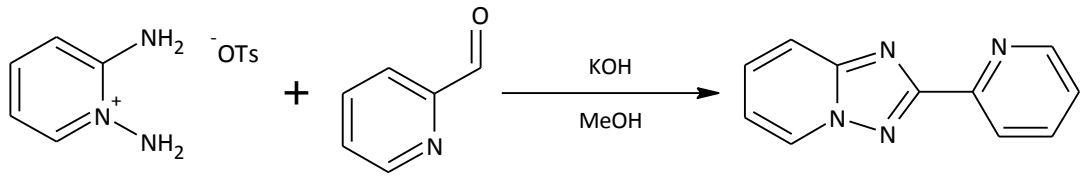

Scheme 4.4 Synthesis of 2-(pyridin-2-yl)[1,2,4]triazolo[1,5-a]pyridine (**12**).

2,2'-Bi[1,2,4]triazolo[1,5-a]pyridine (**13**) was synthesised in a similar manner. The 1,2-diaminopyridinium salt was initially treated with sodium ethoxide, before diethyl oxalate was added and the mixture was brought to reflux for five hours. Dilution of the hot mixture with water prompted the product to crystallise out overnight, in moderate yield (43%) (Scheme 4.5).

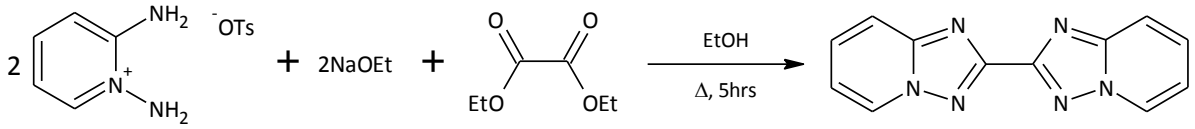

Scheme 4.5 Synthesis of 2,2'-bi[1,2,4]triazolo[1,5-a]pyridine (**13**).

Compounds **12** and **13** were examined by NMR analysis. Full characterisation (^{1}H and ^{13}C) was carried out in deuterated chloroform, while additional ^{1}H spectra were obtained in deuterated acetonitrile, to allow Coordination Induced Shifts (CIS) to be calculated. Full assignments of these compounds proton and carbon spectra, made by a combination of 2-D experiments (COSY, HSQC, HMBC), can be found in the Experimental section (Chapter 6).

4.3 Synthesis and Characterisation of Complexes

4.3.1 Synthesis of Bis(2,2'-bipyridine)[2-(pyridin-2-yl)[1,2,4]triazolo[1,5-a]pyridine]ruthenium(II) bis(hexafluorophosphate) (14)

Complex **14** was synthesised on two separate occasions, by two different methods. This was necessitated by the need for a clean NMR, and the fact that **12** can bind in two different ways; through the N1 nitrogen (as shown in Fig 4.3), and through the N3 nitrogen. The first method, refluxing overnight in ethanol, led to a mixture of isomers which proved difficult to separate. The second method, a microwave synthesis, was carried out in an attempt to quickly form a single product, and efforts were taken to reduce the amount of light the resulting solutions were exposed to, as dissociation and isomerism are often light induced processes.

The first method reacted a 1:1 ratio of ligand **12** and bis(2,2'-bipyridine)ruthenium(II) dichloride, $[Ru(bpy)_2Cl_2]$. The reaction was carried out in a 3:1 mixture of ethanol:water, with stirring at reflux overnight. After standard workup, the product $[Ru(bpy)_2(\mathbf{12})](PF_6)_2$, (**14**), was obtained in excellent yield (87%)

For the second synthesis, ligand **12** was reacted in a 1:1 ratio with $[Ru(bpy)_2Cl_2]$ in a small volume of ethylene glycol. The solution was irradiated at 450 W, with monitoring by TLC in 2 minute intervals for a total of 8 minutes. After the addition of aqueous KPF_6, the product was recrystallised by the addition of excess diethyl ether to the complex dissolved in the minimum amount of acetonitrile, in moderate yield (66%).

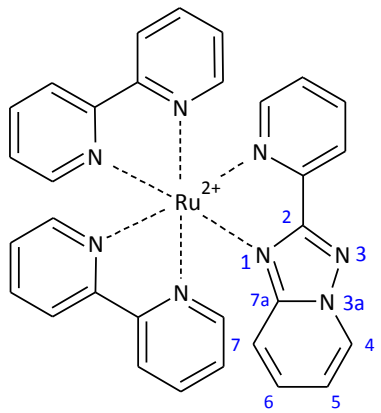

Fig 4.3 Structure of the cation of complex **14**.

Analysing the first sample of **14** by ^{1}H NMR was problematic as ligand **12** can bind to ruthenium through either the N1 or the N3 nitrogen, and the two isomeric forms proved difficult to separate. Worse still, extended exposure of solutions of the complex to light saw the initial 3:1 ratio evolve to roughly 1:1 (observed by the change in integral values over a number of weeks). The second (microwave) sample presented a much cleaner spectrum, with only one isomer being prominently observed. This isomer was the minor product of the first reaction, and is thought to be the thermodynamic product (The high energies involved in microwave synthesis often lead to the thermodynamic product being produced over the kinetic. Further supporting this reasoning is the observation that the major isomer of method 1 began to equilibrate with the minor isomer after periods of extended exposure to light.).

Complex **14** contains a total of 24 aromatic protons; 16 from the two bpy ligands and 8 from ligand **12**. The ^{1}H NMR spectrum of the product displayed all 24 signals, determined by analysing the integral values of the various multiplets. The chemical shifts and CIS values for **12** and **14** are shown in Table 4.1, and the ^{1}H NMR spectrum of **14** is shown in Figure 4.4.

Table 4.1 ^{1}H NMR Chemical Shifts[a] and Coordination Induced Shifts[b] of the coordinated imidazolo[1,2-a]pyridine rings of **14** and the chemical shifts of **12**.

	H4	H5	H6	H7	H3'	H4'	H5'	H6'
14	8.83	7.31	7.53	5.88	8.50	8.11	7.45	7.68
12	8.69	7.07	7.56	7.82	8.36	7.89	7.41	8.83
CIS	+0.14	+0.24	-0.03	-1.94	+0.14	+0.22	+0.04	-1.15

[a] Solvent: deuterated acetonitrile (MeCN-*d3*). [b] CIS = ($\delta_{complex}$ - δ_{ligand}).

In the ^{1}H NMR of the microwave sample, peaks were assigned by a combination of COSY, HSQC and HMBC experiments, and the isomeric form present (chelating through N1) was determined by crystal structure analysis, along with comparisons to the ^{1}H NMR spectra of analogous complexes (**3** and **15**). The key chemical shift to assign is the doublet present far upfield at 5.88 ppm. Like previous examples, this upfield shift is due to anisotropic shielding of a ligand proton by an ancillary bpy ring. When this shift is assigned to the H7 proton, the resulting CIS values for H7 and H4 are comparable to those of **3** (-1.95 and +0.09 ppm, respectively). In comparison, assigning 5.88 ppm to the H4 proton leads to some dramatic CIS values. Values of +1.01 ppm (H7) and -2.81 ppm (H4) are much larger than any previously examined, and are hard to rationalise when more agreeable values are available.

As such, the shift at 5.88 ppm is assigned to H7, and so ligand **12** must be binding through the N1 nitrogen.

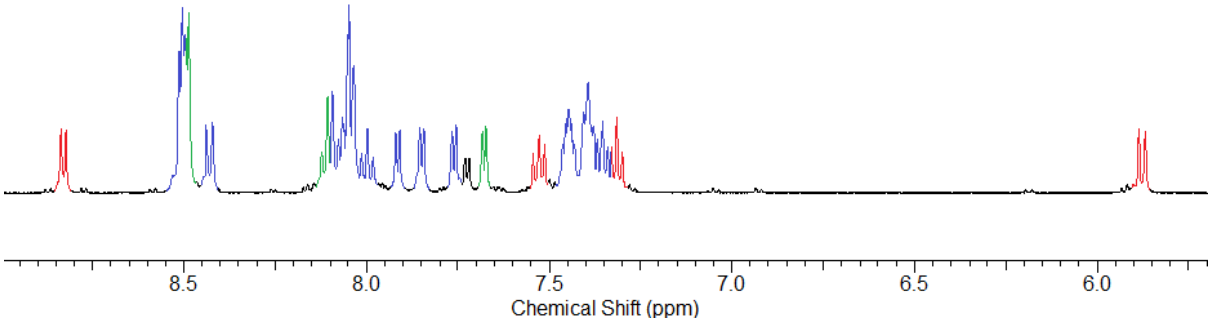

Fig 4.4 ^{1}H NMR spectrum of $[Ru(bpy)_2(\mathbf{12})]^{2+}$, (**14**), in MeCN-*d3*. Red = **12** (H4-H7), Green = **12** (H3'-H6'), Blue = bpy.

The (M)d-(L)π* absorption band of complex **14** occurs at a λ_{max} of 454 nm (Fig 4.5, Table 4.2). This wavelength is slightly longer than that of $[Ru(bpy)_3]^{2+}$, which in turn indicates the HOMO-LUMO gap of **14** is slightly smaller. The extinction coefficient indicates that this complex absorbs light more strongly than the imidazo[1,2-a]pyridines, but not quite as strongly as $[Ru(bpy)_3]^{2+}$ and the imidazo[1,5-a]pyridines.

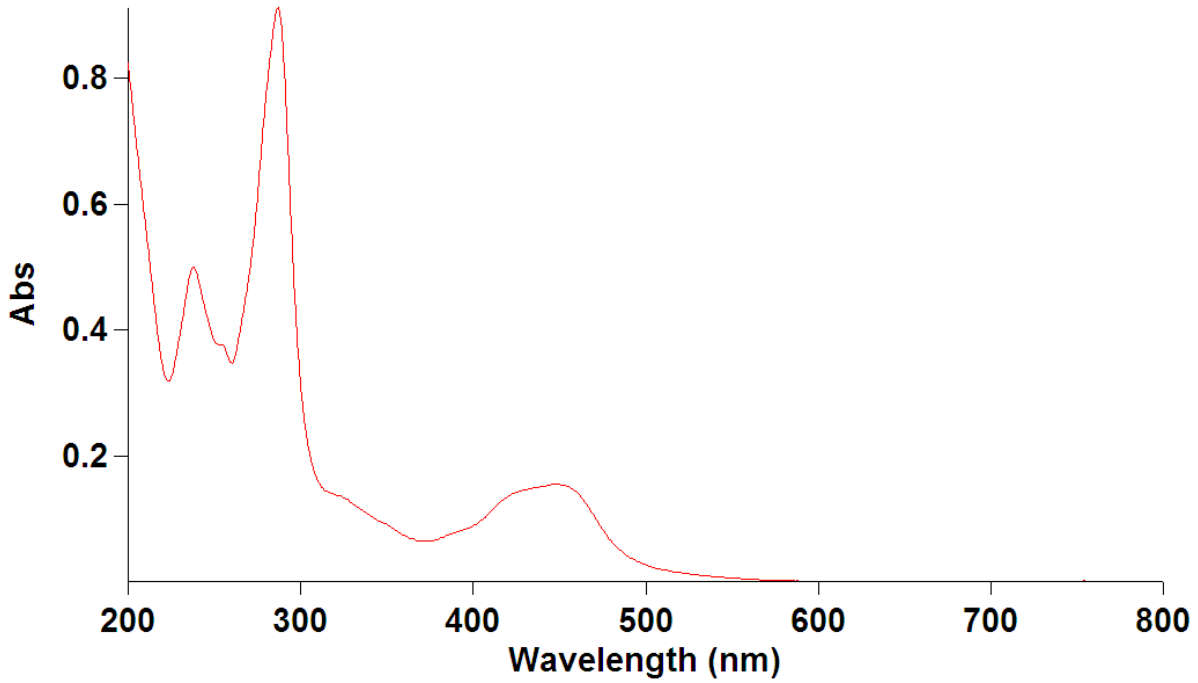

Fig 4.5 UV-Vis spectrum of $[Ru(bpy)_2(\mathbf{12})]^{2+}$, (**14**).

Table 4.2 Absorption Maxima[a] with Molar Absorption Coefficients[b] and Redox Potentials[c] of complex **14**.

Complex	λ_{max} (ε)	E_{ox}	E_{red1}	E_{red2}	E_{red3}	$\Delta E_{ox\text{-}red1}$
$[Ru(bpy)_3]^{2+}$	452 (13600)	+1.26	-1.33	-1.51	-1.79	2.59
14	454 (9800)	+1.13(90)	-1.45(90)	-	-	2.58

[a] In nanometres. [b] $M^{-1}cm^{-1}$. [c] In volts vs SCE.

An unusual result was obtained when **14** was examined by cyclic voltammetry (Fig 4.6). In the previously examined cyclic voltammograms, the lower solvent limit of the acetonitrile solution occurred around -1.8 V (± 100 mV or so). However, for a sample of **14** the solvent limit occurred around -1.5 V, and as such only one reduction peak can be fully observed (the second peak can be seen to start forming immediately before the solvent limit). The solution was further degassed with nitrogen to determine whether oxygen was the cause; unfortunately this was not the case. The shift in the solvent limit is reflected in a shift of the peaks; the ferrocene reference peak of **14** occurs at 460 mV, compared with that of **3** (443 mV, limit ~-1.75V) and **10** (273 mV, limit ~-2 V). This illustrates the importance of recording a reference peak such as ferrocene, as discrepancies in the measured potential can be corrected to a standard value. While the solvent limit has prevented us from observing the second and third reductions, the oxidation and reduction values obtained after correction vs a saturated calomel electrode (SCE, $[E^0(Fc/Fc^+) = 310$ mV]) are within the expected range of values. The cyclic voltammogram of complex **14** shows a reversible oxidation at +1.13 V, and a single reversible bpy-based reduction. Complex **14** is easier to oxidise than $[Ru(bpy)_3]^{2+}$, however it is the hardest of the complexes in this report to oxidise.

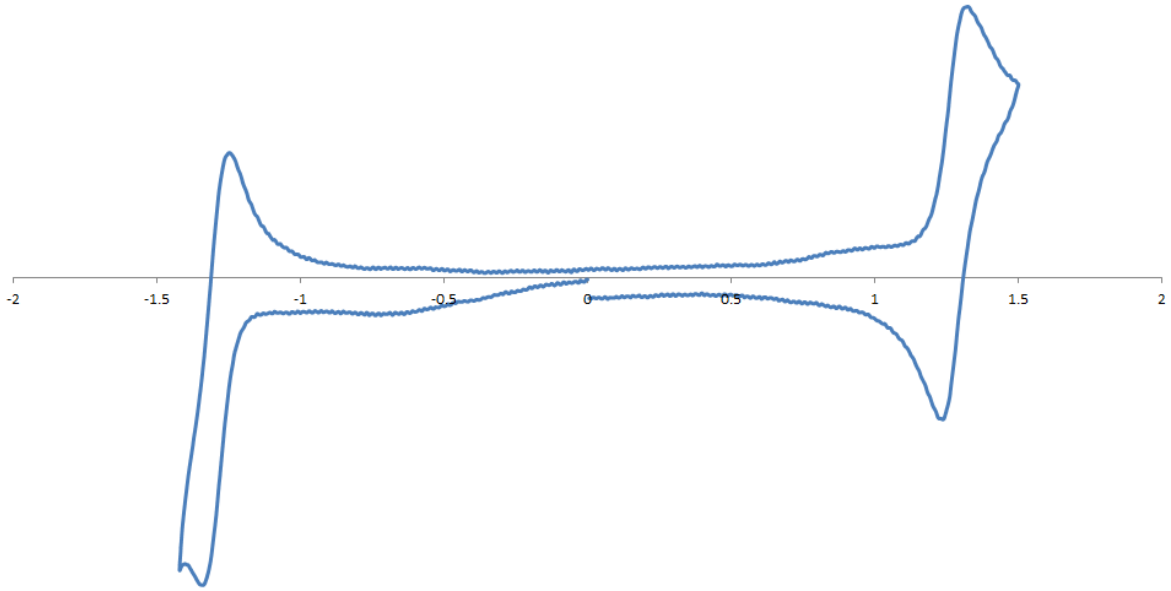

Fig 4.6 Cyclic Voltammogram of $[Ru(bpy)_2(\mathbf{12})]^{2+}$, (**14**), in volts vs silver wire.

Crystals of complex **14** were grown by slow diffusion of petroleum ether into a solution of acetone containing the complex. X-Ray diffraction was used to examine one of these crystals, and the resulting structure solved in the triclinic space group P-1. Contained in the asymmetric unit are one full cation, two hexafluorophosphate counteranions, and two acetone solvate molecules. Figure 4.7 shows a perspective view of the cation, with solvent and counteranions omitted for clarity. Ligand **12** has the potential to bind through either the N1 nitrogen or the N2 nitrogen (N3 in the previous NMR numbering). The mode of binding present here is through the N1 nitrogen, and was rationalised by a number of factors. The structure modelled in Figure 4.7 has the lowest R1 value, in addition to the most regular thermal parameters (when compared to the structure obtained by swapping the N3 and C1 atoms). As discussed previously, this structure is also in the best agreement with the observed ^{1}H NMR data.

With a bond length of [2.077(4) Å] between the ruthenium centre (Ru1) and the triazole nitrogen of **12** (N1), and a distance of [2.098(4) Å] between Ru1 and the pyridyl nitrogen (N3), we have seen an interesting shift between **3** and **14**. Where the pyridyl ring was once located closest to the metal centre, now the triazolopyridine is the closer of the two rings. This indicates that the triazole moiety associates more strongly with the metal centre, perhaps through greater donation from the electron rich triazole. The bite angle of ligand **12**

[77.85(15)°] is in good agreement with previously reported values, as are the bite angles of the ancillary bpy ligands [78.97(17)°, 78.83(15)°].

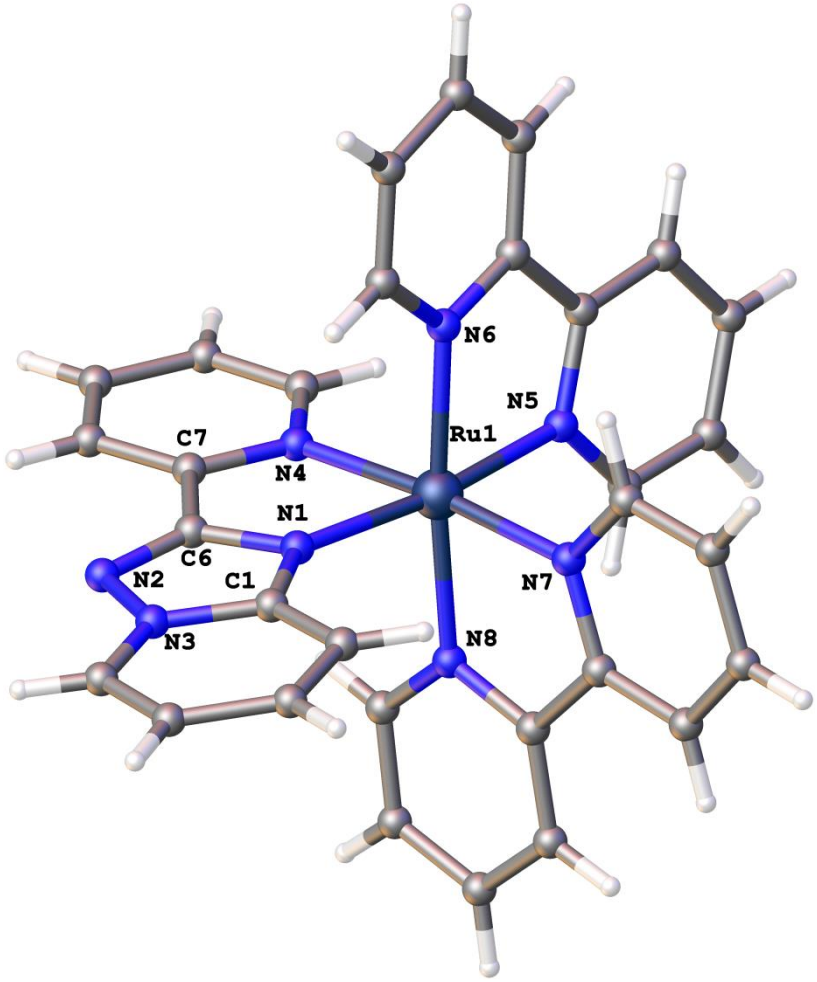

Fig 4.7 Perspective view of **14**, with partial labelling. Selected bond lengths (Å) and angles (°): Ru1-N1 2.077(4), Ru1-N4 2.098(4), Ru1-N5 2.047(4), Ru1-N6 2.065(4), Ru1-N7 2.056(4), Ru1-N8 2.055(4), N1-Ru1-N4 77.85(15), N5-Ru1-N6 78.97(17), N7-Ru1-N8 78.83(15), N1-C1 1.344(6), C1-N3 1.383(7), N3-N2 1.349(6), N2-C6 1.327(6), C6-N1 1.366(6), C6-C7 1.449(7), N1-C1-N3 108.4(4), C1-N3-N2 110.2(4), N3-N2-C6 103.0(4), N2-C6-N1 115.1(4), C6-N1-C1 103.3(4).

4.3.2 Synthesis of Bis(2,2'-bipyridine)[2,2'-bi[1,2,4]triazolo[1,5-a]pyridine]ruthenium(II) bis(hexafluorophosphate) (15)

A 1:1 mixture of 2,2'-bi[1,2,4]triazolo[1,5-a]pyridine and $Ru(bpy)_2Cl_2$ was added to a small volume of ethylene glycol and reacted via microwave irradiation (450 w, 3x2 minutes, with monitoring by TLC). After cooling, the PF_6^- salt was precipitated (addition of aqueous KPF_6) and recrystallised by the addition of excess diethyl ether to the complex dissolved in the minimum volume of acetonitrile, to give the pure product $[Ru(bpy)_2(\mathbf{13})](PF_6)_2$, (**15**), in moderate yield (69%) (Fig 4.8).

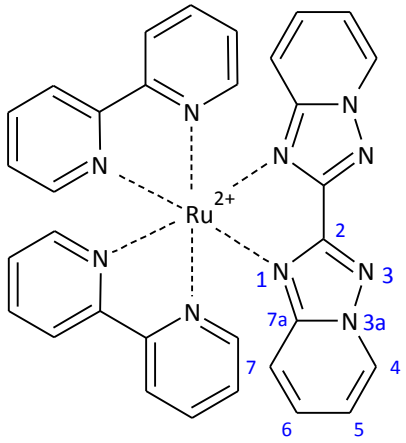

Fig 4.8 Structure of the cation of complex **15**.

Complex **15** contains a two-fold rotational axis of symmetry, and as such the 24 aromatic protons were seen as 12 proton signals; 8 from the two bpy ligands and 4 from ligand **13**. The chemical shifts and CIS values for **13** and **15** are shown in Table 4.3.

Table 4.3 ^{1}H NMR Chemical Shifts[a] and Coordination Induced Shifts[b] of the coordinated imidazolo[1,2-a]pyridine rings of 15 and the chemical shifts of 13.

	H4	H5	H6	H7
15	8.87	7.34	7.56	5.80
13	8.79	7.19	7.67	7.84
CIS	+0.08	+0.23	-0.11	-2.04

[a] Solvent: deuterated acetonitrile (MeCN-*d3*). [b] CIS = ($\delta_{complex}$ - δ_{ligand}).

Like **12**, ligand **13** can potentially bind to ruthenium through either the N1 or the N3 nitrogens. To compound matters, **13** could thus bind to give any one of three isomers. As

such, obtaining a clean, single isomer (^{1}H NMR) after minor purification was an excellent result. Proton signals were assigned by a COSY experiment, and the isomeric form (chelating through both N1 nitrogens) was assigned through the same rationalisation as for complex **14**; by examining and comparing the shifts and their resulting CIS values, and confirmed by X-ray diffraction analysis.

Figure 4.9 shows a clean, single isomer spectrum, with the bpy peaks in their characteristic positions and the peaks of **13** in a similar arrangement to previous complexes (Chapter 2). As has been discussed previously, anisotropic shielding leads to the large negative CIS value for H7, and the shift difference between the two bpy H6's.

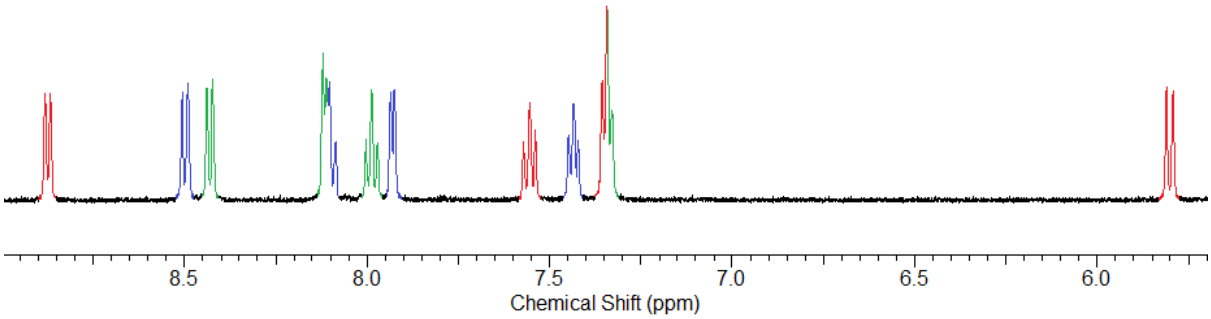

Fig 4.9 ^{1}H NMR spectrum of $[Ru(bpy)_2(\mathbf{13})]^{2+}$, (**15**), in MeCN-*d3*. Red = **13**, Blue/Green = bpy.

By replacing the pyridine moiety of **12** with the additional triazolopyridine of **13**, we have seen a red shift in absorbance (λ_{max} = 461 nm) (Fig 4.10). This places the HOMO-LUMO energy gap of the (M)d-(L)π* transition lower than both $[Ru(bpy)_3]^{2+}$ and **14**. This is also illustrated in the cyclic voltammogram of complex **15**; a $\Delta E_{ox\text{-}red1}$ value of +2.57 V is slightly lower than the comparative value of $[Ru(bpy)_3]^{2+}$ (+2.59 V). Figure 4.11 and Table 4.4 show the single reversible oxidation peak (+1.11 V), and the two reversible bpy-based reductions of this complex. Complex **15** is slightly harder to oxidise than the analogous imidazo[1,2-a]pyridines, and similarly hard to reduce. This indicates that, while more electron rich than pyridine, the triazolopyridine moiety may be less electron rich than the imidazo[1,2-a]pyridines; alternately, as was seen in the crystal structure of **14**, the triazolopyridine moiety may be a good donor for ruthenium.

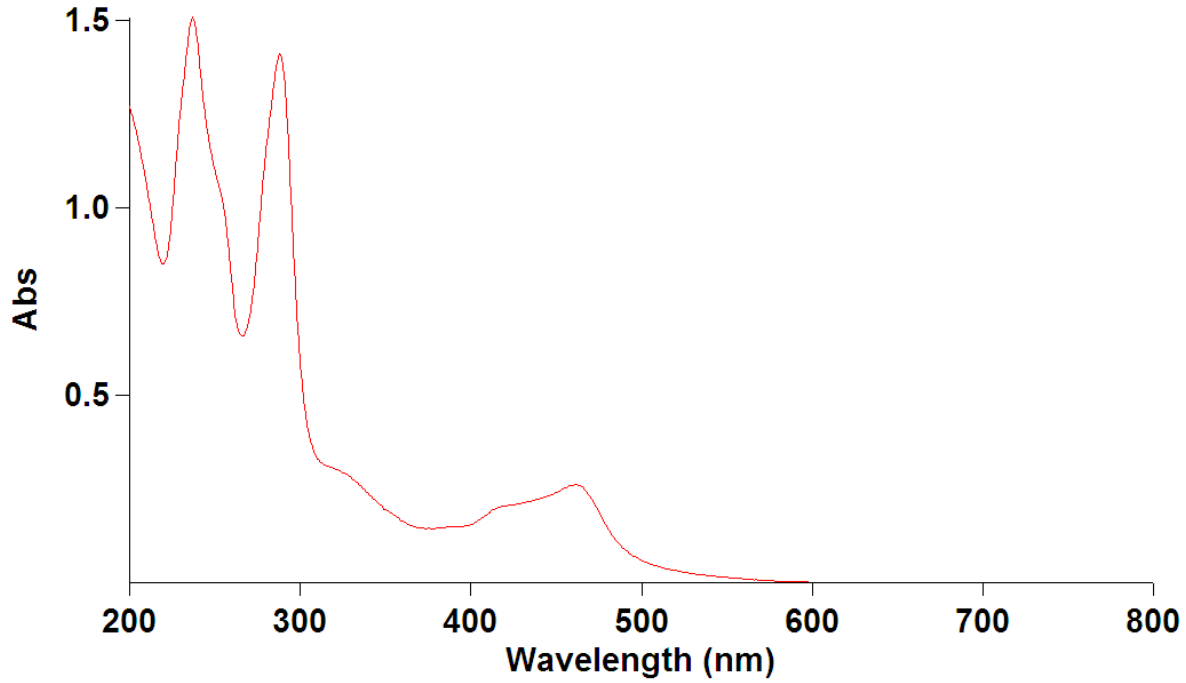

Fig 4.10 UV-Vis spectrum of $[Ru(bpy)_2(\mathbf{13})]^{2+}$, (**15**).

Table 4.4 Absorption Maxima[a] with Molar Absorption Coefficients[b] and Redox Potentials[c] of complex **15**.

Complex	λ_{max} (ε)	E_{ox}	E_{red1}	E_{red2}	E_{red3}	$\Delta E_{ox\text{-}red1}$
$[Ru(bpy)_3]^{2+}$	452 (13600)	+1.26	-1.33	-1.51	-1.79	2.59
15	461 (8600)	+1.11(83)	-1.46(81)	-1.68(89)	-	2.57

[a] In nanometres. [b] $M^{-1}cm^{-1}$. [c] In volts vs SCE.

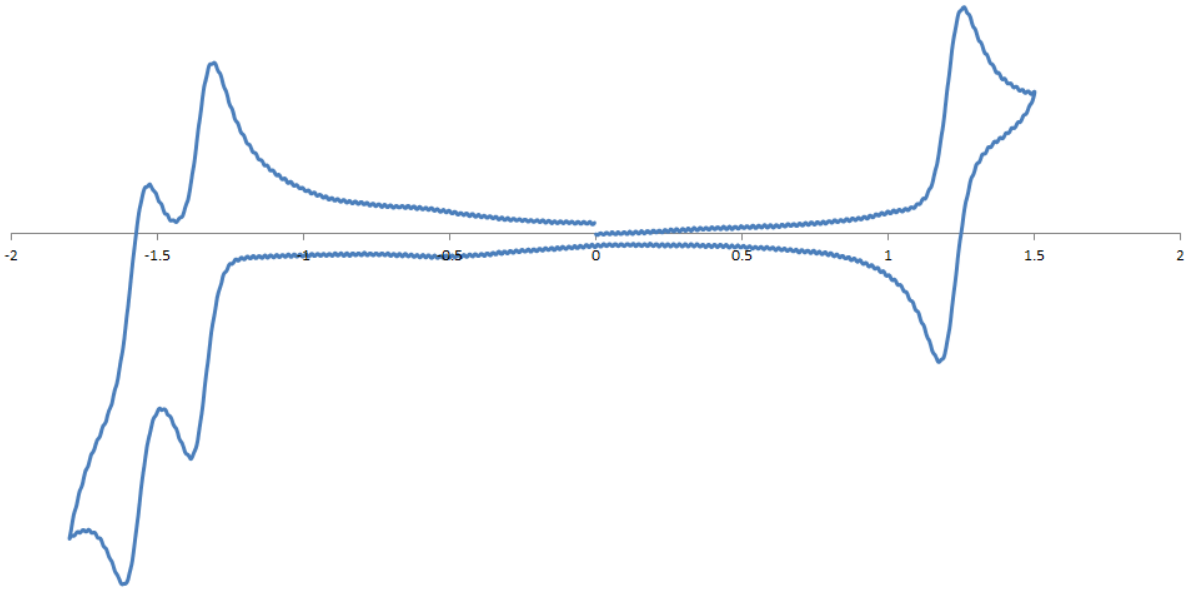

Fig 4.11 Cyclic Voltammogram of $[Ru(bpy)_2(\mathbf{13})]^{2+}$, (**15**), in volts vs silver wire.

Crystals of complex **15** were grown by slow diffusion of petroleum ether into a solution of the complex in acetone. One of the needle-like crystals formed was used for X-ray diffraction analysis. Crystallising in the monoclinic space group $P2_1/n$, the asymmetric unit of **15** contains a full cation, two hexafluorophosphate counteranions and two acetone solvate molecules. Figure 4.12 shows a perspective view of the cation, with the counteranions and solvate molecules omitted for clarity. The crystal structure of **15** shows both halves of ligand **13** coordinating through the N1 nitrogen. Like **14**, this structure gave the lowest R1 factor with the most regular thermal parameters, and is in best agreement with the observed ^{1}H NMR data. The Ru-N bond lengths of the coordinating nitrogens of **13** [2.093(3) Å and 2.109(3) Å] are slightly longer than those of the bpy ligands [2.046(3) Å to 2.069(3) Å], and comparable to those of the imidazolo[1,2-a]pyridine analogue (**4**, 2.100(3) Å and 2.115(3) Å). They are also slightly longer than the equivalent bond in **14** [2.059(13) Å], probably for steric reasons. The bite angle of **13** is 77.14(12)°, compared with those of bpy [79.03(13)° and 79.71(13)°]. For both bond lengths and bite angles, the results for bpy are in agreement with those previously reported for $[Ru(bpy)_3]^{2+}$ in the literature [2.056(6) Å, 78.7(2)°, 79.4(2)°].[47] The large CIS value for H7 can be further explained by examining the distances between protons and the centre of the ring into which they point. The average distance of the H7 proton to the adjacent pyridine ring was calculated as *ca.* 3.04Å, while the average bpy H6 to ligand pyridine was *ca.* 3.83Å, and the average bpy H6 to bpy pyridine was *ca.* 3.17Å. As the H7 proton is much closer to the centre of the pyridine ring, this proton experiences much greater shielding and is thus shifted further upfield.

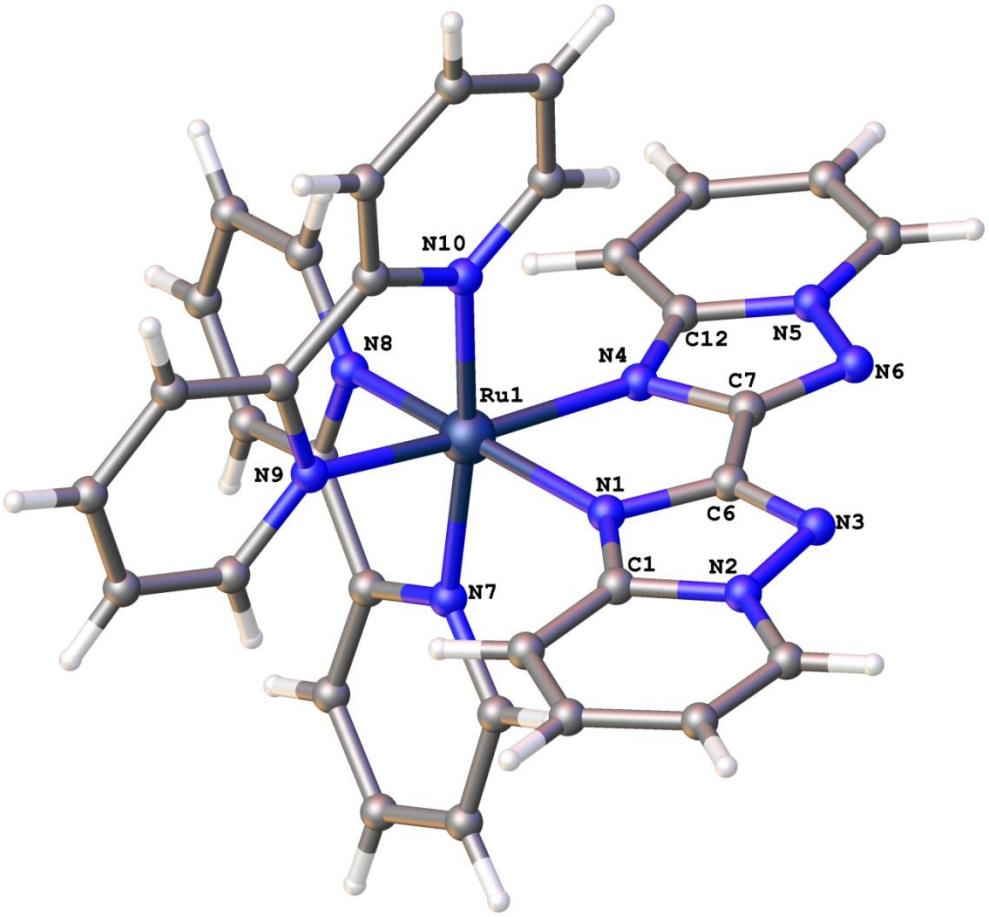

Fig 4.12 Perspective view of **15**, with partial labelling. Selected bond lengths (Å) and angles (°): Ru1-N1 2.093(3), Ru1-N4 2.109(3), Ru1-N7 2.056(3), Ru1-N8 2.046(3), Ru1-N9 2.055(3), Ru1-N10 2.069(3), N1-Ru1-N4 77.14(12), N7-Ru1-N8 79.71(13), N9-Ru1-N10 79.03(13), N1-C1 1.347(5), C1-N2 1.372(5), N2-N3 1.372(5), N3-C6 1.321(5), C6-N1 1.359(5), C6-C7 1.452(5), N1-C1-N2 107.7(3), C1-N2-N3 111.0(3), N2-N3-C6 101.6(3), N3-C6-N1 115.9(3), N1-C6-C7 115.1(3).

The preceding data on complex **15** all comes from a pure sample. The first sample synthesised was not so pure, for an interesting reason. First synthesised by refluxing in aqueous conditions, the ^{1}H NMR of this product indicated there were two compounds present, in an 8:1 ratio. Initially, it was assumed that this was an isomeric form, with ligand **13** binding through one or both of the N3 nitrogens. The mass spectrum of this product showed three ruthenium based peaks; the product **15** cation at *m/z* 325.0609, some $[Ru(bpy)_3]^{2+}$ impurity at *m/z* 285.0544, and an additional peak at *m/z* 365.0670. The identity of this additional peak was later revealed when crystals were grown. After a number of failed attempts to find and analyse a suitable crystal (consistently running into unit cell errors), a structure was finally obtained of the bis-ligand complex (2,2'-bipyridine)bis[2,2'-

bi[1,2,4]triazolo[1,5-a]pyridine]ruthenium(II)-bis(hexafluorophosphate) $[Ru(bpy)(\mathbf{13})_2]^{2+}$, (**16**) (Fig 4.13).

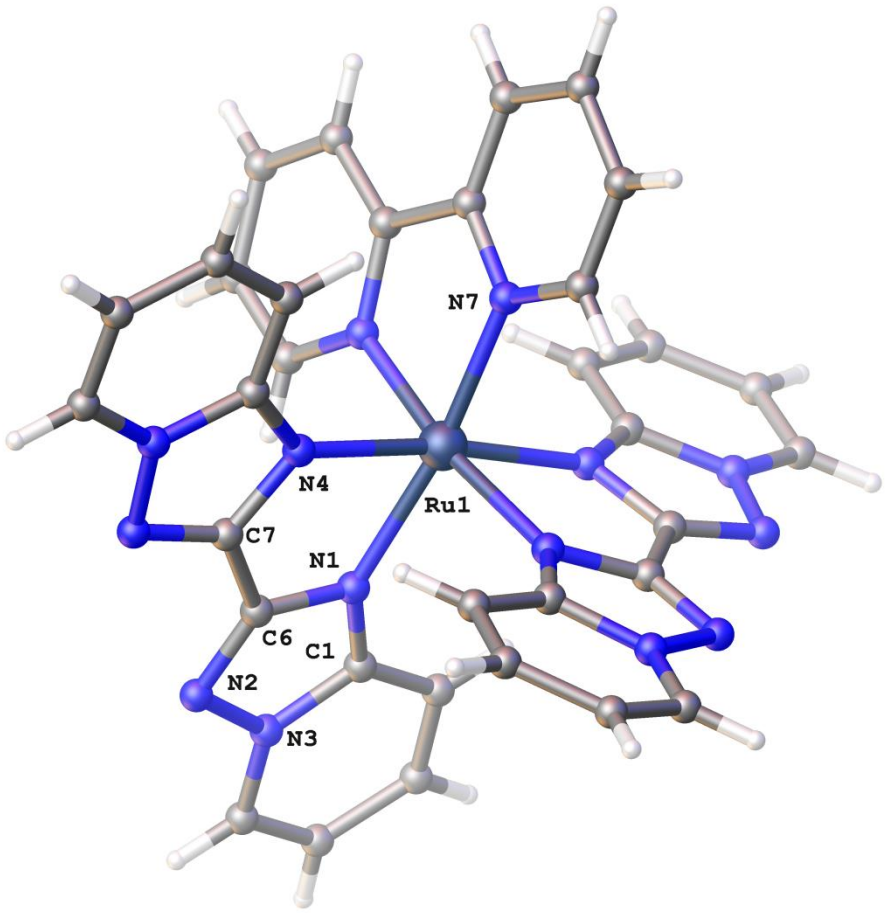

Fig 4.13 Perspective view of **16**, with partial labelling. Selected bond lengths (Å) and angles (°): Ru1-N1 2.118(5), Ru1-N4 2.096(5), Ru1-N7 2.035(5), N1-Ru1-N4 76.7(2), N7-Ru1-N7 79.1(3), N1-C1 1.360(7), C1-N3 1.355(9), N3-N2 1.393(9), N2-C6 1.324(9), C6-N1 1.331(8), C6-C7 1.449(10), N1-C1-N3 107.0(6), C1-N3-N2 111.4(5), N3-N2-C6 100.3(6), N2-C6-N1 116.9(6), C6-N1-C1 104.3(5).

Solving in the monoclinic space group of C2/c, the asymmetric unit of **16** contains half of a full cation, and one hexafluorophosphate counteranion. The structure also contained some amount of diffuse, poorly ordered solvate, which was removed using a solvent mask. Figure 4.13 shows a perspective view of the full cation, with counteranions omitted for clarity. Once again, the ligand binds exclusively through the N1 nitrogen, as this gave the lowest R1 value and the most regular thermal parameters. The bond lengths [2.118(5) and 2.096(5) Å] and bite angle [76.7(2)°] between the coordinating nitrogens of **13** and the central ruthenium are in excellent agreement with the values reported for **15** ([2.093(3) Å] and [2.109(3) Å],

[77.14(12)°]). The values for the ancillary bpy ligands are also in good agreement (**16** [2.035(5) Å, 79.1(3)°], **15** [2.046(3)-2.069(3) Å, 79.03(13)°, 79.71(13)°]).

This was a most unusual result, and it is currently unknown why this product forms. Exposure to light and a light mediated exchange of ligands was proposed as a potential cause. To test the effect of light on this reaction, a sample **15** was prepared in the dark, in aqueous reflux conditions. Care was taken to limit the subsequent workup's exposure to light, and the end result saw the presence of **16** in the mass spectrum. This would indicate there is some other process involved, either instead of or in addition to photoexcitation. Ligand **13** is not the only ligand that this occurs with either. When examining the aqueous complexation of **7** and **8**, peaks were also observed of their respective bis-ligand products. No bis-ligand complex was seen in the products of **12**, **1**, **2**, and **5**. It is possible that the resulting complexes were purified more successfully, or that the bis-ligand complex never formed for these ligands.

Chapter 5

Conclusion

This thesis described the synthesis and analysis of a number of little-studied heterocyclic chelating ligands, and offers a first look at the structure and properties of their ruthenium(II) complexes. The heterocycles examined all contain bridgehead nitrogens, and feature fused pyridine/imidazole or pyridine/triazole functionalities. All ligands were synthesised either using a new procedure or a literature preparation.

Ruthenium(II) complexes formed were of the type $[Ru(bpy)_2(L)]^{2+}$, as this allowed us to compare their properties with the well-studied $[Ru(bpy)_3]^{2+}$ complex. Complexes were formed by reacting ligands with $Ru(bpy)_2Cl_2$, either by aqueous reflux or microwave methods, with purification involving a mixture of column chromatography and recrystallisation. Each complex was analysed by a combination of multinuclear NMR, UV-visible absorption spectroscopy and cyclic voltammetry, and a number of trends were observed.

Coordination induced shifts (CIS) were used to examine the effect of coordination on the ligand; these values originate from the difference between the chemical shifts of the complexed ligand, and those of the free ligand. Small up- or downfield shifts are directly related to coordination, while larger shifts are brought about by other factors. The ^{1}H NMR of complexes **3**, **4**, **14** and **15** all contain a H7 proton with a large upfield shift; this is due to strong anisotropic shielding, a result of H7's close proximity to the centre of an adjacent pyridine system. This is further illustrated in the ^{1}H NMR spectra of complexes **9-11**; no large shifts are observed, as the shape of the ligands involved prevent these protons from experiencing the same anisotropic shielding.

In each ligand, at least one of the coordinating nitrogens is part of an azole system. Azoles are more electron rich than azines like pyridine, and the result of coordinating a more electron

rich ligand could be observed in the UV-visible spectra and electrochemical data. In general, these complexes absorbed at longer wavelengths than $[Ru(bpy)_3]^{2+}$, as the metal based HOMO had been raised and the electron rich ligands provided a lower LUMO. This could also be seen in the electrochemical data, as when compared to $[Ru(bpy)_3]^{2+}$, each complex was observed to be both easier to oxidise and harder to reduce.

In summary, the heterocyclic systems examined here all appear to possess similar properties when complexed as $[Ru(bpy)_2(L)]^{2+}$, relative to $[Ru(bpy)_3]^{2+}$. Complexes were easier to oxidise, harder to reduce, and absorb light at longer wavelengths, which all point towards the electron rich nature of the ligand. Future work on this topic may involve examining ligands containing the pyrazolo[1,5-a]pyridine moiety, substituted derivatives, or even ligands containing two of the examined (or related) moieties.

Chapter 6

Experimental

6.1 General Experimental

NMR spectra were recorded on Agilent 400-MR or Varian INOVA 500 spectrometers with a 5 mm or 3 mm probe and operating at 400MHz and 500MHz, respectively, for ^{1}H and 100MHz and 125MHz respectively for ^{13}C. Spectra recorded in $CDCl_3$ were referenced to an internal Me_4Si standard, while those recorded in CD_3CN were referenced against the respective solvent signal (1.94 ppm). ^{13}C NMR spectra were referenced against the solvent signals; $CDCl_3$ (77.0 ppm) and CD_3CN (117.3 ppm). 1D TOCSY and two dimensional experiments (COSY, HSQC, HMBC) were performed using standard pulse sequences and parameters available with the two spectrometers. Unless otherwise stated the value for the chemical shift is given to the centre of the multiplet.

Cyclic voltammetric measurements were made on an EG&G Princeton Model 362 Scanning Potentiostat. Measurements were made of acetonitrile solutions containing *ca.* 1 mM complex with 0.1 M tetrabutylammonium tetrafluoroborate as the supporting electrode, using a scan rate of 100 mVs^{-1} and a platinum working electrode (area 0.07 cm^{-2}), with a silver wire reference electrode and a gold wire auxiliary electrode. Ferrocene was used as an internal standard and the potentials given in the preceding chapters have been corrected versus the saturated calomel electrode [$E^0(Fc/Fc^+)$ = 0.31 V vs SCE]; the data presented in this experimental section are uncorrected (i.e. vs silver wire). Differential pulse voltammetry measurements were made on an Autolab PGSTAT302N potentiostat/galvanostat. Measurements were made of acetonitrile solutions containing *ca.* 0.1 mM complex, with supporting electrolyte, electrodes and ferrocene reference as above.

Mass Spectra (ESI) were recorded using a Bruker UHR-TOF MaXis 4G mass spectrometer with Dionex UltiMate 3000 UHPLC system. Samples were submitted dissolved in

acetonitrile. UV-Visible spectra were recorded on a Varian Cary 100 Bio UV-Visible spectrophotometer in acetonitrile. Infrared spectra were recorded from solids using a Bruker ALPHA FT-IR Spectrometer with Platinum-ATR attachment. Melting points were determined using an Electrothermal melting point apparatus and are uncorrected. The Chemistry Department, University of Otago, Dunedin, performed elemental analyses.

Unless otherwise stated, reagents were obtained from commercial sources and used as received. The following compounds were prepared using literature procedures: bis(2,2'-bipyridine)ruthenium(II) dichloride,[103,104] 2-(pyridin-2-yl)imidazo[1,2-a]pyridine (**1**),[42] 1-(pyridin-2-yl)imidazo[1,5-a]pyridine (**5**)[72], 1,2-diaminopyridinium tosylate.[102]

6.2 Preparation of Ligands

2-(Pyridin-2-yl)imidazo[1,2-a]pyridine (1)

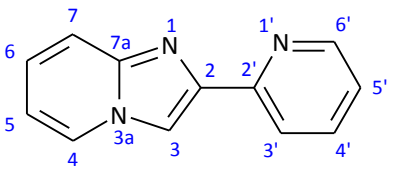

Following a procedure detailed by Cyransi *et al.*,[42] 2-aminopyridine (455 mg, 4.83 mmol), 2-acetylpyridine (0.25 mL, 2.23 mmol) and I_2 (627 mg, 2.47 mmol) were added to a pressure tube, and the mixture was stirred at 110°C for 4 hours. The temperature was subsequently reduced and the mixture continued to stir overnight. After cooling to room temperature, 5 mL H_2O and 10 mL NaOH (45%) was added. After transferring the solution to a beaker, the mixture was heated for a further 2 hours at 100°C. After dilution with DCM (25 mL), the solution was neutralised with HCl (10%). DCM extraction was followed by an alumina column eluting with 1:1 DCM:petroleum ether. ^{1}H NMR analysis of the obtained fractions revealed that a mixture of product and 2-aminopyridine had been recovered. As sufficient pure stocks of this ligand had been synthesised by a previous member of the group, further purification was not pursued.

M.p. 142-144°C.

ESI/MS: calc *m/z* for $C_{12}H_{10}N_3$ (MH^+) 196.0869; found 196.0870.

^{1}H NMR (400 MHz, CD_3CN): δ ppm 6.85 (1 H, t, *J* = 6.6 Hz, H5), 7.20 - 7.30 (2 H, m, H6, H5'), 7.54 (1 H, d, *J* = 9.0 Hz, H7), 7.82 (1 H, td, *J* = 7.6, 1.5 Hz, H4'), 8.15 (1 H, d, *J* = 8.2 Hz, H3'), 8.30 (1 H, s, H3), 8.34 (1 H, d, *J* = 7.0 Hz, H4), 8.58 (1 H, d, *J* = 4.7 Hz, H6').

^{1}H NMR (400 MHz, $CDCl_3$): δ ppm 6.81 (1 H, t, *J* = 6.8 Hz, H5), 7.17 - 7.25 (2 H, m, H6, H5'), 7.65 (1 H, d, *J* = 9.0 Hz, H7), 7.79 (1 H, td, *J* = 7.6, 1.5 Hz, H4'), 8.16 (1 H, d, *J* = 7.0 Hz, H4), 8.21 (1 H, d, *J* = 8.2 Hz, H3'), 8.26 (1 H, s, H3), 8.62 (1 H, d, *J* = 4.7 Hz, H6').

^{13}C NMR (100 MHz, $CDCl_3$): δ ppm 110.9 C3; 112.8 C5; 117.8 C7; 120.5 C3'; 122.7 C5'; 125.1 C6; 126.0 C4; 136.9 C4'; 145.5 C7a; 145.6 C2; 149.4 C6'; 152.8 C2'.

IR: ν cm^{-1} 3126, 1594, 1421, 1370, 1252, 1202, 1080, 760, 506, 435.

2,2'-Biimidazo[1,2-a]pyridine (2)

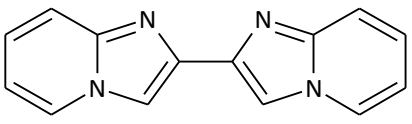

2-Aminopyridine (0.94 g, 0.01 mol) and 1,4-dibromo-2,3-butanedione (1.22 g, 5 mmol) were mixed in ethanol (30

mL) and stirred at room temperature over a weekend. The solution was reduced *in vacuo* and redissolved in water, before being basified with $NaHCO_3$. After extracting with EtOAc and washing with brine, the product was added to an alumina column eluting with EtOAc. The resulting fractions contained both 2-aminopyridine and product, and while reducing the volume *in vacuo* the desired product precipitated. Yield 14.2 mg (1%)

M.p. >300°C.

ESI/MS: calc *m/z* for $C_{14}H_{11}N_4$ (MH^+) 235.0978; found 235.0976.

^{1}H NMR (400 MHz, CD_3CN): δ ppm 6.83 (2 H, t, *J* = 6.8 Hz, H5), 7.22 (2 H, t, *J* = 7.8 Hz, H6), 7.51 (2 H, d, *J* = 9.0 Hz, H7), 8.15 (2 H, s, H3), 8.33 (2 H, d, *J* = 7.0 Hz, H4).

^{1}H NMR (400 MHz, $CDCl_3$): δ ppm 6.82 (2 H, t, *J* = 7.0 Hz, H5), 7.22 (2 H, t, *J* = 7.8 Hz, H6), 7.65 (2 H, d, *J* = 9.0 Hz, H7), 8.18 (2 H, d, *J* = 6.6 Hz, H4), 8.24 (2 H, s, H3).

^{13}C NMR (100 MHz, $CDCl_3$): δ ppm 110.0 C3; 112.7 C5; 117.1 C7; 125.3 C6; 125.99 C4; 140.1 C2; 145.4 C7a.

IR: ν cm^{-1} 3128, 1511, 1447, 1329, 1287, 1220, 1090, 914, 750, 426.

1-(Pyridin-2-yl)imidazo[1,5-a]pyridine (5)

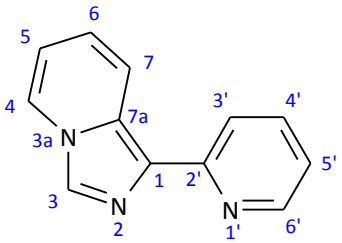

Following a procedure detailed by Grigg *et al.*,[72] di(2-pyridyl)ketone (0.686 g, 378 mmol) and glycine (0.288 g, 3.8 mmol) were added to a solution of methanol containing a few drops of glacial acetic acid. The reaction mixture was refluxed for 24 hours, and the solvent was subsequently removed *in vacuo*. The resulting residue was subjected to column chromatography (silica, EtOAc). Yield 28.7 mg (39%).

M.p. 106-109°C.

ESI/MS: calc *m/z* for $C_{12}H_{10}N_3$ (MH^+) 196.0869; found 196.0876.

^{1}H NMR (400 MHz, CD_3CN): δ ppm 6.71 (1 H, t, *J* = 6.8 Hz, H5), 6.97 (1 H, dd, *J* = 8.8, 6.8 Hz, H6), 7.12 (1 H, dd, *J* = 6.8, 5.2 Hz, H5'), 7.75 (1 H, td, *J* = 8.2, 1.0 Hz, H4'), 8.11 (1 H, d, *J* = 7.8 Hz, H3'), 8.16 (1 H, d, *J* = 7.0 Hz, H4), 8.22 (1 H, s, H3), 8.54 (1 H, d, *J* = 9.3 Hz, H7), 8.57 (1 H, d, *J* = 4.3 Hz, H6').

^{1}H NMR (400 MHz, $CDCl_3$): δ ppm 6.65 (1 H, t, *J* = 7.0 Hz, H5), 6.90 (1 H, t, *J* = 8.2 Hz, H6), 7.08 (1 H, ddd, *J* = 7.4, 5.0, 1.1 Hz, H5'), 7.71 (1 H, td, *J* = 7.7, 1.7 Hz, H4'), 7.95 (1 H, dd, *J* = 7.0, 0.7 Hz, H4), 8.10 - 8.17 (2 H, m, H3, H3'), 8.58 - 8.65 (2 H, m, H6', H7).

^{13}C NMR (100 MHz, $CDCl_3$): δ ppm 113.7 C5; 119.6 C3'; 120.4 C5'; 121.2 C6; 121.5 C7; 122.3 C4; 129.0 C7a; 130.2 C1; 136.3 C4'; 148.9 C6'; 154.9 C2'.
IR: ν cm^{-1} 1583, 1517, 1438, 1302, 1000, 969, 783, 741, 973, 421.

1,1'-Biimidazo[1,5-a]pyridine (6)

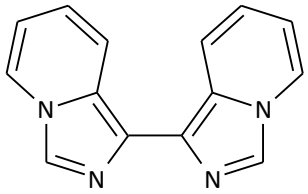

Attempted synthesis
2,2'-Pyridil (403 mg, 1.90 mmol) and glycine (441 mg, 5.87 mmol) were added to a solution of methanol (20 mL) containing a few drops of glacial acetic acid, and refluxed overnight. After cooling to room temperature, the solution was filtered to remove unreacted glycine, and was run through a silica column eluting EtOAc. ^{1}H NMR and ESI/MS was used to determine that there was none of the desired product present.

2,2'-Pyridil (1.06 g, 5 mmol), formaldehyde (0.60 g) and ammonium acetate (1.93 g, 25 mmol), were added to glacial acetic acid (50 mL) and refluxed under nitrogen for 5 hours. After cooling, the reaction mixture was neutralised by addition of NaCl and $NaHCO_3$. The mixture was extracted with DCM, and dried *in vacuo*. The solid was further extracted with petroleum ether. ^{1}H NMR and ESI/MS of the resulting oil indicated that there was none of the desired product present.

3-(Pyridin-2-yl)imidazo[1,5-a]pyridine (7)

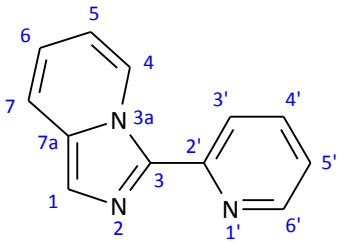

Ligand **7** was received with gratitude from Dr Chris Richardson.
M.p. 114-116°C.
ESI/MS: calc *m/z* for $C_{12}H_{10}N_3$ (MH^+) 196.0869; found 196.0869.
^{1}H NMR (400 MHz, CD_3CN): δ ppm 6.82 (1 H, t, *J* = 6.8 Hz, H5), 6.93 (1 H, dd, *J* = 9.0, 6.6 Hz, H6), 7.28 (1 H, dd, *J* = 6.8, 5.2 Hz, H5'), 7.57 (1 H, s, H1), 7.63 (1 H, d, *J* = 9.0 Hz, H7), 7.85 (1 H, t, *J* = 8.2 Hz, H4'), 8.31 (1 H, d, *J* = 8.2 Hz, H3'), 8.66 (1 H, d, *J* = 5.0 Hz, H6'), 9.95 (1 H, d, *J* = 7.4 Hz, H4).
^{1}H NMR (400 MHz, $CDCl_3$): δ ppm 6.74 (1 H, t, *J* = 7.0 Hz, H5), 6.87 (1 H, ddd, *J* = 9.0, 6.4, 0.9 Hz, H6), 7.20 (1 H, ddd, *J* = 7.4, 4.8, 0.9 Hz, H5'), 7.54 (1 H, d, *J* = 9.0 Hz, H7),

7.60 (1 H, s, H1), 7.78 (1 H, td, *J* = 7.8, 1.9 Hz, H4'), 8.36 (1 H, d, *J* = 7.8 Hz, H3'), 8.64 (1 H, d, *J* = 4.7 Hz, H6'), 9.97 (1 H, dd, *J* = 7.4, 0.7 Hz, H4).

^{13}C NMR (100 MHz, $CDCl_3$): δ ppm 113.6 C5; 118.0 C7; 120.2 C6; 120.8 C1; 121.6 C5'; 121.8 C3'; 126.0 C4; 132.9 C7a; 135.3 C3; 136.5 C4'; 148.1 C6'; 151.0 C2'.

IR: ν cm^{-1} 1584, 1493, 1419, 1353, 1250, 1008, 756, 739, 685, 424.

3,3'-Biimidazo[1,5-a]pyridine (8)

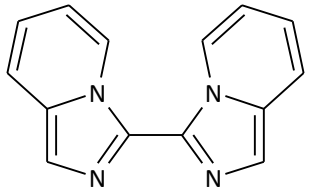

Ligand **8** was received with gratitude from Dr Chris Richardson.

M.p. 160-162°C.

ESI/MS: calc *m/z* for $C_{14}H_{11}N_4$ (MH^+) 235.0978; found 235.0974.

^{1}H NMR (400 MHz, CD_3CN): δ ppm 6.87 (2 H, t, *J* = 6.6 Hz, H5), 6.96 (2 H, t, *J* = 7.0 Hz, H6), 7.65 (2 H, s, H1), 7.67 (2 H, d, *J* = 9.3 Hz, H7), 9.82 (2 H, d, *J* = 7.8 Hz, H4).

^{13}C NMR (100 MHz, CD_3CN): δ ppm 113.4 C5; 118.0 C7; 119.8 C6; 120.2 C1; 124.8 C4; C3, C7a not recorded.

IR: ν cm^{-1} 1503, 1349, 1249, 1004, 905, 777, 732, 668, 556, 421.

2-(Pyridin-2-yl)[1,2,4]triazolo[1,5-a]pyridine (12)

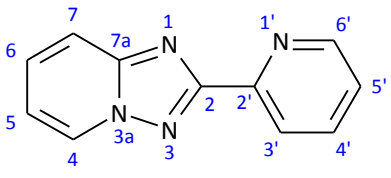

1,2-Diaminopyridinium tosylate (1.41 g, 5.00 mmol) and 2-pyridinecarboxaldehyde (1.07g, 10 mmol) were added to a solution of methanol (50 mL) containing potassium hydroxide (50 mmol). The reaction was stirred at room temperature and monitored by TLC. Once complete, the reaction mixture was evaporated under reduced pressure, before being redissolved in water (100 mL) and extracted with DCM (40 mL). After further washing the organic layer with water and brine, the product was dried over Na_2SO_4 and purified on an alumina plug eluting with 1:1 EtOAc:DCM. Yield 0.898 g (91%).

M.p. 166-167°C.

ESI/MS: calc *m/z* for $C_{11}H_9N_4$ (MH^+) 197.0821; found 197.0826.

^{1}H NMR (400 MHz, CD_3CN): δ ppm 7.15 (1 H, t, *J* = 7.0 Hz, H5), 7.44 (1 H, dd, *J* = 7.4, 4.7 Hz, H5'), 7.63 (1 H, t, *J* = 7.4 Hz, H6), 7.79 (1 H, d, *J* = 9.0 Hz, H7), 7.91 (1 H, td, *J* = 7.6, 1.5 Hz, H4'), 8.31 (1 H, d, *J* = 8.2 Hz, H3'), 8.74 (2 H, m, H4, H6').

^{1}H NMR (400 MHz, $CDCl_3$): δ ppm 7.06 (1 H, td, *J* = 6.8, 1.1 Hz, H5), 7.39 (1 H, ddd, *J* = 7.4, 4.7, 1.1 Hz, H5'), 7.55 (1 H, ddd, *J* = 7.0, 5.4, 1.5 Hz, H6), 7.81 (1 H, d, *J* = 9.0 Hz, H7), 7.86 (1 H, td, *J* = 7.7, 1.7 Hz, H4'), 8.34 (1 H, d, *J* = 7.8 Hz, H3'), 8.68 (1 H, d, *J* = 6.6 Hz, H4), 8.81 (1 H, d, *J* = 5.1 Hz, H6')

^{13}C NMR (100 MHz, $CDCl_3$): δ ppm 114.26 C5; 116.9 C7; 122.6 C3'; 124.5 C5'; 128.7 C4; 129.8 C6; 136.8 C4'; 149.7 C2'; 150.2 C6'; 151.7 C7a; 163.5 C2.

IR: ν cm^{-1} 1635, 1503, 1411, 1385, 1332, 1262, 1152, 759, 737, 429

2,2'-Bi[1,2,4]triazolo[1,5-a]pyridine (13)

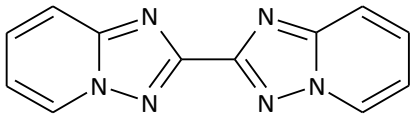

Sodium ethoxide (0.55 g, 8.08 mmol) was dissolved in 25 mL EtOH. 1,2-Diaminopyridinium tosylate (1.51 g, 5.37 mmol) was added to the solution and stirred for five minutes, at which point diethyl oxalate (0.40 mL, 2.66 mmol) was added and the mixture was brought to reflux for five hours. Water (70 mL) was added to the hot solution, and the mixture was left to crystallise overnight. The crystals were filtered and washed with water, before being dried *in vacuo*. Yield 0.27 g (43%).

M.p. >300°C.

ESI/MS: calc *m/z* for $C_{12}H_9N_6$ (MH^+) 237.0883; found 237.0880.

^{1}H NMR (400 MHz, CD_3CN): δ ppm 7.19 (2 H, t, *J* = 6.8 Hz, H5), 7.67 (2 H, t, *J* = 7.8 Hz, H6), 7.84 (2 H, d, *J* = 9.0 Hz, H7), 8.79 (2 H, d, *J* = 6.6 Hz, H4).

^{1}H NMR (400 MHz, $CDCl_3$): δ ppm 7.11 (2 H, t, *J* = 6.8 Hz, H5), 7.59 (2 H, t, *J* = 7.8 Hz, H6), 7.87 (2 H, d, *J* = 9.0 Hz, H7), 8.71 (2 H, d, *J* = 7.0 Hz, H4).

^{13}C NMR (100 MHz, $CDCl_3$): δ ppm 114.5 C5; 117.3 C7; 128.7 C4; 130.0 C6; 151.7 C7a; 157.6 C2.

IR: ν cm^{-1} 3076, 1634, 1495, 1324, 1257, 956, 915,763, 739, 440.

6.3 Preparation of Complexes

Bis(2,2'-bipyridine)[2-(pyridin-2-yl)imidazo[1,2-a]pyridine]ruthenium(II)-bis(hexafluorophosphate) (3)

2-(Pyridin-2-yl)imidazo[1,2-a]pyridine (**1**) (26 mg, 0.13mmol) and $Ru(bpy)_2Cl_2$ (63 mg, 0.13 mmol) were refluxed in 3:1 ethanol:water (8 mL) overnight. After cooling, the reaction mixture was concentrated to dryness *in vacuo*. The residue was redissolved in the minimum amount of water, filtered to remove unreacted ligand, and the complex was precipitated out by the addition of an aqueous solution of KPF_6. The aqueous solution was extracted with DCM, dried over Na_2SO_4, and loaded onto a column of alumina eluting 95:5 DCM:MeOH. The fractions were dried *in vacuo.* Yield 110 mg (95%).

M.p. >300°C.

EA: found C:44.93, H:3.56, N:9.94. Calculated for $[(bpy)_2Ru(L)](PF_6)_2 \cdot 2(C_3H_6O)$ C:44.98, H:3.68, N:9.66.

ESI/MS: calc *m/z* for $C_{32}H_{25}N_7Ru$ (M^{2+}) 304.5606; found 304.5609

^{1}H NMR (400 MHz, CD_3CN): δ ppm 5.59 (1 H, d, *J* = 9.0 Hz, H7), 7.00 (1 H, t, *J* = 7.0 Hz, H5), 7.11 (1 H, t, *J* = 7.8 Hz, H6), 7.25 (1 H, t, *J* = 7.0 Hz, H5'), 7.30 - 7.45 (4 H, m, bpy H5), 7.55 (1 H, d, *J* = 5.4 Hz, H6'), 7.75 (1 H, d, *J* = 5.4 Hz, bpy H6), 7.86 (1 H, d, *J* = 5.4 Hz, bpy H6), 7.88 - 7.93 (2 H, m, bpy H6), 7.93 - 8.11 (5 H, m, H4', bpy H4), 8.23 (1 H, d, *J* = 8.2 Hz, H3'), 8.43 (2 H, d, *J* = 8.2 Hz, H4, bpy H3), 8.49 (3 H, d, *J* = 8.2 Hz, bpy H3), 8.65 (1 H, s, H3)

^{13}C NMR (100 MHz, CD_3CN) δ ppm 112.9 C7; 114.1 C3; 114.8 C5; 122.3 C6'; 123.9, 124.0_1, 124.0_4, 124.2 bpy C6; 125.6 C4'; 127.2_5, 127.2_9, 127.4, 127.5 bpy C4; 129.3 C4; 129.6 C6; 137.1, 137.2_8, 137.3_3, 137.6, 137.8 bpy C5/C5'; 143.5 C2; 146.3 C7a; 151.4 C3'; 151.6, 152.1, 152.2, 152.3 bpy C3; 153.7 C2'; 157.1_8, 157.2_0, 157.9_5, 158.0_4 bpy C2.

IR: ν cm^{-1} 1708, 1605, 1464, 1445, 1223, 1122, 828, 759, 554, 422

UV-Vis (CH_3CN)

λ_{max} 463 nm, ε = 8000 $cm^{-1}M^{-1}$, log ε = 3.904

λ_{max}(sh) 427 nm, ε = 7600 $cm^{-1}M^{-1}$, log ε = 3.883

λ_{max}(sh) 326 nm, ε = 11900 $cm^{-1}M^{-1}$, log ε = 4.075

λ_{max} 289 nm, ε = 49300 $cm^{-1}M^{-1}$, log ε = 4.693

λ_{max}(sh) 255 nm, ε = 22600 $cm^{-1}M^{-1}$, log ε = 4.354

λ_{max} 241 nm, ε = 28400 $cm^{-1}M^{-1}$, log ε = 4.453

E^0 (CH_3CN) Ru^{2+}/Ru^{3+} +1.12(78) V; E^0_{red} -1.34(81) V; E^0_{red} -1.56(83) V; E^0 Fc/Fc^+ +443(75) mV

Bis(2,2'-bipyridine)[2,2'-biimidazo[1,2-a]pyridine]ruthenium(II)-bis(hexafluorophosphate) (4)

2,2'-Biimidazo[1,2-a]pyridine (**2**) (9.90 mg, 0.042 mmol) and $Ru(bpy)_2Cl_2$ (21.50 mg, 0.044 mmol) in ethylene glycol (8 mL) were reacted via microwave irradiation (450 W, 3x2 minutes). After cooling, the solution was diluted with distilled water and filtered through a Celite plug. The complex was precipitated by the addition of an aqueous solution of KPF_6, and the settled precipitate was filtered. The complex was recrystallised by the addition of excess diethyl ether to an acetonitrile solution. Yield 26.1 mg (66%).

M.p. >300°C.

EA: found C:41.03, H:2.91, N:11.20. Calculated for $[(bpy)_2Ru(L)](PF_6)_2 \cdot 3H_2O$ C:41.18, H:3.25, N:11.30.

ESI/MS: calc *m/z* for $C_{34}H_{26}N_8Ru$ (M^{2+}) 324.0661; found 324.0665

^{1}H NMR (400 MHz, CD_3CN): δ ppm 5.48 (2 H, d, *J* = 9.0 Hz, H7), 6.95 (2 H, t, *J* = 6.6 Hz, H5), 7.06 (2 H, t, *J* = 7.8 Hz, H6), 7.30 (2 H, t, *J* = 6.8 Hz, bpy H5), 7.40 (2 H, t, *J* = 6.6 Hz, bpy H5), 7.89 - 7.99 (6 H, m, bpy H6, bpy H4, bpy H6), 8.06 (2 H, t, *J* = 8.0 Hz, bpy H4), 8.38 - 8.45 (6 H, m, H4, bpy H3, H3), 8.48 (2 H, d, *J* = 8.2 Hz, bpy H3)

^{13}C NMR (100 MHz, CD_3CN): δ ppm 111.1 C3; 112.6 C7; 114.3 C5; 123.7, 124.0 bpy C3; 127.1, 127.3 bpy C5; 128.9 C6; 129.0 C4; 136.7, 137.2 bpy C4; 138.7 C2; 146.1 C7a; 152.1, 152.6 bpy C6; 157.4, 158.9 bpy C2.

IR: ν cm^{-1} 1638, 1510, 1464, 1445, 1422, 1316, 831, 758, 556, 423

UV-Vis (CH_3CN)

λ_{max} 480 nm, ε = 8100 $cm^{-1}M^{-1}$, log ε = 3.910

λ_{max}(sh) 430 nm, ε = 5400 $cm^{-1}M^{-1}$, log ε = 3.731

λ_{max}(sh) 365 nm, ε = 8400 $cm^{-1}M^{-1}$, log ε = 3.924

λ_{max} 329 nm, ε = 17600 $cm^{-1}M^{-1}$, log ε = 4.245

λ_{max} 291 nm, ε = 60300 $cm^{-1}M^{-1}$, log ε = 4.780

λ_{max}(sh) 252 nm, ε = 36200 $cm^{-1}M^{-1}$, log ε = 4.559

λ_{max} 238 nm, ε = 43500 $cm^{-1}M^{-1}$, log ε = 4.638

λ_{max}(sh) 223 nm, ε = 40000 $cm^{-1}M^{-1}$, log ε = 4.602

E^0 (CH_3CN) Ru^{2+}/Ru^{3+} +895(80) mV; E^0_{red} -1.50(70) V; E^0_{red} -1.73(85) V; E^0 Fc/Fc^+ +313(85) mV.

Bis(2,2'-bipyridine)[1-(pyridin-2-yl)imidazo[1,5-a]pyridine]ruthenium(II)-bis(hexafluorophosphate) (9)

1-(Pyridin-2-yl)imidazo[1,5-a]pyridine (**5**) (24.7 mg, 0.127 mmol) and $Ru(bpy)_2Cl_2$ (62.4 mg, 1.29 mmol) were refluxed in 3:1 ethanol:water (8 mL) overnight. After cooling, the reaction mixture was concentrated to dryness *in vacuo*. The residue was redissolved in the minimum amount of water, filtered to remove unreacted ligand, and the complex was precipitated out by the addition of an aqueous solution of KPF_6. The aqueous solution was extracted with DCM, dried over Na_2SO_4, and loaded onto a column of alumina eluting with 95:5 DCM:MeOH. The fractions were dried *in vacuo.* Yield 102 mg (90%).

M.p. ~215-218°C.

EA: found C:42.75, H:2.97, N:10.95. Calculated for $[(bpy)_2Ru(L)](PF_6)_2$ C:42.77, H:2.80, N:10.91.

ESI/MS: calc *m/z* for $C_{32}H_{25}N_7Ru$ (M^{2+}) 304.5606; found 304.5610

^{1}H NMR (400 MHz, CD_3CN): δ ppm 6.97 (1 H, t, *J* = 7.2 Hz, H5), 7.10 (1 H, t, *J* = 6.4 Hz, H5'), 7.31 - 7.42 (5 H, m, H6, bpy H5), 7.53 (1 H, d, *J* = 5.8 Hz, H6'), 7.80 (1 H, d, *J* = 5.8 Hz, bpy H6), 7.82 - 7.86 (2 H, m, bpy H6), 7.87 (1 H, s, H3), 7.88 - 7.95 (2 H, m, bpy H6, H4'), 7.98 - 8.07 (4 H, m, bpy H4), 8.08 - 8.13 (2 H, m, H7, H4), 8.16 (1 H, d, *J* = 8.2 Hz, H3'), 8.43 - 8.53 (4 H, m, bpy H3)

^{13}C NMR (100 MHz, CD_3CN): δ ppm 115.0 C5; 116.2 C7; 120.3 C3' 123.0 C5'; 123.7, 123.8, 123.9, 124.1 bpy C3; 124.6 C4; 126.2 C6; 126.9, 127.1, 127.2_8, 127.3_4 bpy C5; 128.9 C1; 130.2 C7a; 137.2_4, 137.2_8, 137.3_1, 137.5 C4'/bpy H4; 151.2 H6'; 151.7, 151.8, 151.9, 152.2 bpy C6; 154.4 C2'; 157.1, 157.2, 157.5, 157.7 bpy C2; C3 not recorded

IR: ν cm^{-1} 1603, 1528, 1445, 1259, 1092, 1017, 821, 758, 554, 423

UV-Vis (CH_3CN)

λ_{max} 462 nm, ε = 10000 $cm^{-1}M^{-1}$, log ε = 3.999

λ_{max}(sh) 423 nm, ε = 9400 $cm^{-1}M^{-1}$, log ε = 3.972

λ_{max}(sh) 361 nm, ε = 14700 $cm^{-1}M^{-1}$, log ε = 4.167

λ_{max} 347 nm, ε = 15000 $cm^{-1}M^{-1}$, log ε = 4.174

λ_{max} 288 nm, ε = 55800 $cm^{-1}M^{-1}$, log ε = 4.747

λ_{max} 254 nm, ε = 21400 $cm^{-1}M^{-1}$, log ε = 4.330

λ_{max} 244 nm, ε = 22700 $cm^{-1}M^{-1}$, log ε = 4.357

E^0 (CH_3CN) Ru^{2+}/Ru^{3+} +1.16(90) V; E^0_{red} -1.41(102) V; E^0_{red} -1.61(100) V; E^0 Fc/Fc^+ +388(85) mV.

Bis(2,2'-bipyridine)[3-(pyridin-2-yl)imidazo[1,5-a]pyridine]ruthenium(II)-bis(hexafluorophosphate) (10)

3-(Pyridin-2-yl)imidazo[1,5-a]pyridine (**7**) (12.8 mg, 0.0656 mmol) and $Ru(bpy)_2Cl_2$ (32.1 mg, 0.0663 mmol) in ethylene glycol (8 mL) were reacted via microwave irradiation (450 W, 3x2 minutes). After cooling, the solution was diluted with distilled water and filtered through a Celite plug. The complex was precipitated by the addition of an aqueous solution of KPF_6, and the precipitate was filtered. The complex was recrystallised by the addition of excess diethyl ether to an acetonitrile solution. Yield 34.6 mg (58%).

M.p. ~212-215°C.

EA: found C:40.35, H:2.68, N:10.37. Calculated for $[(bpy)_2Ru(L)](PF_6)_2 \cdot 3H_2O$ C:40.35, H:3.28, N:10.29.

ESI/MS: calc *m/z* for $C_{32}H_{25}N_7Ru$ (M^{2+}) 304.5606; found 304.5603

^{1}H NMR (400 MHz, CD_3CN): δ ppm 7.03 (1 H, s, H1), 7.15 - 7.26 (3 H, m, H5, H6', H6), 7.30 - 7.43 (4 H, m, bpy H5), 7.63 (1 H, d, *J* = 9.0 Hz, H7), 7.68 - 7.74 (2 H, m, H6', bpy H6), 7.79 (1 H, d, *J* = 5.4 Hz, bpy H6), 7.83 (2 H, d, *J* = 5.4 Hz, bpy H6), 7.97 - 8.09 (5 H, m, bpy H4, H4'), 8.31 (1 H, d, *J* = 8.6 Hz, H3'), 8.43 - 8.52 (4 H, m, bpy H3), 8.83 (1 H, d, *J* = 7.0 Hz, H4)

^{13}C NMR (100 MHz, CD_3CN-d_3) δ ppm 116.8 C5; 118.1 C7; 120.7 C3'; 121.9 C1; 123.4, 123.5, 123.7, 123.8, 124.0, 124.2, 124.3 C4/C6/C5'/bpy C3; 127.0, 127.2, 127.3_6, 127.3_9 bpy C5; 135.2 C7a; 137.3_3, 137.3_8, 137.4_1, 137.6 bpy C4/C4'; 149.4 C2'; 151.8, 152.0_5, 152.1_4, 152.4 bpy C6/C6'; 157.0, 157.4, 157.5 bpy C2; C3 not recorded.

IR: ν cm^{-1} 1602, 1479, 1444, 1422, 1370, 827, 763, 687, 556, 422.

UV-Vis (CH_3CN)

λ_{max} 454 nm, ε = 11500 $cm^{-1}M^{-1}$, log ε = 4.065

λ_{max}(sh) 424 nm, ε = 11500 $cm^{-1}M^{-1}$, log ε = 4.059

λ_{max}(sh) 380 nm, ε = 14400 $cm^{-1}M^{-1}$, log ε = 4.160

λ_{max}(sh) 359 nm, ε = 15600 $cm^{-1}M^{-1}$, log ε = 4.193

λ_{max}(sh) 318 nm, ε = 21100 $cm^{-1}M^{-1}$, log ε = 4.323

λ_{max} 288 nm, ε = 56700 $cm^{-1}M^{-1}$, log ε = 4.754

λ_{max}(sh) 253 nm, ε = 21200 $cm^{-1}M^{-1}$, log ε = 4.327

λ_{max} 243 nm, ε = 28300 $cm^{-1}M^{-1}$, log ε = 4.452

E^0 (CH_3CN) Ru^{2+}/Ru^{3+} +1.07(84) V; E^0_{red} -1.50(83) V; E^0_{red} -1.71(88) V; E^0 Fc/Fc^+ +273(75) mV.

Bis(2,2'-bipyridine)[3,3'-biimidazo[1,5-a]pyridine]ruthenium(II)-bis(hexafluorophosphate) (11)

3,3'-Biimidazo[1,5-a]pyridine (**8)** (15.2 mg, 0.034 mmol) and $Ru(bpy)_2Cl_2$ (32.1 mg, 0.062 mmol) in ethylene glycol (8 mL) were reacted via microwave irradiation (450 W, 4x2 minutes). After cooling, the solution was diluted with distilled water and filtered through a Celite plug. The complex was precipitated by the addition of an aqueous solution of KPF_6, and the precipitate was filtered. The complex was recrystallised by the addition of excess diethyl ether to an acetonitrile solution, and subjected to column chromatography (alumina, DCM:MeOH 95:5). Yield 5.2 mg (16%).

M.p. >300°C.

ESI/MS: calc *m/z* for $C_{34}H_{26}N_8Ru$ (M^{2+}) 324.0661; found 324.0660

^{1}H NMR (400 MHz, CD_3CN): δ ppm 6.96 (2 H, s, H1), 6.99 - 7.10 (4 H, m, H5, H6), 7.33 (2 H, t, *J* = 6.2 Hz, bpy H5), 7.38 (2 H, t, *J* = 6.2 Hz, bpy H5), 7.51 (2 H, d, *J* = 8.2 Hz, H7), 7.84 (2 H, d, *J* = 5.0 Hz, bpy H6), 7.88 (2 H, d, *J* = 5.0 Hz, bpy H6), 7.98 (2 H, t, *J* = 7.8 Hz, bpy H4), 8.03 (2 H, t, *J* = 7.8 Hz, bpy H4), 8.45 (1 H, d, *J* = 8.2 Hz, bpy H3), 8.48 (1 H, d, *J* = 7.8 Hz, bpy H3), 8.61 (1 H, d, *J* = 6.6 Hz, H4)

^{13}C NMR (100 MHz, CD_3CN): δ ppm 116.0 C5; 118.1 C7; 121.9 C6; 122.3 C1; 123.5, 123.7 bpy C3; 124.5 C4; 126.8, 127.1 bpy C5; 133.7 C7a; 137.0 bpy C4; 152.2, 152.3 bpy C6; C3, bpy C2 not recorded.

IR: ν cm^{-1} 1602, 1445, 1422, 1363, 1242, 829, 759, 728, 555, 420

UV-Vis (CH_3CN)

λ_{max} 469 nm, ε = 9208.29 $cm^{-1}M^{-1}$, log ε = 3.964

λ_{max} 428 nm, ε = 11200.97 $cm^{-1}M^{-1}$, log ε = 4.049

λ_{max} 347 nm, ε = 20058.43 $cm^{-1}M^{-1}$, log ε = 4.302

λ_{max} 290 nm, ε = 45675.30 $cm^{-1}M^{-1}$, log ε = 4.660

E^0 (CH_3CN) Ru^{2+}/Ru^{3+} +987 mV; E^0_{red} -1.36 V; E^0_{red} -1.59 V; E^0 Fc/Fc^+ +418 mV

Bis(2,2'-bipyridine)[2-(pyridin-2-yl)[1,2,4]triazolo[1,5-a]pyridine]ruthenium(II)-bis(hexafluorophosphate) (14)

2-(Pyridin-2-yl)[1,2,4]triazolo[1,5-a]pyridine (**12**) (12.5 mg, 0.066 mmol) and $Ru(bpy)_2Cl_2$ (32.1 mg, 0.063 mmol) in ethylene glycol (8 mL) were reacted via microwave irradiation (450 W, 3x2 minutes). After cooling, the solution was diluted with distilled water and filtered through a Celite plug. The complex was precipitated by the addition of an aqueous solution of KPF_6, and the precipitate was filtered. The complex was recrystallised by the addition of excess diethyl ether to an acetonitrile solution. Yield 38.8 mg (66%).

M.p. >300°C.

EA: found C:40.67, H:2.63, N:12.10. Calculated for $[(bpy)_2Ru(L)](PF_6)_2 \cdot H_2O$ C:40.58, H:2.86, N:12.21.

ESI/MS: calc *m/z* for $C_{31}H_{24}N_8Ru$ (M^{2+}) 305.0582; found 305.0578

^{1}H NMR (500 MHz, CD_3CN): δ ppm 5.88 (1 H, d, *J* = 9.0 Hz, H7), 7.28 - 7.48 (6 H, m, H5, bpy H5, H5'), 7.53 (1 H, t, *J* = 8.0 Hz, H6), 7.68 (1 H, d, *J* = 5.6 Hz, H6'), 7.76 (1 H, d, *J* = 5.6 Hz, bpy H6), 7.85 (1 H, d, *J* = 4.8 Hz, bpy H6), 7.91 (1 H, d, *J* = 5.6 Hz, bpy H6), 8.00 (1 H, t, *J* = 7.8 Hz, bpy H4), 8.02 - 8.14 (6 H, m, bpy H4, bpy H6, H4'), 8.43 (1 H, d, *J* = 8.3 Hz, bpy H3), 8.46 - 8.54 (4 H, m, H3', bpy H3), 8.83 (1 H, d, *J* = 6.8 Hz, H4).

^{13}C NMR (125 MHz, CD_3CN): δ ppm 112.9 C7; 117.1 C5; 123.90, 124.0, 124.1, 124.2_9, 124.3_2 C3'/bpy C3; 127.3, 127.4, 127.5, 127.7, 128.3 C5'/bpy C5; 131.3 C4; 134.2 C6; 137.4_8, 137.5_4, 137.6, 138.0, 138.5 C4'/bpy C4; 149.5 C2'; 151.0 C7a; 151.7, 151.9, 152.3, 152.5, 152.6 C6'/bpy C6; 157.0_7,157.1_2, 158.0, 158.1 bpy C2; C2 not recorded.

IR: ν cm^{-1} 1638, 1605, 1448, 1427, 1330, 1160, 831, 757, 556, 421

UV-Vis (CH_3CN)

λ_{max} 454 nm, ε = 9800 $cm^{-1}M^{-1}$, log ε = 3.991

λ_{max}(sh) 426 nm, ε = 9200 $cm^{-1}M^{-1}$, log ε = 3.963

λ_{max} 287 nm, ε = 58200 $cm^{-1}M^{-1}$, log ε = 4.765

λ_{max} 238 nm, ε = 32100 $cm^{-1}M^{-1}$, log ε = 4.507

E^0 (CH_3CN) Ru^{2+}/Ru^{3+} +1.28(90) V; E^0_{red} -1.30(90) V; E^0 Fc/Fc^+ +460(80) mV.

Bis(2,2'-bipyridine)[2,2'-bi[1,2,4]triazolo[1,5-a]pyridine]ruthenium(II)-bis(hexafluorophosphate) (15)

2,2'-Bi[1,2,4]triazolo[1,5-a]pyridine (**13**) (15.67 mg, 0.066 mmol) and $Ru(bpy)_2Cl_2$ (31.31 mg, 0.065 mmol) in ethylene glycol (8 mL) were reacted via microwave irradiation (450 W, 3x2 minutes). After cooling, the solution was diluted with distilled water and filtered through a Celite plug. The complex was precipitated by the addition of an aqueous solution of KPF_6, and the precipitate was filtered. The complex was recrystallised by the addition of excess diethyl ether to an acetonitrile solution. Yield 41.95 mg (69%).

M.p. >300°C.

EA: found C: 40.32, H: 2.54, N: 14.46. Calculated for $[(bpy)_2Ru(L)](PF_6)_2 \cdot H_2O$ C: 40.14, H: 2.74, N: 14.63.

ESI/MS: calc *m/z* for $C_{32}H_{24}N_{10}Ru$ (M^{2+}) 325.0613; found 325.0611.

^{1}H NMR (500 MHz, CD_3CN): δ ppm 5.80 (2 H, d, *J* = 9.0 Hz, H7), 7.32 - 7.37 (4 H, m, H5, bpy H5), 7.43 (2 H, t, *J* = 6.6 Hz, bpy H5), 7.56 (2 H, t, *J* = 8.0 Hz, H6), 7.93 (2 H, d, *J* = 5.8 Hz, bpy H6), 7.99 (2 H, t, *J* = 7.7 Hz, bpy H4), 8.07 - 8.15 (4 H, m, bpy H4, bpy H6), 8.43 (2 H, d, *J* = 8.3 Hz, bpy H3), 8.50 (2 H, d, *J* = 8.3 Hz, bpy H3), 8.87 (2 H, d, *J* = 6.8 Hz, H4).

^{13}C NMR (125 MHz, CD_3CN): δ ppm 112.9 C7; 117.5 C5; 123.8, 124.1 bpy C3; 127.3, 127.5 bpy C5; 131.6 C4; 134.5 C6; 137.3, 137.8 bpy C4; 151.0 C7a; 152.8, 153.0 bpy C6; 157.2, 158.9 bpy C2; C2 not recorded.

IR: ν cm^{-1} 1638, 1517, 1446, 1386, 1347, 1261, 828, 758, 555, 429.

UV-Vis (CH_3CN)

λ_{max} 461 nm, ε = 8600 $cm^{-1}M^{-1}$, log ε = 3.933

λ_{max}(sh) 417 nm, ε = 6700 $cm^{-1}M^{-1}$, log ε = 3.823

λ_{max}(sh) 322 nm, ε = 10000 $cm^{-1}M^{-1}$, log ε = 3.997

λ_{max} 288 nm, ε = 56200 $cm^{-1}M^{-1}$, log ε = 4.750

λ_{max} 237 nm, ε = 67100 $cm^{-1}M^{-1}$, log ε = 4.827

E^0 (CH_3CN) Ru^{2+}/Ru^{3+} +1.22(83) V; E^0_{red} -1.34(81) V; E^0_{red} -1.57(89) V; E^0 Fc/Fc^+ +423(65) mV

Chapter 7

Crystallography

Tables 7.1 and 7.2 list crystal data and X-ray experimental details for the six crystal structures discussed in this thesis. Selected bond lengths and angles are listed in the discussion of the structures, and the remaining distances and angles, as well as atom coordinates, anisotropic displacement parameters and hydrogen atom coordinates, are available from the Department of Chemistry, University of Canterbury.

All measurements were made on an Oxford-Agilent SuperNova diffractometer with focused microsource Cu Kα [λ = 1.54184 Å] or Mo Kα [0.71073 Å] radiation, and ATLAS CCD area detector. CrysAlisPro was used for the data collection and data processing. The structures were solved by direct methods using SHELXS[105] and refined, using SHELXL,[106] on F^2 using all data. The latest version Olex2[107] was used for visualisation. The hydrogen atoms were included in calculated positions and assigned isotropic displacement parameters 1.3 times the isotropic equivalent of their carrier atoms. Graphical presentation of crystallographic data was prepared using Olex2.

Table 7.1 Crystal Data and X-ray Experimental Details for **3**, **4** and **9**

Compound	**3**	**4**	**9**
Empirical formula	$C_{36.5}H_{32.5}F_{12}N_7O_{1.5}P_2Ru$	$C_{74.3}H_{64.6}F_{24}N_{16}O_{2.1}P_4Ru_2$	$C_{32}H_{25}F_{12}N_7P_2Ru$
Formula weight	984.20	1997.24	898.60
Temperature (K)	120	120	120
Crystal system	Monoclinic	Monoclinic	Monoclinic
Space group	C2/c	C2/c	$P2_1/n$
Unit cell dimensions: a/Å	22.8380(4)	24.1893(4)	10.739(2)
Unit cell dimensions: b/Å	14.3814(2)	13.8139(2)	19.539(4)
Unit cell dimensions: c/Å	24.2375(4)	24.8135(4)	15.769(3)
Unit cell dimensions: α/°	90	90	90
Unit cell dimensions: β/°	91.0244(16)	96.4497(16)	94.94(3)
Unit cell dimensions: γ/°	90	90	90
Volume ($Å^3$)	7959.4(2)	8238.9(2)	3296.7(11)
Z	8	4	4
Density (calculated) (mg/mm^3)	1.643	1.610	1.810
μ/mm^{-1}	4.845	4.690	0.679
F(000)	3956	4013	1792
Crystal size (mm^3)	0.32 × 0.26 × 0.19	0.22 × 0.10 × 0.09	0.42 × 0.05 × 0.04
Radiation	CuKα (λ = 1.54184)	CuKα (λ = 1.54184)	MoKα (λ = 0.71073)
Theta range for data collection (°)	7.2 to 141.9°	7.1 to 133.9°	3.3 to 52.7°
Reflections collected	27189	15482	22904
Independent reflections [R(int)]	7661 (0.0359)	7358 (0.0281)	6646 (0.0345)
Data / restraints / parameters	7661 / 0 / 564	7358 / 0 / 572	6646 / 0 / 487
Goodness-of-fit on F^2	1.091	1.067	1.050
R1 [I>=2σ (I)]	0.0735	0.0446	0.0377
wR2 [all data]	0.1730	0.1308	0.1003

Table 7.2 Crystal Data and X-ray Experimental Details for **14**, **15** and **16**

Compound	**14**	**15**	**16**
Empirical formula	$C_{37}H_{36}F_{12}N_8O_2P_2Ru$	$C_{38}H_{36}F_{12}N_{10}O_2P_2Ru$	$C_{34}H_{24}F_{12}N_{14}P_2Ru$
Formula weight	1015.75	1055.78	1019.68
Temperature (K)	120	120	120
Crystal system	Triclinic	Monoclinic	Monoclinic
Space group	P-1	$P2_1/n$	C2/c
Unit cell dimensions: a/Å	12.2146(4)	10.20205(13)	25.0157(4)
Unit cell dimensions: b/Å	13.2552(5)	10.01137(13)	14.16880(19)
Unit cell dimensions: c/Å	14.3847(5)	41.2557(7)	14.0775(3)
Unit cell dimensions: α/°	63.309(3)	90	90
Unit cell dimensions: β/°	81.771(3)	96.7094(14)	102.3682(17)
Unit cell dimensions: γ/°	88.771(3)	90	90
Volume ($Å^3$)	2056.97(13)	4184.85(11)	4873.86(14)
Z	2	4	4
Density (calculated) (mg/mm^3)	1.640	1.676	1.390
μ/mm^{-1}	4.723	4.685	3.999
F(000)	1024	2128	2032
Crystal size (mm^3)	0.18 × 0.15 × 0.05	0.50 × 0.09 × 0.02	0.19 × 0.10 × 0.10
Radiation	CuKα (λ = 1.54184)	CuKα (λ = 1.54184)	CuKα (λ = 1.54184)
Theta range for data collection (°)	6.9 to 147.4°	8.6 to 133.9°	7.2 to 147.9°
Reflections collected	39335	26405	42488
Independent reflections [R(int)]	8212 (0.0836)	7439 (0.0358)	4918 (0.0525)
Data / restraints / parameters	8212 / 0/ 563	7439 / 6 / 590	4918 / 0 / 285
Goodness-of-fit on F^2	1.181	1.143	1.127
Final R indexes [I>=2σ (I)]	R1 = 0.0546, wR2 = 0.1610	R1 = 0.0475, wR2 = 0.1126	R1 = 0.0777, wR2 = 0.1891
Final R indexes [all data]	R1 = 0.0758, wR2 = 0.1655	R1 = 0.0498, wR2 = 0.1136	R1 = 0.0791, wR2 = 0.1897

Chapter 8

References

(1) Kauffman, G. B. *Alfred Werner: Founder of Coordination Chemistry*; Springer-Verlag, 1966.

(2) Ernst, K.-H.; Wild, F. R. W. P.; Blacque, O.; Berke, H. *Angew. Chem., Int. Ed.* **2011**, *50*, 10780.

(3) Wilkinson, G.; Dillard, R. D.; McCleverty, J. A. *Comprehensive Coordination Chemistry* Pergamon, Oxford, 1987.

(4) *Comprehensive Coordination Chemistry II*; McCleverty, J. A.; Meyer, T. J., Eds.; Elsevier, 2003.

(5) Joule, J. A.; Mills, K. *Heterocyclic Chemistry*; 5th Edition ed.; Wiley-Blackwell, 2010.

(6) Herlocker, D. W.; Rosenthal, M. R. *Inorg. Chim. Acta* **1970**, *4*, 501.

(7) Blau, F. *Chem. Ber.* **1888**, *21*, 1077.

(8) Constable, E. C. *Adv. Inorg. Chem.* **1989**, *34*, 1.

(9) Elfring, W. H., Jr.; Crosby, G. A. *J. Am. Chem. Soc.* **1981**, *103*, 2683.

(10) Thompson, D. W.; Ito, A.; Meyer, T. J. *Pure Appl. Chem.* **2013**, *85*, 1257.

(11) Juris, A.; Balzani, V.; Barigelletti, F.; Campagna, S.; Belser, P.; Von Zelewsky, A. *Coord. Chem. Rev.* **1988**, *84*, 85.

(12) Paris, J. P.; Brandt, W. W. *J. Am. Chem. Soc.* **1959**, *81*, 5001.

(13) Montalti, M.; Credi, A.; Prodi, L.; Gandolfi, M. T.; Editors *Handbook of Photochemistry - Third Edition*; CRC Press LLC, 2006.

(14) Stoll, T.; Gennari, M.; Fortage, J.; Castillo, C. E.; Rebarz, M.; Sliwa, M.; Poizat, O.; Odobel, F.; Deronzier, A.; Collomb, M.-N. *Angew. Chem., Int. Ed.* **2014**, *53*, 1654.

(15) Constable, E. C.; Steel, P. J. *Coord. Chem. Rev.* **1989**, *93*, 205.

(16) Richardson, C.; Fitchett, C. M.; Keene, F. R.; Steel, P. J. *Dalton Trans.* **2008**, 2534.

(17) Downard, A. J.; Steel, P. J.; Steenwijk, J. *Aust. J. Chem.* **1995**, *48*, 1625.

(18) Richardson, C.; Steel, P. J. *Aust. J. Chem.* **2002**, *55*, 783.

(19) Richardson, C.; Steel, P. J. *Acta Crystallographica, Section C: Crystal Structure Communications* **2001**, *57*, 197.

(20) Richardson, C.; Steel, P. J.; D'Alessandro, D. M.; Junk, P. C.; Keene, F. R. *J. Chem. Soc., Dalton Trans.* **2002**, 2775.

(21) Richardson, C.; Steel, P. J. *Inorg. Chem. Comm.* **2007**, *10*, 884.

(22) Richardson, C.; Steel, P. J. *Dalton Trans.* **2003**, 992.

(23) Richardson, C.; Keene, F. R.; Steel, P. J. *Aust. J. Chem.* **2008**, *61*, 183.

(24) Pradhan, B.; Das, S. *Chem. Mater.* **2008**, *20*, 1209.

(25) Fitchett, C. M.; Keene, F. R.; Richardson, C.; Steel, P. J. *Inorg. Chem. Comm.* **2008**, *11*, 595.

(26) Chichibabin, A. E. *Ber. Dtsch. Chem. Ges. B* **1925**, *58B*, 1704.

(27) Mosby, W. L. *Heterocyclic Systems with Bridge-head Nitrogen Atoms*; Interscience Pubs.: New York, 1961; Vol. 1.

(28) Roe, A. M. *J. Chem. Soc.* **1963**, 2195.

(29) Hand, E. S.; Paudler, W. W. *J. Org. Chem.* **1978**, *43*, 2900.

(30) Adib, M.; Sheikhi, E.; Rezaei, N. *Tetrahedron Lett.* **2011**, *52*, 3191.

(31) Mishra, S.; Ghosh, R. *Synthesis* **2011**, 3463.

(32) Chernyak, N.; Gevorgyan, V. *Angew. Chem., Int. Ed.* **2010**, *49*, 2743.

(33) Liu, P.; Fang, L.-s.; Lei, X.; Lin, G.-q. *Tetrahedron Lett.* **2010**, *51*, 4605.

(34) Reddy, B. V. S.; Sivaramakrishna Reddy, P.; Jayasudhan Reddy, Y.; Yadav, J. S. *Tetrahedron Lett.* **2011**, *52*, 5789.

(35) Elhakmaoui, A.; Gueiffier, A.; Milhavet, J.-C.; Blache, Y.; Chapat, J.-P.; Chavignon, O.; Teulade, J.-C.; Snoeck, R.; Andrei, G.; De Clercq, E. *Bioorg. Med. Chem. Lett.* **1994**, *16*, 1937.

(36) Lhassani, M.; Chavignon, O.; Chezal, J.-M.; Teulade, J.-C.; Chapat, J.-P.; Snoeck, R.; Andrei, G.; Balzarini, J.; De Clercq, E.; Gueiffier, A. *Eur. J. Med. Chem.* **1999**, *34*, 271.

(37) Lacerda, R. B.; de Lima, C. K. F.; da Silva, L. L.; Romeiro, N. C.; Miranda, A. L. P.; Barreiro, E. J.; Fraga, C. A. M. *Bioorg. Med. Chem.* **2009**, *17*, 74.

(38) Langer, S. Z.; Arbilla, S.; Benavides, J.; Scatton, B. *Adv. Biochem. Psychopharmacol.* **1990**, *46*, 61.

(39) Harrison, T. S.; Keating, G. M. *CNS Drugs* **2005**, *19*, 65.

(40) Mizushige, K.; Ueda, T.; Yukiiri, K.; Suzuki, H. *Cardiovasc. Drug Rev.* **2002**, *20*, 163.

(41) Bagdi, A. K.; Rahman, M.; Santra, S.; Majee, A.; Hajra, A. *Adv. Synth. Catal.* **2013**, *355*, 1741.

(42) Stasyuk, A. J.; Banasiewicz, M.; Cyranski, M. K.; Gryko, D. T. *J. Org. Chem.* **2012**, *77*, 5552.

(43) Chandra Mohan, D.; Reddy Donthiri, R.; Nageswara Rao, S.; Adimurthy, S. *Adv. Synth. Catal.* **2013**, *355*, 2217.

(44) Aries, R. 1968, p FR1536351.

(45) Ortoleva, G. *Gaz. Chim. Ital.* **1899**, *29*, 503.

(46) King, L. C. *J. Am. Chem. Soc.* **1944**, *66*, 894.

(47) Rillema, D. P.; Jones, D. S.; Levy, H. A. *J. Chem. Soc., Chem. Commun.* **1979**, 849.

(48) Eggleston, D. S.; Goldsby, K. A.; Hodgson, D. J.; Meyer, T. J. *Inorg. Chem.* **1985**, *24*, 4573.

(49) Bower, J. D.; Ramage, G. R. *J. Chem. Soc.* **1955**, 2834.

(50) Shibahara, F.; Kitagawa, A.; Yamaguchi, E.; Murai, T. *Org. Lett.* **2006**, *8*, 5621.

(51) Tahara, S.; Shibahara, F.; Maruyama, T.; Murai, T. *Chem. Commun.* **2009**, 7009.

(52) Shibahara, F.; Sugiura, R.; Yamaguchi, E.; Kitagawa, A.; Murai, T. *J. Org. Chem.* **2009**, *74*, 3566.

(53) Shibahara, F.; Yamaguchi, E.; Kitagawa, A.; Imai, A.; Murai, T. *Tetrahedron* **2009**, *65*, 5062.

(54) Yamaguchi, E.; Shibahara, F.; Murai, T. *Chem. Lett.* **2011**, *40*, 939.

(55) Bluhm, M. E.; Ciesielski, M.; Gorls, H.; Döring, M. *Angew. Chem., Int. Ed.* **2002**, *41*, 2962.

(56) Bluhm, M. E.; Folli, C.; Pufky, D.; Kroeger, M.; Walter, O.; Döring, M. *Organometallics* **2005**, *24*, 4139.

(57) Moulin, A.; Garcia, S.; Martinez, J.; Fehrentz, J.-A. *Synthesis* **2007**, 2667.

(58) Ostermeier, M.; Limberg, C.; Ziemer, B.; Karunakaran, V. *Angew. Chem., Int. Ed.* **2007**, *46*, 5329.

(59) Niyomura, O.; Yamaguchi, Y.; Tamura, S.; Minoura, M.; Okamoto, Y. *Chem. Lett.* **2011**, *40*, 449.

(60) Wang, J.; Mason, R.; VanDerveer, D.; Feng, K.; Bu, X. R. *J. Org. Chem.* **2003**, *68*, 5415.

(61) Wang, J.; Dyers, L., Jr.; Mason, R., Jr.; Amoyaw, P.; Bu, X. R. *J. Org. Chem.* **2005**, *70*, 2353.

(62) Siddiqui, S. A.; Potewar, T. M.; Lahoti, R. J.; Srinivasan, K. V. *Synthesis* **2006**, 2849.

(63) Crawforth, J. M.; Paoletti, M. *Tetrahedron Lett.* **2009**, *50*, 4916.

(64) Salassa, L.; Garino, C.; Albertino, A.; Volpi, G.; Nervi, C.; Gobetto, R.; Hardcastle, K. I. *Organometallics* **2008**, *27*, 1427.

(65) Nakamura, H.; Yamamoto, H.; Idemitsu Kosan Co., Ltd., Japan . 2005, p WO2005043630A1.

(66) Burstein, C.; Lehmann, C. W.; Glorius, F. *Tetrahedron* **2005**, *61*, 6207.

(67) Alcarazo, M.; Roseblade, S. J.; Cowley, A. R.; Fernandez, R.; Brown, J. M.; Lassaletta, J. M. *J. Am. Chem. Soc.* **2005**, *127*, 3290.

(68) Hahn, F. E. *Angew. Chem., Int. Ed.* **2006**, *45*, 1348.

(69) Kim, D.; Wang, L.; Hale, J. J.; Lynch, C. L.; Budhu, R. J.; MacCoss, M.; Mills, S. G.; Malkowitz, L.; Gould, S. L.; DeMartino, J. A.; Springer, M. S.; Hazuda, D.; Miller, M.; Kessler, J.; Hrin, R. C.; Carver, G.; Carella, A.; Henry, K.; Lineberger, J.; Schleif, W. A.; Emini, E. A. *Bioorg. Med. Chem. Lett.* **2005**, *15*, 2129.

(70) Davey, D.; Erhardt, P. W.; Lumma, W. C., Jr.; Wiggins, J.; Sullivan, M.; Pang, D.; Cantor, E. *J. Med. Chem.* **1987**, *30*, 1337.

(71) Ford, N. F.; Browne, L. J.; Campbell, T.; Gemenden, C.; Goldstein, R.; Gude, C.; Wasley, J. W. F. *J. Med. Chem.* **1985**, *28*, 164.

(72) Grigg, R.; Kennewell, P.; Savic, V.; Sridharan, V. *Tetrahedron* **1992**, *48*, 10423.

(73) Hajos, G.; Riedl, Z. *Sci. Synth.* **2002**, *12*, 613.

(74) Alvarez, C. M.; Alvarez-Miguel, L.; Garcia-Rodriguez, R.; Miguel, D. *Dalton Trans.* **2012**, *41*, 7041.

(75) Abushanab, E. *Tetrahedron Lett.* **1971**, 1441.

(76) Huang, C.; Giokaris, A.; Gevorgyan, V. *Chem. Lett.* **2011**, *40*, 1053.

(77) Garino, C.; Ruiu, T.; Salassa, L.; Albertino, A.; Volpi, G.; Nervi, C.; Gobetto, R.; Hardcastle, K. I. *Eur. J. Inorg. Chem.* **2008**, 3587.

(78) Richardson, C. Ph.D., Canterbury University, 1999.

(79) Fitchett, C. M.; Richardson, C.; Steel, P. J. *Org. Biomol. Chem.* **2005**, *3*, 498.

(80) ACD/ChemSketch, version 12.01, Advanced Chemistry Development, Inc., Toronto, ON, Canada, www.acdlabs.com, 2014.

(81) ACD/3D Viewer, version 12.01, Advanced Chemistry Development, Inc., Toronto, ON, Canada, www.acdlabs.com, 2014.

(82) Cruz, A. J.; Kirgan, R.; Siam, K.; Heiland, P.; Rillema, D. P. *Inorg. Chim. Acta* **2010**, *363*, 2496.

(83) Bower, J. D.; Ramage, G. R. *J. Chem. Soc.* **1957**, 4506.

(84) Grenda, V. J.; Jones, R. E.; Gal, G.; Sletzinger, M. *J. Org. Chem.* **1965**, *30*, 259.

(85) Potts, K. T.; Burton, H. R.; Bhattacharyya, J. *J. Org. Chem.* **1966**, *31*, 260.

(86) Potts, K. T.; Burton, H. R.; Roy, S. K. *J. Org. Chem.* **1966**, *31*, 265.

(87) Potts, K. T.; Surapaneni, C. R. *J. Heterocycl. Chem.* **1970**, *7*, 1019.

(88) Okamoto, T.; Hirobe, M.; Tamai, Y.; Yabe, E. *Chem. Pharm. Bull.* **1966**, *14*, 506.

(89) Banks, R. E.; Hitchen, S. M. *J. Fluorine Chem.* **1982**, *20*, 373.

(90) Ueda, S.; Nagasawa, H. *J. Am. Chem. Soc.* **2009**, *131*, 15080.

(91) Mammoliti, O.; Quinton, E. M.; Loones, K. T. J.; Nguyen, A. T.; Wouters, J.; Van Lommen, G. *Tetrahedron* **2013**, *69*, 1669.

(92) Jin, C. H.; Krishnaiah, M.; Sreenu, D.; Subrahmanyam, V. B.; Rao, K. S.; Mohan, A. V. N.; Park, C.-Y.; Son, J.-Y.; Sheen, Y. Y.; Kim, D.-K. *Bioorg. Med. Chem. Lett.* **2011**, *21*, 6049.

(93) Guba, W.; Nettekoven, M.; Puellmann, B.; Riemer, C.; Schmitt, S. *Bioorg. Med. Chem. Lett.* **2004**, *14*, 3307.

(94) Nettekoven, M. *Synlett* **2001**, 1917.

(95) Kuroyanagi, J.-i.; Kanai, K.; Sugimoto, Y.; Fujisawa, T.; Morita, C.; Suzuki, T.; Kawakami, K.; Takemura, M. *Bioorg. Med. Chem.* **2010**, *18*, 5845.

(96) Jones, P.; Altamura, S.; Boueres, J.; Ferrigno, F.; Fonsi, M.; Giomini, C.; Lamartina, S.; Monteagudo, E.; Ontoria, J. M.; Orsale, M. V.; Palumbi, M. C.; Pesci, S.; Roscilli, G.; Scarpelli, R.; Schultz-Fademrecht, C.; Toniatti, C.; Rowley, M. *J. Med. Chem.* **2009**, *52*, 7170.

(97) Edmondson, S. D.; Mastracchio, A.; Mathvink, R. J.; He, J.; Harper, B.; Park, Y.-J.; Beconi, M.; Di Salvo, J.; Eiermann, G. J.; He, H.; Leiting, B.; Leone, J. F.; Levorse, D. A.; Lyons, K.; Patel, R. A.; Patel, S. B.; Petrov, A.; Scapin, G.; Shang, J.; Roy, R. S.; Smith, A.; Wu, J. K.; Xu, S.; Zhu, B.; Thornberry, N. A.; Weber, A. E. *J. Med. Chem.* **2006**, *49*, 3614.

(98) Kiyogo, S.; Kyorin Pharmaceutical Co., Ltd., Japan . 1979, p JP54039094A.

(99) Tsukamoto, G.; Takano, T.; Kawashima, T.; Ito, K.; Tajima, S.; Nose, H.; Uchiumi, I.; Kanebo, Ltd., Japan . 1981, p JP56061315A.

(100) Tsukamoto, G.; Takano, T.; Kawashima, T.; Ito, K.; Tajima, S.; Nose, H.; Uchiumi, I.; Kanebo, Ltd., Japan . 1981, p JP56100783A.

(101) Tsukamoto, G.; Takano, T.; Kawashima, T.; Ito, K.; Tajima, S.; Nose, H.; Uchiumi, I.; Kanebo, Ltd., Japan . 1981, p JP56063983A.

(102) Glover, E. E.; Rowbottom, K. T. *J. Chem. Soc., Perkin Trans. 1* **1976**, 367.

(103) Nakabayashi, Y.; Watanabe, Y.; Nakao, T.; Yamauchi, O. *Inorg. Chim. Acta* **2004**, *357*, 2553.

(104) Viala, C.; Coudret, C. *Inorg. Chim. Acta* **2006**, *359*, 984.

(105) Sheldrick, G. M. *Acta Crystallogr., Sect. A: Found. Crystallogr.* **2008**, *64*, 112.

(106) Sheldrick, G. M. University of Göttingen, SHELXL.

(107) Dolomanov, O. V. B., L.J.; Gildea, R.J.; Howard, J.A.K.; Puschmann, H., *J. Appl. Cryst.* **2009**, *42*, 339.